

SOILS and ROCKS

An International Journal of Geotechnical and Geoenvironmental Engineering

Editor Waldemar Coelho Hachich - University of São Paulo, Brazil

Co-editor Manuel Matos Fernandes - University of Porto, Portugal

Executive Board

Alberto Sayão

Pontifical Catholic University of Rio de Janeiro, Brazil

Jorge Almeida e Sousa

University of Coimbra, Portugal

Ian Schumann Martins

Federal University of Rio de Janeiro, Brazil

João Maranhã

LNEC, Portugal

Associate Editors

H. Einstein

MIT, USA

John A. Hudson

Imperial College, UK

Kenji Ishihara

University of Tokyo, Japan

Michele Jamiolkowski

Studio Geotecnico Italiano, Italy

Willy A. Lacerda

COPPE/UF RJ, Brazil

E. Maranhã das Neves

Lisbon Technical University, Portugal

Nielen van der Merve

University of Pretoria, South Africa

Paul Marinou

NTUA, Greece

James K. Mitchell

Virginia Tech., USA

Lars Persson

SGU, Sweden

Harry G. Poulos

University of Sidney, Australia

Niek Rengers

ITC, The Netherlands

Fumio Tatsuoka

Tokyo University of Science, Japan

Luíz González de Vallejo

UCM, Spain

Roger Frank

LCPC, France

Editorial Board Members

Roberto F. Azevedo

Federal University of Viçosa, Brazil

Milton Kanji

University of São Paulo, Brazil

Antonio M.S. Oliveira

University of Guarulhos, Brazil

Omar Y. Bitar

IPT, Brazil

Lázaro V. Zuquette

University of São Paulo, Brazil

Fabio Taioli

University of São Paulo, Brazil

Tarcisio Celestino

University of São Paulo-SC, Brazil

Roberto Q. Coutinho

Federal Univ. of Pernambuco, Brazil

Nilo C. Consoli

Federal Univ. Rio Grande do Sul, Brazil

Sandro S. Sandroni

Consultant, Brazil

Sérgio A.B. Fontoura

Pontifical Catholic University, Brazil

Ennio M. Palmeira

University of Brasília, Brazil

Luciano Décourt

Consultant, Brazil

Faíçal Massad

University of São Paulo, Brazil

Marcus Pacheco

University of the State of Rio de Janeiro, Brazil

Paulo Maia

University of Northern Rio de Janeiro, Brazil

Renato Cunha

University of Brasília, Brazil

Orencio Monje Vilar

University of São Paulo at São Carlos, Brazil

Maria Eugenia Boscov

University of São Paulo, Brazil

Vinod Garga

University of Ottawa, Canada

Richard J. Bathurst

Royal Military College of Canada

Robert Mair

University of Cambridge, UK

Nick Barton

Consultant, Norway

Serge Leroueil

University of Laval, Canada

Mario Manassero

Politécnico di Torino, Italy

Luis Valenzuela

Consultant, Chile

Jorge G. Zornberg

University of Texas/Austin, USA

Andrew Whittle

MIT, USA

Pierre Bérest

LCPC, France

Peter Kaiser

Laurentian University, Canada

He Manchao

CUMT, China

Teruo Nakai

Nagoya Inst. Technology, Japan

Claudio Olalla

CEDEX, Spain

Frederick Baynes

Baynes Geologic Ltd., Australia

R. Kerry Rowe

Queen's University, Canada

R. Jonathan Fannin

University of British Columbia, Canada

Laura Caldeira

LNEC, Portugal

António S. Cardoso

University of Porto, Portugal

José D. Rodrigues

Consultant, Portugal

António G. Coelho

Consultant, Portugal

Luís R. Sousa

University of Porto, Portugal

Rui M. Correia

LNEC, Portugal

João Marcelino

LNEC, Portugal

António C. Mineiro

University of Lisbon, Portugal

António P. Cunha

LNEC, Portugal New

António G. Correia

University of Minho, Portugal

Carlos D. Gama

Lisbon Technical University, Portugal

José V. Lemos

LNEC, Portugal

Nuno Grossmann

LNEC, Portugal

Luís L. Lemos

University of Coimbra, Portugal

Ricardo Oliveira

COBA, Portugal

Soils and Rocks publishes papers in English in the broad fields of Geotechnical Engineering, Engineering Geology and Geo-environmental Engineering. The Journal is published in April, August and December. Subscription price is US\$ 90.00 per year. The journal, with the name “Solos e Rochas”, was first published in 1978 by the Graduate School of Engineering, Federal University of Rio de Janeiro (COPPE-UFRJ). In 1980 it became the official magazine of the Brazilian Association for Soil Mechanics and Geotechnical Engineering (ABMS), acquiring the national character that had been the intention of its founders. In 1986 it also became the official Journal of the Brazilian Association for Engineering Geology and the Environment (ABGE) and in 1999 became the Latin American Geotechnical Journal, following the support of Latin-American representatives gathered for the Pan-American Conference of Guadalajara (1996). In 2007 the journal acquired the status of an international journal under the name of Soils and Rocks, published by the Brazilian Association for Soil Mechanics and Geotechnical Engineering (ABMS), Brazilian Association for Engineering Geology and the Environment (ABGE) and Portuguese Geotechnical Society (SPG). In 2010, ABGE decided to publish its own journal and left the partnership.

Soils and Rocks

1978,	1 (1, 2)
1979,	1 (3), 2 (1,2)
1980-1983,	3-6 (1, 2, 3)
1984,	7 (single number)
1985-1987,	8-10 (1, 2, 3)
1988-1990,	11-13 (single number)
1991-1992,	14-15 (1, 2)
1993,	16 (1, 2, 3, 4)
1994-2010,	17-33 (1, 2, 3)
2011,	34 (1, 2, 3, 4)
2012-2013,	35-36 (1, 2, 3)
2014,	37 (1, 2,

ISSN 1980-9743

CDU 624.131.1

SOILS and ROCKS

An International Journal of Geotechnical and Geoenvironmental Engineering

Publication of**ABMS - Brazilian Association for Soil Mechanics and Geotechnical Engineering****SPG - Portuguese Geotechnical Society****Volume 37, N. 2, May-August 2014****Table of Contents***VICTOR DE MELLO LECTURE**Lessons From The Lives of Two Dams*

J.K. Mitchell

99

*ARTICLES**Theoretical and Experimental Studies on the Resilience of Driven Piles*

Faïçal Massad

113

*Suggested Methodology for Rehabilitation of Ancient Masonry Castles and Forts on Rock Hills*A. Viana da Fonseca, L. Ribeiro e Sousa, A. Arêde, J. Guedes, E. Paupério, K. Karam, A. Costa,
J.E.Q. Menezes

133

*Influence of the Fibre Component of Soft Plastic on Shear Strength Parameters of Pre-Treated
Municipal Solid Waste*

A.V.A. Borgatto, C.F. Mahler, K. Münnich, A.D. Webler

151

*TECHNICAL NOTES**Impacts on the Groundwater Quality Within a Cemetery Area in Southeast Brazil*

A.G. Fineza, E.A.G. Marques, R.K.X. Bastos, L.S. Betim

161

*The Influence of Cement Content and Water to Cement Ratio on Capillary Absorption
of Root-Pile Mortars*

E. Laister, P.J.R. Albuquerque, G. Camarini, D. Carvalho

171

Victor de Mello Lecture



The Victor de Mello Lecture was established in 2008 by the Brazilian Association for Soil Mechanics and Geotechnical Engineering (ABMS), the Brazilian Association for Engineering Geology and the Environment (ABGE) and the Portuguese Geotechnical Society (SPG) to celebrate the life and professional contributions of Prof. Victor de Mello. Prof. de Mello was a consultant and academic for over 5 decades and made important contributions to the advance of geotechnical engineering. Every second year a worldwide acknowledged geotechnical expert is invited to deliver this special lecture, on occasion of the main conferences of ABMS and SPG. The fourth Victor de Mello Lecture is delivered by Prof. James K. Mitchell, whose name requires no introduction as author, professor, researcher and engineer. Prof. de Mello used to exchange ideas with his friend, Prof. Mitchell, most recently on topics related to the book he was writing. Prof. Mitchell chose for the lecture a theme that was one of Prof. de Mello's passions: dams. In his thorough review of the upgrading process of two old dams, focused on effective risk mitigation, Prof. Mitchell revisits and expands many of the concepts put forth by Prof. de Mello in his Rankine Lecture of 1977.



Prof. JAMES K. MITCHELL is University Distinguished Professor, Emeritus, at Virginia Tech and Consulting Geotechnical Engineer. He received his B.C.E. from R.P.I. in 1951, and M.S. and Sc.D. degrees from M.I.T. in 1953 and 1956. He was a professor at the University of California, Berkeley, from 1958 to 1994 before moving to Virginia Tech, and was Chairman of the Civil Engineering Department there during 1979-1984. His teaching, research and consulting have focused on soil properties and behavior, soil stabilization and improvement, ground reinforcement, in-situ measurement of soil properties, and mitigation of ground failure risk during earthquakes. He has authored 400 publications, including three editions of the book, "Fundamentals of Soil Behavior." Dr. Mitchell is a Distinguished Member of the American Society of Civil Engineers and was Vice President of the International Society for Soil Mechanics and Geotechnical Engineering from 1989-1994. He is a member of the United States National Academies of Engineering and Sciences.

Soils and Rocks
v. 37, n. 2

Lessons From The Lives of Two Dams

J.K. Mitchell

Abstract. Many embankment dams completed during the first six decades of the 20th century have been found deficient relative their ability to resist currently anticipated levels of seismic shaking and probable maximum flood. In this Fourth Victor de Mello Lecture, two recent case histories are described. One is a hydraulic fill structure completed in 1920 that is founded on alluvial material, some zones of which are susceptible to liquefaction. The other is a zoned earthfill dam completed in 1956 that is founded over a channel filled with loose, uncompacted, hydraulically placed tailings from gold mining operations. Each dam has been upgraded in phases over periods of several decades using different strategies and ground improvement technologies to improve stability and reduce failure risks. Several take away lessons from these experiences concerning current risk mitigation strategies, the importance of correct soil and site characterization, and implementation and effectiveness of different ground stabilization and improvement methods are presented.

Keywords: earthquakes, embankment dams, liquefaction, risk mitigation, site characterization, soil improvement.

1. Introduction

Dr. Victor de Mello was one of the “Giants of Geotechnics” of the 20th century who leaves a legacy of exceptional contributions from his major accomplishments as a practicing civil and geotechnical engineer, as a teacher both inside and outside the classroom, as a researcher, as a leader in his profession, and as a dynamic, yet philosophical and congenial colleague and friend. I am greatly honored by the invitation to deliver this lecture in celebration of his life and professional contributions, while at the same time daunted and humbled by the challenge of contributing something worthy of the honor.

Victor de Mello devoted his 1977 Rankine Lecture to considerations in embankment dam design (de Mello, 1977), with special focus on filters, drainage and seepage control, as well as stability issues. He discussed factors of safety and their meaning, introducing considerations of probability and variability that, while relatively new then, are now central to assessment of dam safety. I have also chosen to address embankment dams, but in this lecture, the focus is on dealing with problems that arise in existing dams resulting from age and from risks caused by extreme events, especially earthquakes and floods, that were incompletely understood and accounted for at the time of original construction many decades ago.

Many large embankment dams were constructed in the U.S.A. during the first six decades of the 20th Century. The M 9.2 Great Alaska Earthquake and the M 7.5 Niigata Earthquake in Japan, both in 1964, focused attention on soil liquefaction, and the near catastrophic failure of the Lower San Fernando Dam in southern California in the 1971 M 6.6 San Fernando Earthquake led to reevaluation of the seismic vulnerability of many other dams. The Maximum Credible Earthquakes, Maximum Probable Floods, and populations at risk have increased significantly at many

sites. Risk analyses have led to unacceptably high potential consequences requiring implementation of mitigation measures at many dams. Two of these dams are described in this paper.

San Pablo Dam, near Oakland, California and completed in 1921, is a hydraulic fill structure founded on alluvial deposits. Mormon Island Auxiliary Dam (MIAD), near Sacramento, California, is a compacted fill embankment founded on hydraulically deposited dredger tailings resulting from gold mining operations; completed in 1956. Each dam was subsequently deemed unsafe under the anticipated seismic loading conditions. Several modifications have been made to each dam to improve resistance to anticipated earthquake loadings and updated flood risks. These modifications took place from 1967 to 2010 at San Pablo Dam and have extended from the late 1980's to a planned final completion in 2016 at the Mormon Island Auxiliary Dam. Some conclusions and lessons learned about the development of geotechnical earthquake engineering for dams, seismic remediation strategies, the importance of proper site and material characterization, and the advantages and limitations of some ground improvement methods can be derived from these two case histories.

2. San Pablo Dam

This dam is a 53.3 m (170 ft) high, 38.1 m (125 ft) crest width, 366 m (1200 ft) long hydraulic fill dam founded on alluvial sediments that contain some zones that are susceptible to liquefaction. The hydraulic fill material used for construction of the embankment consists of weathered sandstone and shale that was obtained from the East Bay Hills near Oakland, California. The site is located within a few kilometers of several major faults, and it is estimated that there is a 62 percent probability of one or more earthquakes of magnitude 6.7 or greater during the period 2003 to 2032.

Photos of the construction of the dam illustrating the excavation for the core trench and placement of the hydraulic fill embankment materials are shown in Fig. 1. The original hydraulic fill embankment construction was completed in 1921. Tests on a few sandy samples of the embankment materials in the 1960's and 1970's indicated potentially liquefiable behavior. Evidently this led to the assumption of a liquefiable embankment because it was a hydraulic fill, and hydraulic fills of cohesionless materials are invariably of low relative density and high liquefaction potential unless densified following deposition.

A small downstream buttress fill was constructed in 1967 to improve seismic stability. Then, following the 1971 San Fernando Earthquake in southern California, a much larger upstream compacted fill buttress extending to bedrock was completed in 1979. Construction of this buttress required draining the reservoir, with its attendant depletion of the area's water supply capacity and disruption of recreational use of the reservoir. A cross section of the maximum embankment section with both the 1967 downstream stabilizing berm and the much larger 1979 upstream berm in place is shown in Fig. 2.

A new seismic stability evaluation was completed in 2004 assuming a liquefiable embankment and a M7.25 earthquake on the Hayward Fault which passes just 3 km southwest of the dam. The results indicated the potential for vertical slumping of up to 10.7 m and overtopping of the dam by the impounded reservoir. To provide additional freeboard for the short term, the reservoir level was lowered by 6 m. Consideration was given to completely rebuilding the dam; however, this would have required again draining the reservoir, an action that had considerable opposition. Instead, an in-place alternative was chosen that consisted of Cement Deep Soil Mixing (CDSM) to bedrock at depths of up to 36.5 m in the downstream foundation alluvial soils and construction of a large buttress fill on the downstream embankment slope, shown as Initial Remedial Concept in Fig. 3, from Yiadom & Roussel (2012).

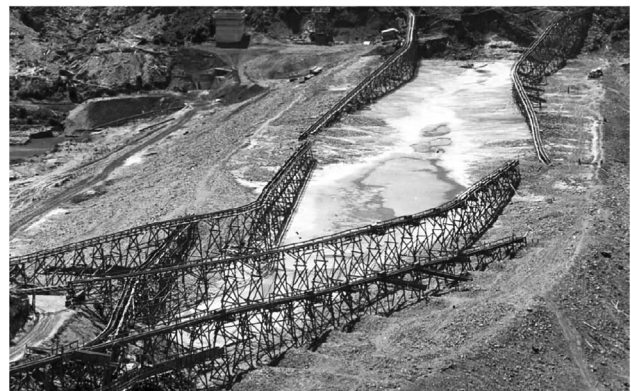
An extensive new field investigation program was then completed that included many cone penetration tests (CPT) and borings into both the embankment and foundation materials. The results of these field investigations and laboratory tests on representative samples are described in detail by Moriwaki, *et al.* (2008). They described the sampled hydraulically placed material as consistently very clayey, very "lumpy", and over-consolidated. Of special interest is Fig. 4, taken from that reference, which shows CPT and plasticity data for the hydraulic fill embankment shell materials, zones (1) and (2) in Fig. 2. This data shows clearly that this material is not susceptible to liquefaction, as had been assumed for the previous evaluations of San Pablo Dam and for the Initial Remedial Concept in Fig. 3. In retrospect this finding is not surprising given that the material used for the hydraulic fill came from the colluvial



(a) Core trench to bedrock with shoring in 1917



(b) Hydraulic fill construction site in 1919



(c) Hydraulic fill transportation and deposition in 1920

Figure 1 - Stages in the construction of San Pablo Dam (East Bay Municipal District construction photos Reproduced and reported by TNM Terra Engineers, Inc., Ninyo and Moore, 2007). (a) Core trench to bedrock with shoring in 1917; (b) Hydraulic fill construction site in 1919; (c) Hydraulic fill transportation and deposition in 1920.

slopes of the surrounding hills where the soil type is known to be largely silty and clayey.

This re-characterization of the hydraulic fill embankment material from liquefiable to non-liquefiable, fine-grained soil enabled significant reductions in the required sizes of the 2010 buttress and CDSM block, as may be seen in Fig. 3 by comparing the Final Remediation Design with the Initial Remedial Concept. Seismic deformation analyses of the maximum composite dam cross-section were done using computer program FLAC with input ground motions that had a peak acceleration of 0.98 g and associ-

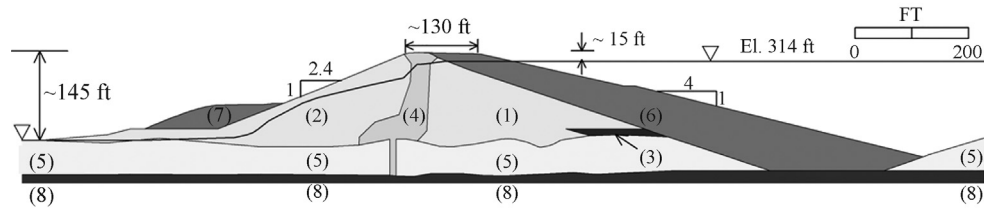


Figure 2 - Composite maximum section of San Pablo dam after buttress additions. (adapted from Moriwaki *et al.*, 2008). (1) upstream shell (hydraulic fill); (2) downstream shell (hydraulic fill); (3) ponded clay/silt; (4) core and key trench (hydraulic fill); (5) alluvial foundation soils; (6) upstream buttress (well-compacted) completed in 1979; (7) downstream buttress (less-compacted) added in 1967; and (8) bedrock.

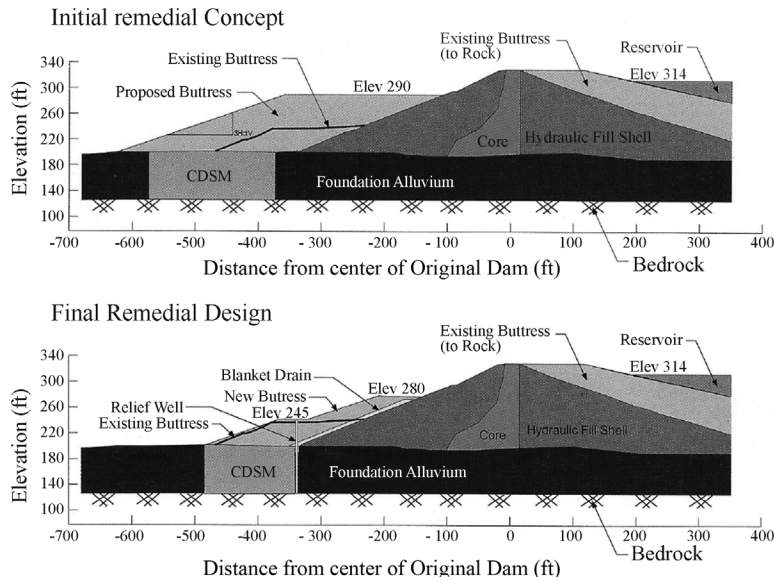


Figure 3 - Remedial designs for mitigation of seismic risk to San Pablo Dam (from Yiadom & Roussel, 2012).

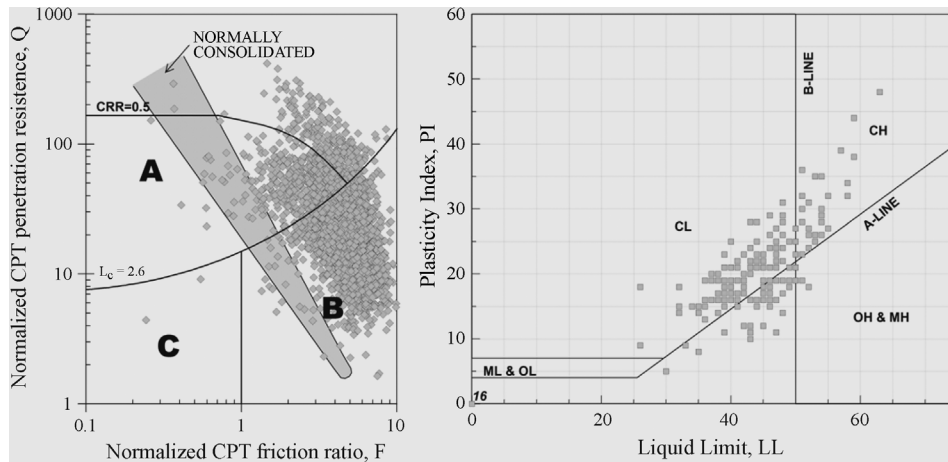


Figure 4 - CPT and Classification data for the San Pablo Dam hydraulic fill shell material. Zone A: Cyclic liquefaction possible; Zone B: Cyclic liquefaction unlikely; Zone C: Flow/cyclic liquefaction possible (from Moriwaki *et al.*, 2008).

ated spectral content consistent with the occurrence of a M7 earthquake on the nearby Hayward Fault. The results indicated maximum seismically induced permanent displacements in the range of 0.3 to 0.6 m (1 to 2 ft) (Kirby *et al.*, 2010), which were considered well within the range for acceptable performance.

The reduced volumes of required CDSM and the new downstream buttress fill realized a cost saving of about US \$40 million, a very significant amount for a project with a construction cost of about \$60 million. Kirby *et al.* (2010) describe the design of the CDSM foundation block, the construction process, and the methods used for quality con-

trol of the material. Another cost saving feature was that the spoils from the deep cement mixing could be incorporated into the new downstream buttress. An aerial photo (Google, 2012) of the project after completion is shown in Fig. 5. This project is an excellent illustration of the importance of correct soil identification and classification prior to analysis and design of risk mitigation strategies for existing dams.

3. Mormon Island Auxiliary Dam

The Mormon Island Auxiliary Dam (MIAD) forms a part of the Folsom Project located on the American River about 32 km (20 miles) northeast of Sacramento, California. This project provides water supply, hydroelectric power, and flood protection for a large metropolitan area. It consists of a concrete main dam, right and left wing dams, the zoned and rolled earthfill MIAD, and eight earthfill dikes that are needed to contain Folsom Lake. A plan showing these features is given in Fig. 6. Figure 7 is an aerial photo showing MIAD as it appears at present (Google Earth, 2013).

MIAD was constructed by the U.S. Army Corps of Engineers and completed in 1953, after which operation and maintenance activities have been the responsibility of the U.S. Bureau of Reclamation. The dam is comprised of a thin central impervious core bounded by fine and coarse filter transition zones extending to weathered metamorphic bedrock and compacted earthfill shells both upstream and downstream, as shown in Fig. 8. The embankment shells are composed of alluvium dredged from the site. The design width of the dam crest is 7.77 m (25.5 ft), the upstream slope varies from 3H:1V to 4.5H:1V, the downstream slope varies from 2.5H:1V to 3.5H:1V. The structural height of the embankment is 50.3 m (165 ft), and the dam is 1470 m (4820 ft) long.

The alluvial foundation materials, consisting of varying amounts of gravels, sands, silts and clays, were dredged and re-dredged to depths of very near the bedrock along an approximately 300 m (900 ft) long strip adjacent to the



Figure 5 - San Pablo Dam in 2010 after seismic remediation using cement deep soil mix in the downstream foundation and a downstream stability berm (Google Earth, Imagery Date 10/2/2009).

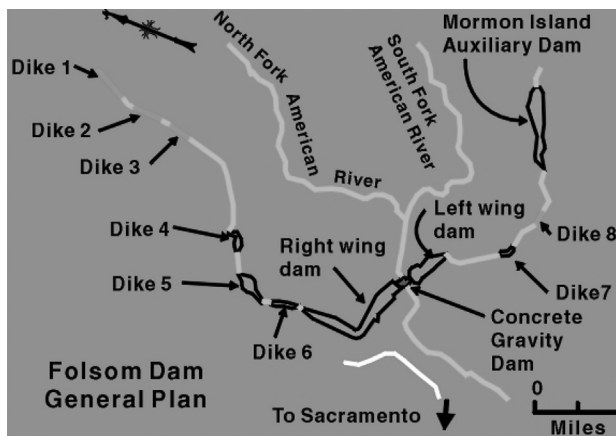


Figure 6 - Components of the Folsom Project near Sacramento, California.



Figure 7 - Aerial view of Mormon Island Auxiliary Dam as it appeared in August 2013. Critical section over potentially liquefiable foundation material extends about 300 m from the left abutment (Google Earth, Imagery Date 8/13/2013).

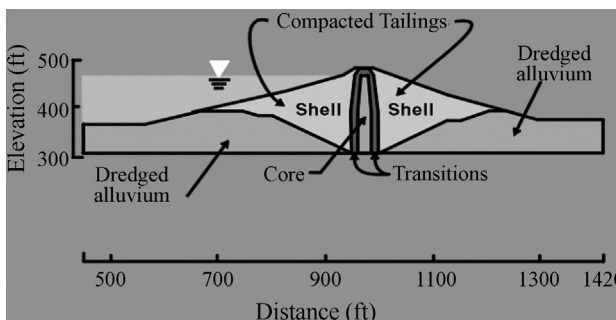


Figure 8 - Cross section of the Mormon Island Auxiliary Dam as constructed in 1956.

present location of the left abutment of the dam as a part of gold mining operations during the latter part of the 19th Century. As a result of this dredging and re-deposition, these materials were left in a loose state. The upstream and downstream toes of the embankment are underlain by an approximately 20 m (60 ft) thick layer of loose tailings for

this 300 m length of the dam. Evaluation of the seismic safety of the dam during the 1980s indicated that liquefaction of these tailings was likely during the design earthquake. A series of dam and foundation modifications for risk mitigation have been undertaken since then, and these activities are described below.

The results of field and laboratory tests were used to develop the distributions of normalized SPT (Standard Penetration Test) values of $(N_1)_{60}$ in the foundation that are shown in Fig. 9. These values were used to evaluate factors of safety against liquefaction and for the establishment of parameters needed for dynamic deformation analyses. Ground improvement was implemented beneath both the upstream and downstream embankment toe areas to mitigate the liquefaction risk and to limit dynamic displacements.

Owing to severe drought conditions in California in the late 1980s the reservoir level was low, and this made it possible to undertake deep dynamic compaction (DDC) in the dry from the upstream embankment. As shown in Fig. 10, an access excavation was made to provide level ground for carrying out the work. A block of densified soil was formed by repeated dropping of a 2.0 m (6.5 ft) diameter steel drop weight of 31.75 tonnes (35 tons) over a 244 by 46 m (800 by 150 ft) treatment area. The drop height of 32.9 m (108 ft) corresponded to a free fall distance of 30 m (98.4 ft). Three coverages of the area were made, with 30 drops at 15.2 m (50 ft) center to center drop point spacing for the first, or primary, coverage, 30 drops at points splitting the primary coverage spacing for the second coverage, and 15 drops at points splitting the secondary coverage for the third coverage. Finally surface "ironing" was accomplished using 2 weight drops from a height of 10 m (30 ft) at adjacent points to cover the entire area. Finally, the access excavation was re-filled, and a post treatment berm was placed on the upstream slope, as shown schematically in Fig. 10. The photograph in Fig. 7 shows this berm extending from the upstream slope into the reservoir following subsequent increase in the reservoir water level.

The effectiveness of the DDC can be seen in Fig. 11, which shows values of Becker Penetration Test (BPT) re-

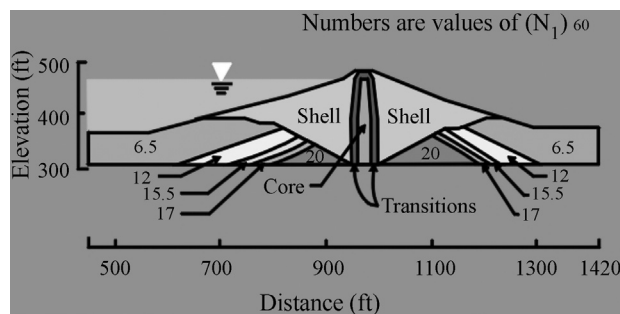


Figure 9 - Characterization of the MIAD foundation material in terms of SPT values of $(N_1)_{60}$ for use in liquefaction potential assessments.

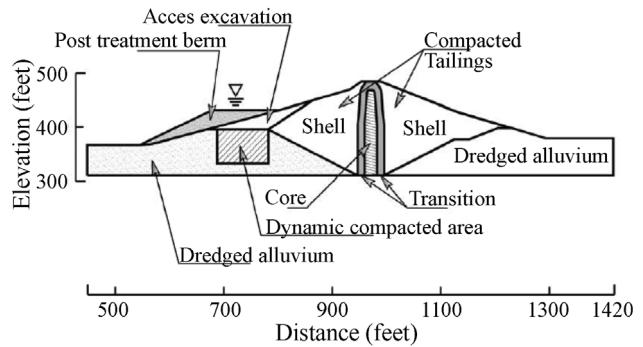


Figure 10 - Ground improvement design intended for mitigation of liquefaction risk beneath upstream embankment of Mormon Island Auxiliary Dam. DDC completed in 1990.

sistance, converted to equivalent SPT values of $(N_1)_{60}$, as a function of elevation. The BPT measures the number of blows to drive a 168 mm (6.6 in) outside diameter double-walled casing a distance of 0.3 m using a double-acting diesel pile driving hammer. This test is useful in soils containing gravel and cobbles, where difficulties are often encountered when using the SPT. The decrease in penetration resistance with depth in Fig. 11 is characteristic of the DDC method for soil improvement, with an effective treatment depth of about 10 m (35 ft) being about the maximum attainable when heavy weights are used in soils of no to low plasticity. As shown in Fig. 11, the DDC was unable to densify the soil within the treatment zone over the full depth to the underlying bedrock.

Following an extensive testing program for determination of the most suitable methods for in-place improvement of the downstream foundation material, the system shown schematically in Fig. 12 was designed, with construction completed during 1993-1994. The improvement zone was a strip along the downstream toe of the dam that is

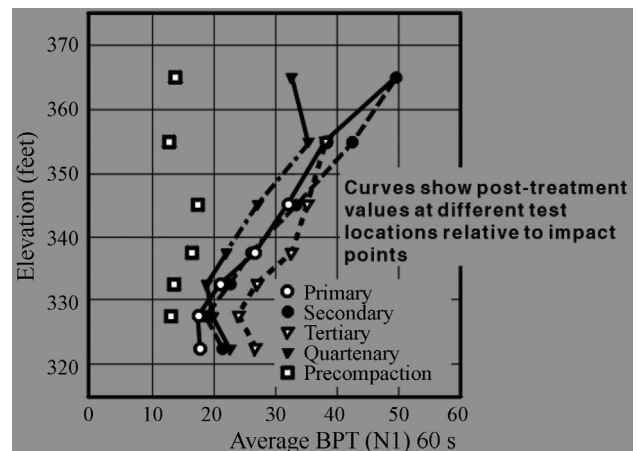


Figure 11 - Pre- and post-deep dynamic compaction Becker Penetration Test equivalent $(N_1)_{60}$ values beneath the upstream slope of Mormon Island Auxiliary Dam.

900 ft (275 m) long by 200 ft (61 m) wide in plan, in the area labeled “Downstream improvement” in Fig. 7. Excavation into the existing downstream embankment was required in order to develop a level working platform, Fig. 13, for installation of 1.2 m (4 ft) diameter wet, bottom feed, vibro-replacement stone columns and the upstream and downstream drainage zones that are composed of 250 mm diameter gravel columns on 1.0 m centers installed using a vibro-pipe. It is important to note that excavation into the downstream slopes of embankment dams is not without risk owing to reduced seepage paths and lower factors of safety against stability failure while the excavation is open, both of which must be accounted for in assessing risk during construction.

The primary purpose of the stone columns was to densify the loose liquefiable dredged alluvium foundation material so that it would not liquefy under the design earthquake. The upstream and downstream drainage zones are intended to intercept pore pressure plumes migrating towards the stone column treated zone in the event liquefaction develops in the adjacent untreated dredged alluvium during an earthquake. Prevention of pore pressure increases in the stone column zone is important for maintenance of shear strength during and after shaking.

The profile through the dredge spoils in the stone column area indicated that the upper 4.5 to 6 m contains coarse sand to cobble size material, and the lower 3 to 6 m is silty sand to silty clay with 10 to 77 percent fines, with an average fines content of 30 percent (Allen *et al.*, 1995). The pre- and post-treatment penetration resistance values shown in Fig. 14 are consistent with these conditions. A cross-section of the embankment showing all the modifications and ground improvement work through 1994 is shown in Fig. 15.

Subsequent investigations and risk analyses were initiated in 2001. These studies took into account that a poten-



Figure 13 - Installation of stone columns and gravel mini-column drains beneath the downstream embankment of Mormon Island Auxiliary Dam in 1994. Note the excavation and steepened slope needed for development of a working platform and for optimization of the improvement zone location for its effectiveness as a key block.

tially liquefiable zone remains beneath the upstream block of material that had been densified by deep dynamic compaction. After extensive re-analyses of available data and further in-situ testing, it was concluded also that the necessary downstream foundation densification was not achieved in the lower part of the soil profile during installation of the downstream stone columns, owing primarily to the fine-grained nature of the material. Furthermore, contamination of the stone columns by the fines resulted in lower column strength than had been anticipated and impeded the drainage capability as well. These re-analyses led to the conclusion that the most critical seismic failure mode

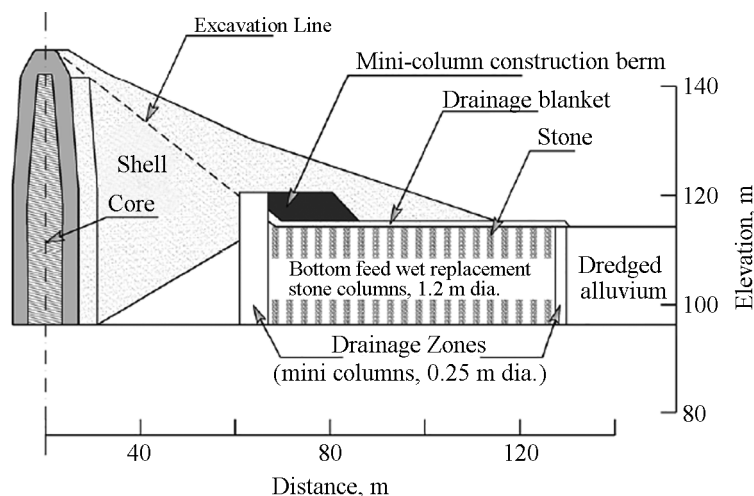


Figure 12 - Downstream foundation improvement for reduction of seismic failure risk at Mormon Island Auxiliary Dam. Construction was completed in 1994.

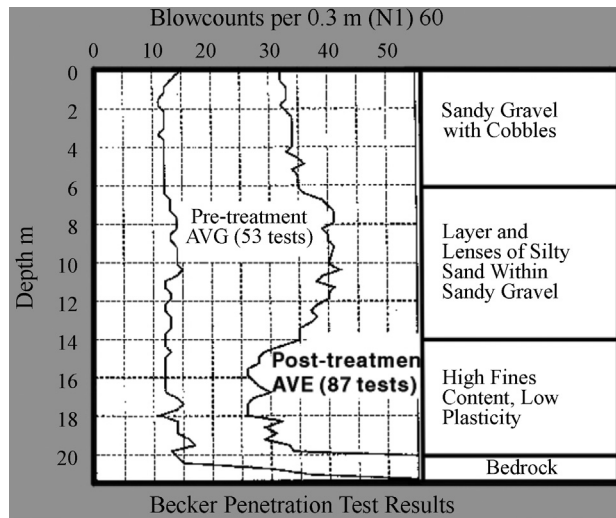


Figure 14 - Penetration resistance profiles in the downstream stone column treatment area, Mormon Island Auxiliary Dam.

would result from liquefaction of the upstream and downstream foundation materials leading to significant deformations of the dam in the downstream direction, with vertical displacements sufficient to result in overtopping for high reservoir levels.

A risk analysis done in 2007 showed that both the Annual Failure Probability and the Annualized Life Loss were above the Bureau of Reclamation guideline values. Corrective Action Studies for Seismic and Static Risk Reduction completed in 2010 led to a design that included a concrete key block with compacted soil above in the downstream

stone column area and a compacted soil buttress fill over the downstream embankment slope that includes underlying filters and drains. No further remedial work is planned for mitigation of the upstream liquefaction risk; i.e., the key block and buttress design is considered sufficiently robust that if any deformations develop in the upstream direction, the remaining downstream core, filters, and berm will still be adequate to maintain stability and the necessary free-board.

An additional point of interest is that jet grouting was proposed initially for construction of the key block. However, the results of an extensive test program indicated that the required continuity and strength of soilcrete could not be obtained owing to the presence of gravel, cobbles, and stone columns in the treatment zone. Jet grouting was ultimately judged to be technically and economically unfeasible for this purpose at this site. As a result, construction of the key block was accomplished within a series of contiguous cells, each being formed within an open, braced excavation. A photograph of this work in progress is shown in Fig. 16.

The final configuration of MIAD will be as shown schematically in Fig. 17. The key block construction was completed in February 2013, and the buttress fill is scheduled for completion in 2016.

4. Take-Away Lessons From These Two Projects

Several lessons and conclusions can be drawn from the San Pablo Dam and Mormon Island Auxiliary Dam seismic remediation work, and other projects within the au-

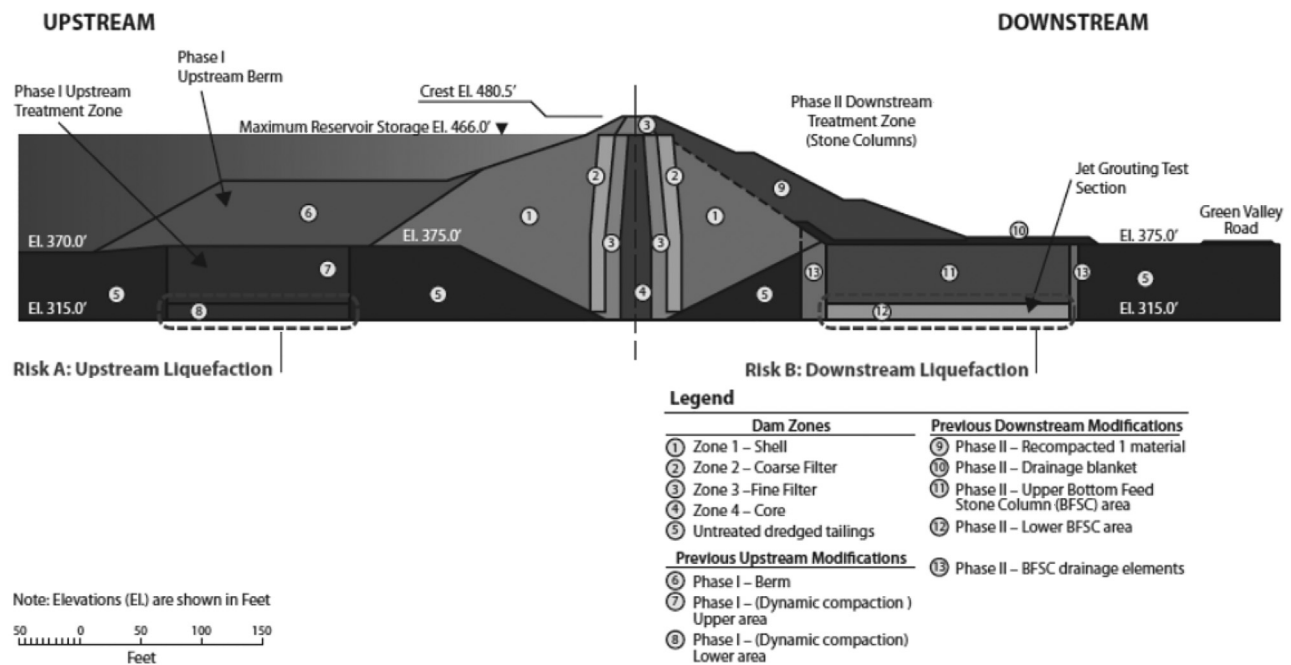


Figure 15 - Cross-section of Mormon Island Auxiliary Dam showing conditions after modifications completed in 1994 (adapted from U.S. Bureau of Reclamation, 2010).

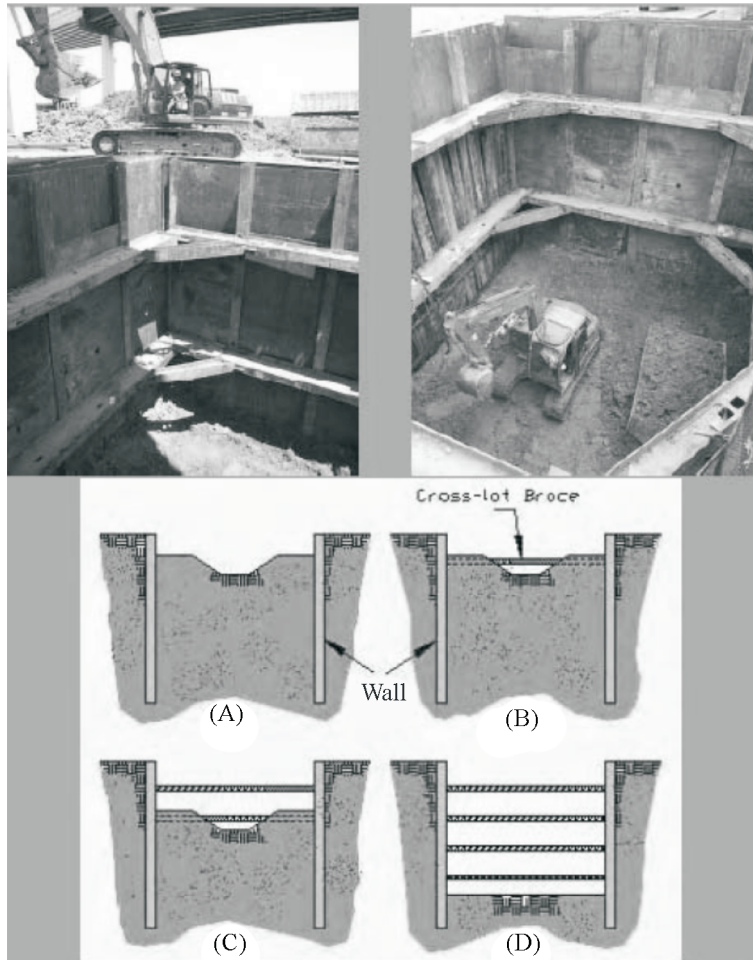


Figure 16 - Schematic diagram and photos of the excavation and bracing system for construction of the concrete key block in the downstream toe area of Mormon Island Auxiliary Dam (adapted from U.S. Bureau of Reclamation).

thor's experience, that relate to geotechnical engineering of existing embankment dams, strategies for mitigation of risk, site and material characterization, and ground improvement methods and their applicability.

4.1. Geotechnical engineering and failure risk mitigation for existing embankment dams

Most existing large embankment dams in the U.S. were constructed prior to the 1960s. Little attention was paid to seismic issues in their design. However, large earthquakes in Alaska and Japan in 1964, and the failure of the Lower San Fernando Dam in California in 1971 triggered assessment of the seismic resistance of major dams. Many dams have required modifications to protect against cracking and excessive deformations in the event of future earthquakes. In addition, seismicity reevaluations and redefinitions of maximum credible earthquake at a site, along with increases in the probable maximum flood and the populations at risk have resulted in increased demands.

Potential failure mode analyses and formal risk analyses are now widely used for determining the urgency of un-

dertaking risk mitigation activities, evaluation of the effectiveness of various types of remediation to be employed, and for prioritizing projects within available time and budget. Risk management guidelines and details of the risk assessment and evaluation process have been developed by several water resources and regulatory agencies. Publications by the U.S. Bureau of Reclamation and by the U.S. Army Corps of Engineers, many of which are available on-line, provide extensive information on these procedures and interpretation of the results.

A reasonable goal is to bring the safety of the dam, as measured by global stability, resistance to deformation sufficient to prevent overtopping resulting from excessive crest settlement, filter protection, safety against cracking, and drainage provisions downstream of the seepage barrier to states that are as safe as would be attainable if the dam were being designed and constructed today.

Remediation strategies for achieving the needed levels of stability, mitigation of liquefaction, controlling deformations under seismic loading, and prevention of overtopping seem to have followed a path over the past 50

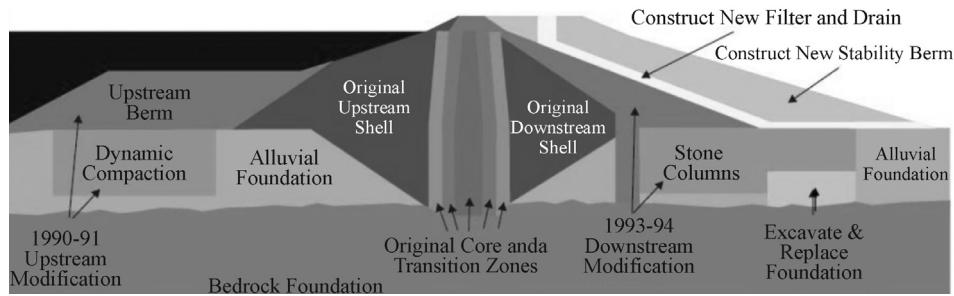


Figure 17 - Mormon Island Auxiliary Dam after completion (est. 2016) of modifications to assure seismic safety (adapted from U.S. Bureau of Reclamation).

years or so from adding a simple buttress fill, to incorporating different types of in-situ ground improvement such as deep dynamic compaction, vibro-compaction, vibro-replacement, and/or compaction piles both upstream and downstream, to a focus on downstream work only.

The downstream only option avoids the need for working over and through water, unless the reservoir level can be drawn down. An upstream embankment failure can be allowed provided the downstream embankment is buttressed sufficiently to prevent excessive loss of freeboard and the upstream failure zone does not encroach on the dam core at a point beneath the reservoir level. Satisfying these conditions must be demonstrated by suitable analyses. A downstream buttress fill overlay above a block of foundation soil treated in-situ, as done for the San Pablo Dam, is simple and reliable. The same is true for the buttress fill over a key block, now under construction at the Mormon Island Auxiliary Dam.

It is imperative to keep in mind, however, that whenever a project involves excavation into the downstream slope; e.g., during the stone column and drain installation, Fig. 13, or into the foundation, as was necessary for the key block construction at MIAD, Fig.16, there may be increased seepage as well as a temporary decrease in factor of safety against stability failure while the excavation is open that must be evaluated and assessed in terms of increased failure risk.

Limit equilibrium and deformation analyses under both static and dynamic loading conditions are necessary. These analyses, if properly carried out, provide critical information about the current condition of the embankment, the potential impacts of different seismic or other new loading conditions, the locations of potential failure surfaces and large deformation zones and patterns, whether the deformations may have detrimental effects on the dam core, filters, and seepage control components, and the effectiveness of different remediation methods and designs in assuring that adequate stability and deformation limits can be achieved.

A number of readily available computer programs is available for the limit equilibrium evaluations; the deformation analyses are usually done using finite difference;

e.g., FLAC and/or finite element; e.g. PLAXIS programs. The most critical input parameter for any of these analyses is the shear strength (Duncan, 2013). Determination of the appropriate strength value is often challenging, especially in situations involving liquefaction where knowledge of the post-triggering strength of the liquefied soil is required in order to assess the potential consequences.

4.2. Site and material characterization

The validity and reliability of all the analyses, selection of risk mitigation methods, and predictions of future behavior hinge on proper knowledge of the subsurface materials, their boundaries, the groundwater conditions, and how the relevant properties are measured and assigned. Review of available, original geological and geotechnical reports and construction records is essential. Information about past modifications to the dam must be carefully assessed. At the same time, the information about the actual present characteristics of the embankment and foundation soils may not be available or totally correct, as was found to be the case at San Pablo Dam.

Incorrect identification and characterization of materials can lead to significant overestimates or underestimates of both the dam safety and the needed extent, time, and cost of ground improvement.

4.3. Ground improvement methods and their applications in embankment dams

Ground improvement is now a major sub-discipline within geotechnical engineering and geo-construction. There are many methods and materials that can be used to meet a variety of ground improvement and reinforcement applications in embankment dams. A comprehensive description and classification of methods was developed by the ISSMGE Technical Committee on Ground Improvement (Chu *et al.*, 2009). An open access web-site, GeoTechTools.org, described by Schaefer *et al.* (2012) is now available that provides information and interactive selection guidance on 46 technologies useful for soil stabilization, ground improvement and reinforcement, and geo-construction. The information provided for each technology includes a technology fact sheet, photos, case histories,

design guidance, quality control and quality assurance information, cost information, specifications, and a bibliography.

The choice of the most appropriate ground improvement method or methods for mitigation of failure risks to dams is critical. In retrospect, the use of deep dynamic compaction for upstream foundation improvement at MIAD was later deemed not effective because of the unimproved zone that remained beneath the densified block, Fig. 10 and Zone 8 in Fig. 15. The presence of the high fines content in the lower portion of the downstream foundation soil at MIAD, Fig. 14 and Zone 12 in Fig. 15, was later deemed responsible for the stone columns to provide the improvement needed.

A few general observations concerning trends in the use of different ground improvement methods for mitigation of liquefaction risk and excessive deformations in dam foundations are:

- The use of vibro-compaction and vibro-replacement is decreasing
- The use of deep soil mixing is increasing.
- Buttress fills and downstream overlay fills are among the most cost-effective treatment methods provided suitable fill material and the necessary space are available.
- The promise of jet grouting for use in dam foundations is yet to be realized.
- What you can see, measure, and test is invariably a better and more reliable option than what you can't see, provided cost and construction risks are acceptable.

5. Some Continuing and Unresolved Problems

A number of unknowns, uncertainties, and problems can be identified that, if resolved, could lead to better risk evaluations, more optimized selection of mitigation strategies and ground treatment methods, and improved predictions of future behavior. A desirable goal is to “get it right the first time” so that subsequent mitigation measures, as were needed at both San Pablo Dam and Mormon Island Auxiliary Dam, will not be necessary. Among these unknowns, uncertainties and problems are:

- Anticipating (predicting) future increases in demand on the facility; e.g., greater seismic loading, larger probable maximum flood, adverse consequences of climate change, increased population at risk
- Interpreting and communicating the results of a risk analysis
- Deciding the acceptable level of risk
- Assessing the liquefaction potential of soils containing gravel and cobbles
- Assessing the liquefaction potential of silty soils
- Assessing the post-earthquake residual strength of liquefied soil

- Selecting and implementing the appropriate soil constitutive model for use in liquefaction and dynamic deformation analyses
- Assessing the reliability and accuracy of dynamic deformation analyses. A widely accepted “rule of thumb” has been that actual deformations may be within about +/- 100 percent of the computed or estimated value; however, it is not really known how valid this estimate is.
- Accounting for time (aging) effects following densification and/or admixture stabilization of foundation and embankment soils
- Writing enforceable specifications that will produce the needed end results, but also allow for inherent variability in materials and other site-specific conditions
- Assessing compliance with the ground improvement specifications for uniformity and post-treatment strength and stiffness requirements

6. Concluding Comments

Getting it right the first time can be very difficult given the unknowns and uncertainties at the time of initial design and construction of an embankment dam. The two case histories described in this paper illustrate that getting the remediation of a deficient existing dam right the first time can also be very difficult. The potential consequences of climate change, increasing numbers and magnitudes of extreme events (floods, storms, earthquakes, fires, etc.) must be considered from the outset of a project. Simple, observable, and measurable methods for dam strengthening and risk mitigation should be used wherever possible. A reasonable overall goal should be to make an existing, deficient embankment dam as safe as if you were starting a new project today. Resolution of the issues listed in the previous section should be instrumental in helping to reach this goal by enabling better selection and optimization of methods for mitigation of risks to existing dams in the future.

References

- Allen, M.G.; Jones, R. & Gularte, F.B. (1995) Bottom-feed stone columns, wet replacement construction method: Mormon Island Auxiliary Dam modifications. *Soil Improvement for Earthquake Hazard Mitigation, Geotechnical Special Publication 49, ASCE*, p. 82-95.
- Chu, S.; Varaksin, S.; Klotz, U., & Menge, P. (2009) *Construction processes. Proc. Int. Conf. on Soil Mechanics and Geotechnical Engineering, Alexandria, Egypt, IOS Press.*
- de Mello, V.F.B. (1977) Reflections on design decisions of practical significance to embankment dams. *The Seventeenth Rankine Lecture, Geotechnique, v. 27:3*, p. 281-355.
- Duncan, J.M. (2013) Slope stability then and now. *Proceedings of the GeoCongress 2013: Stability and Performance of Slopes and Embankments III*, p. 2191-210.

- Kirby, R.C.; Roussel, G.L.; Barneich, J.A.; Yiadom, A.B. & Todaro, S.M. (2010) Design and construction of seismic upgrades at San Pablo Dam using CDSM. Proc. U.S. Society of Dams Conference, p. 137-152.
- Mitchell, J.K. (2008) Recent developments in ground improvement for mitigation of seismic risk to existing embankment dams. Geotechnical Earthquake Engineering and Soil Dynamics IV, ASCE Geotechnical Special Publication 181, p. 1-20.
- Moriwaki, Y.; Dinsick, A.; Barneich, J.; Roussel, G.; Yiadom, A.; Starr, F., & Tan, P. (2008) Seismic characterization and its limited implication for San Pablo Dam. Geotechnical Earthquake Engineering and Soil Dynamics IV, p. 1-10.
- Schaefer, V.R.; Mitchell, J.K.; Berg, R.R.; Filz, G.M. & Douglas, S.C. (2012) Ground improvement in the 21st century: a comprehensive web-based information system. Rollins, K. & Zekkos, D. (eds) Geotechnical Engineering State of the Art and Practice. ASCE Geotechnical Special Pub. No. 226, p. 272-293.
- TNM Terra Engineers Ninyo and Moore (2007) Site characterization of Dam Area, Report, Design Services for San Pablo Dam Seismic Upgrade, April 2007, 347 p.
- U.S. Bureau of Reclamation (2010) Mormon Island Auxiliary Dam Modification Project, Final Supplemental Environmental Impact Statement/Environmental Impact Report. Folsom California, Mid-Pacific Region, State Clearing House #2009042077. May 2010.
- Yiadom, A.B. & Roussel, G.L. (2012) Seismic upgrades of San Pablo Dam. Geo-Strata, May/June 2012, p. 34-39.

Articles

Soils and Rocks
v. 37, n. 2

Theoretical and Experimental Studies on the Resilience of Driven Piles

Façal Massad

Abstract. This paper deals with the resilient condition that may be reached by driven piles, during its installation as well as under static cyclic and monotonic loading tests. During the 1950's Van Weele observed its effect in the context of a method for the separation of the toe and shaft loads at failure using the results of static cyclic loading tests on driven piles. Under this condition and based on a mathematical model that uses Cambeftor's Relations and takes into account pile compressibility and residual loads, this paper shows that there is a homothetic relation between the loading and the unloading-movement curves at pile head. A graphical construction is presented along with a numerical procedure allowing to improve the understanding of pile behavior and to determine significant parameters of pile-soil interaction under static or driving loadings. Application of the homothetic relations is made to several piles and particularly a new procedure was developed to analyze dynamic loading tests with a single blow record, considering the residual load at the toe.

Keywords: resilience, driven piles; homothety, residual loads, unloading.

1. Introduction

During pile driving or under static cyclic or monotonic loading a state of resilience may be reached in the soil along the shaft and at the toe, that is to say they respond elastically to the imposed loads. Without mentioning this term, Van Weele (1957) observed its effect in the context of a method for the separation of the toe and shaft loads at failure using the results of a static cyclic loading test on driven piles. The method requires: a) the full mobilization of lateral friction in the final cycles of loading-unloading; and b) the knowledge of the relationship between the mean and the total shaft load at failure. It consists of plotting a graph of maximum applied load as a function of elastic rebound, measured at the pile head. In the range associated to the shaft load full mobilization a straight line was obtained which enabled the mentioned separation. As will be dealt with later, the resilience effect was incorporated in the Smith Wave Equation Model (see, *e.g.*, Rausche, 2002).

The application of Van Weele's Method was extended by Massad (2001) to dynamic loading tests with increasing energy. In addition, a more general linear equation was derived relating the maximum applied load, shaft friction at failure, the residual toe load, the soil stiffness at the toe and the pile elastic rebound. This was done in the light of a mathematical model that incorporates, as load transfer functions, the modified Cambeftor's Relations and considers pile compressibility and the residual stresses.

In this paper it is shown how to use these findings and that the resilient state during repeated loading implies a homothety of the curves of loading and unloading movements at pile head.

2. The Resilient state According to Van Weele

The static cyclic loading test introduced by Van Weele (1957) consists of applying increasing loads in multiple cycles, such that at the end of each cycle the load is zero at the pile head. Figure 1 illustrates one complete cycle. In the load test analyzed by this author the concrete pile had a square section (0.38 cm x 0.38 cm), 14.05 m in length, and it was instrumented with strain gauges, installed in 4 levels along the shaft. In addition, movement measurements were taken at the pile head. There was also a portion of reference 1 m in height, at the top, which allowed the assessment of the modulus of elasticity of the concrete, of the order of 38.3 GPa.

Figures 2 and 3 show: a) toe load (Q_p) in function of toe quake (C_3) and b) the maximum load in each cycle (P_o^{\max}) as a function of the elastic rebound at the pile head (ρ) (see list of symbols at the end of the text). While Fig. 1 illustrates how C_3 and ρ were determined for one cycle, Fig. 2 allows the determination of the coefficient of subgrade reaction, as termed by Van Weele, or the Cambeftor parameter R_{reb} that measure the resilient elastic response of the soil at pile toe (see Baguelin & Venon, 1971 and Massad, 1995, 2001). In general, and using the notations of Randolph & Wroth (1978), it is possible to write $R = (2 \cdot D \cdot G_b) / [(1 - \nu) \cdot \eta \cdot S]$, where G_b is the Shear Modulus of the soil at pile toe (base).

The linear relationship displayed by Fig. 2 characterizes the effect of the resilience at the toe, which manifests itself in many geotechnical engineering problems with repeated loadings.

Façal Massad, Full Professor and Geotechnical Consultant, Escola Politécnica, Universidade de São Paulo, Av. Prof. Almeida Prado 271, trav. 2, São Paulo, SP, Brazil. e-mail: faissal@usp.br.

Submitted on June 19, 2014; Final Acceptance on August 18, 2014; Discussion open until December 31, 2014.

Based on Fig. 3 Van Weele proposed a method to separate the load in ultimate shaft friction and toe resistance. A condition for its application is the full mobilization of the shaft load in the last cycles. In the case of the load test analyzed by this author, this occurred above the maximum load (P_o^{\max}) of 1000 kN, when the experimental points in Fig. 3 lined up. Van Weele obtained the following results:

- $A_r = 625$ kN for the ultimate shaft resistance, which compared with the measured figure of 608 kN; and
- $Q_{p\max} = 1,750 - 625 = 1,125$ kN for the maximum toe load.

The Van Weele method still requires the knowledge of the relationship between the mean and the total shaft load at failure estimated in his case as 24.7% based on Begegnann CPT.

3. The Meaning of the Van Weele's Equation

Leonards & Lovell (1979), coincidentally aiming at taking advantage of the Van Weele's achievement, proposed an equation to estimate the shortening of vertical piles, under axial compression loading at the head (P_o), not necessarily at failure, which can be written as follows:

$$\Delta e = \frac{Q_p}{K_r} + c \cdot \frac{A_l}{K_r} \quad (1)$$

where Q_p and A_l are toe and shaft loads, respectively, so that:

$$P_o = Q_p + A_l \quad (2)$$

K_r is the pile stiffness, with height h , cross sectional area S and modulus of elasticity E , given by:

$$K_r = \frac{E \cdot S}{h} \quad (3)$$

In the expression 1 c is the ratio of the average value of the transferred lateral load ($A_l - A'_l$) and the total shaft load (A_l), i.e.:

$$c = \frac{A_l - A'_l}{A_l} \quad (4)$$

It depends on the distribution of the unit shaft friction (f). If the shaft load is fully mobilized ($A_l = A'_l$), then $c = 0.5$ for $f_u = \text{const}$ along depth and $c = 2/3$ for f_u increasing linearly with depth. Values of c for other simple forms of distribution of f_u can be obtained rapidly using the nomograms prepared by Leonards & Lovell (1979) or the equations proposed by Fellenius (1980). For most common cases of heterogeneous layers c varies in the range 0.5-0.8. In the case of Van Weele's pile, $c = 1 - 24.7\% \cong 0.75$.

These equations remain valid for unloading, that is, in tension. Imagine that a static cyclic loading has reached the maximum load P_o^{\max} at the pile head and that, after unloading ($P_o = 0$), the elastic rebound, measured at the top, is ρ . In the usual form, it can be written:

$$\rho = C_2 + C_3 \quad (5)$$

where C_2 e C_3 are, respectively, the shaft and toe quakes (see Fig. 1).

Obviously, the absolute value of C_2 , which is now elongation, is given by the expression 1 suitably rewritten, namely:

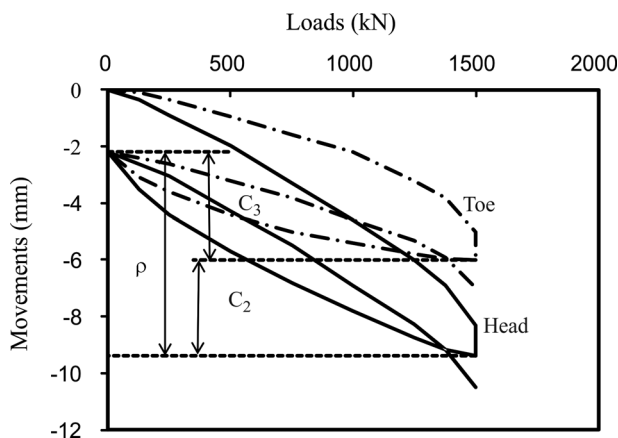


Figure 1 - Static cyclic loading test – Adapted from Van Weele (1957).

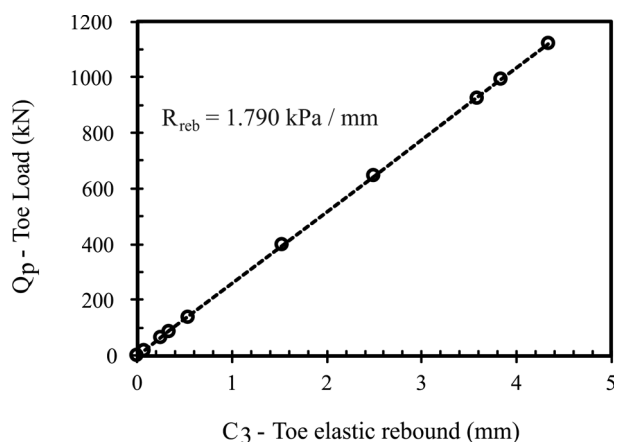


Figure 2 - Relation between Q_p and C_3 (Van Weele, 1957).

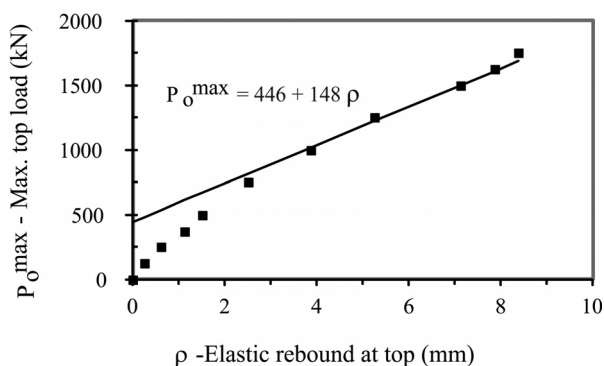


Figure 3 - P_o^{\max} vs. ρ (Van Weele, 1957).

$$C_2 = \frac{P_o^{\max} - A_l}{K_r} + c \cdot \frac{A_l}{K_r} \quad (6)$$

No consideration, for now, is being made with respect to any residual loads on the pile toe. The total shaft load decreases from A_l , end of loading, to zero, end of unloading ($P_o = 0$). The same happens with the toe, whose reaction falls from $Q_p = P_o^{\max} - A_l$ to zero.

The value C_3 may be expressed by the following equation:

$$C_3 = \frac{P_o^{\max} - A_l}{R_{reb} \cdot S_p} \quad (7)$$

where S_p is the area of the pile toe and R_{reb} is one of the basic parameter of the second Cambeftor Relation for unloading ("rebound"), as mentioned before. The hypothesis that R_{reb} is constant is plausible in a cyclic loading test as seen above in the context of Fig. 2.

Substituting Eqs. 6 and 7 into Eq. 5 and after several transformations results:

$$P_o^{\max} = A_l \left(1 - c \cdot \frac{d_{2R}}{K_r} \right) + d_{2R} \cdot \rho \quad (8)$$

where d_{2R} , given by:

$$\frac{1}{d_{2R}} = \frac{1}{K_r} + \frac{1}{R_{reb} \cdot S_p} \quad (9)$$

is a measure of the pile-soil (at the toe) stiffness.

If the shaft load in a cycle has been fully mobilized, *i.e.*, $A_l = A_{lr}$ at the end of unloading ($P_o = 0$), the parameter c becomes constant, and the expression 8 turns into:

$$P_o^{\max} = A_{lr} \left(1 - c \cdot \frac{d_{2R}}{K_r} \right) + d_{2R} \cdot \rho \quad (10)$$

which is the meaning of the straight line of Fig. 3. In a plot of $P_o^{\max} - \rho$, there is a linear relationship, which occurred above 1000 kN in the case of concrete pile analyzed by Van Weele, illustrated in Fig. 3. Applying Eq. 10 in this case and taken into account that $K_r = 394$ kN/mm and $c = 1 - 0.247 \cong 0.75$ it follows that:

$$d_{2R} = 148 \text{ kN/mm} \quad (11)$$

$$A_{lr} = \frac{446}{l - (1 - 0.247) \cdot \frac{148}{394}} = 622 \text{ kN} \quad (12)$$

and so:

$$Q_{p\max} = 1750 - 622 = 1128 \text{ kN} \quad (13)$$

which are in agreement with the figures gotten by Van Weele. Equation 9 leads to $d_{2R} = 156$ kN/mm, close to the value given by Eq. 11.

The existence of residual load has been known for a long time. Certainly it does not affect the pile load capacity but the skin friction and the end bearing values. According to Fellenius (2002), it is not easy to demonstrate its influence on test data and yet more difficult to quantify its effect. And this author adds: "Practice is, regrettably, to consider the residual load to be small and not significant to the analysis and to proceed with an evaluation based on "zeroing" all gages immediately before the start of the test. That is, the problem is solved by declaring it not to exist". In spite of this assessment, the interference of residual loads on pile behavior will be considered now.

In general, residual stresses can be dealt with a magnifier factor (μ) (Massad, 1995), given by:

$$\mu = 1 + \frac{P_h}{A_{lr}} \quad \text{or} \quad \mu = 1 + \frac{|f'_{res}|}{f'_u} \quad (14)$$

where P_h is the residual toe load, that is in equilibrium with the residual shaft friction, whose mean value is f'_{res} and f'_u is the mean value of the ultimate unit shaft friction.

Note that $\mu A_{lr} = A_{lr} + P_h$, *i.e.*, the residual loads act as a shaft load due to the need to reverse the residual shaft friction. In general, this coefficient, that is greater than 1, is bounded by the smaller value between 2 and $1 + Q_{pr}/A_{lr}$, where Q_{pr} is the toe load at failure.

Assuming now that at the end of a cycle of loading-unloading, with $P_o = 0$, a residual load (P_h^{reb}) arises at the toe of a driven pile, which is in equilibrium with the residual shaft friction, and introducing the factor $\mu_{reb} = 1 + P_h^{reb}/A_{lr}$, the expressions 6, 7 and 10 change to:

$$C_2 = \frac{P_o^{\max} - \mu_{reb} \cdot A_{lr}}{K_r} + c \cdot \frac{\mu_{reb} \cdot A_{lr}}{K_r} \quad (15)$$

$$C_3 = \frac{P_o^{\max} - \mu_{reb} \cdot A_{lr}}{R_{reb} \cdot S_p} \quad (16)$$

$$P_o^{\max} = \mu_{reb} \cdot A_{lr} \left(1 - c \cdot \frac{d_{2R}}{K_r} \right) + d_{2R} \cdot \rho \quad (17)$$

Expression 17 is the general form of the Van Weele's Equation (straight line of Fig. 3).

The difficulty in applying Eq. 17 is that c depends on the amount of shaft friction mobilized in the rebound. Massad (2001) presented results of a parametric study, using a mathematical model, to be presented later, based on the Cambeftor's Relations showing that at the end of rebound c varies from 0.4 to 0.5 (see Fig. 4-a) if the maximum unit skin friction (f'_u) is constant; for friction full mobilization $c = 0.5$, as mentioned before. In Fig. 4-a:

$$Q = \frac{C_3}{y_1} \quad (18)$$

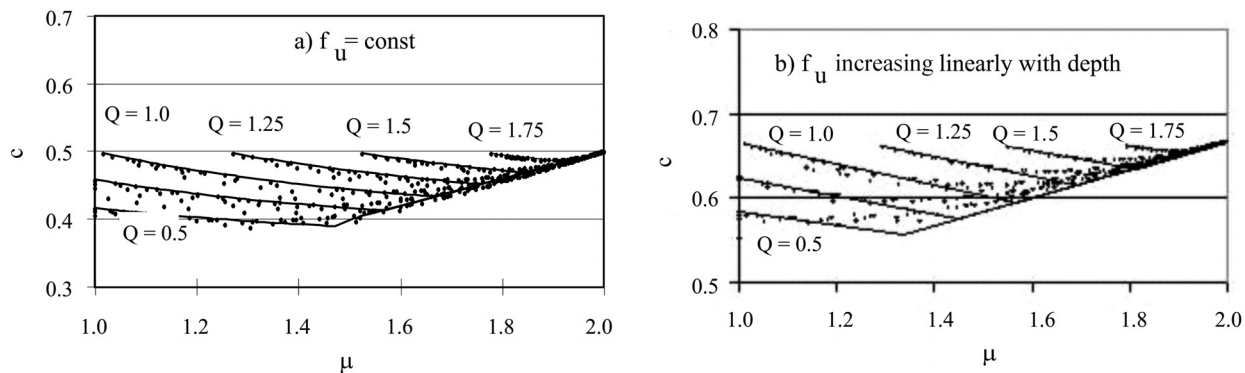


Figure 4 - Theoretical relations between c and μ , at the end of rebound ($P_o = 0$).

Thus, in a first approximation, c can be taken equal to $1/2$, for f_u constant with depth.

If f_u varies linearly with depth, it can be proved that c ranges between 0.57 to 0.67 , and again the last figure is associated with full mobilization of friction (see Fig. 4-b). Thus, in a first approximation, c can be taken equal $2/3$ for f_u increasing linearly with depth.

4. Homothetic Relations Between the Loading and Unloading-Movement Curves at Pile Head

During pile driving or under static cyclic loading the state of resilience implies a homothetic relation between the loading and unloading (“rebound”)–movement curves.

To demonstrate this similarity it will be used the already mentioned mathematical model that assumes the modified Cambeft’s Relations (Fig. 5-a and 5-b, with $y_3 = \mu \cdot y_1$) and takes into account pile compressibility (*i.e.* progressive failure) and residual loads due to driving or repeated loadings. It incorporates most of the features of the model developed by Baguelin & Venon (1971), in a simpler way and can be applied to bored, jacked or driven piles, first or subsequent loadings and unloadings. Initially, the soil will be admitted to be homogeneous, with $f_u = \text{const}$.

One advantage of using μ is that it allows to take the residual loads as friction loads in the model (Massad, 1995).

4.1. Basic equations

A coefficient that measures the relative stiffness of the pile-soil (around the shaft) system was introduced by Massad (1995) and is defined as follows:

$$k = \frac{A_{lr}}{K_r \cdot y_1} \quad \text{and} \quad z = \sqrt{k} \tag{19}$$

where y_1 is the pile displacement, of the order of some mm, required to mobilize the full shaft resistance (see Fig. 5-a). Note that: a) the maximum and the residual shaft frictions (f_u and f_{res}) are supposed to be constant along the pile; and b) the coefficient k is the term $(\mu h)^2$ of Randolph and Wroth (1978), with his notations, not to be confused with the symbol μ used in this paper.

The model gave a further insight on pile behavior and led to a new pile classification, with respect to k values: “short” or rigid ($k \leq 2$); intermediate ($2 \leq k \leq 8$); and “long” or compressible ($k \geq 8$) (see Massad, 1995).

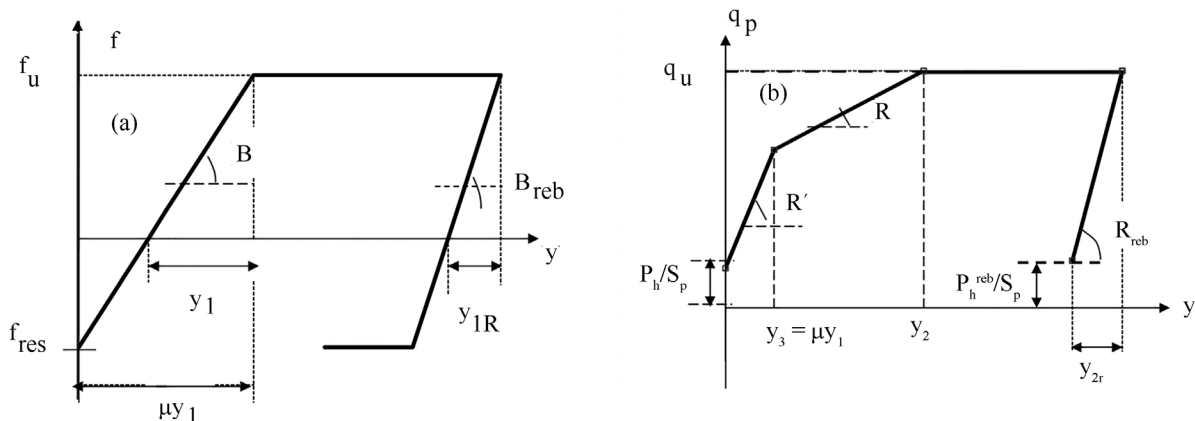


Figure 5 - Modified First and Second Cambeft’s Law.

The load (P_o)-movement (y_o) curve at pile head (see Fig. 6), during loading and unloading, may be expressed by the equations shown in Table 1.

Reporting to Table 1 and Fig. 6, the range 0-3 corresponds to the initial pseudo elastic lines of Fig. 5, with inclinations B and R' ; the range 3-4 refers to the progressive mobilization of shaft resistance, from top to bottom, and also the point resistance up to $y_3 = \mu \cdot y_1$; and finally the range 4-5 is the free development of toe resistance, $y > y_3 = \mu \cdot y_1$. Point 5 is not necessarily associated with the failure load. The coefficients β_1 and β_2 depends on the characteristics of the soil-pile system and the toe parameter R' . But, for compressible piles ("long piles") they approach 1 and the influence of the toe is very small in ranges 0-3 and 3-4. Note that if $\beta_2 \cong 1$, the range 3-4 turns to be a parabola. For very rigid piles, this range vanishes, that is, Points 3 and 4 coincide but the influence of R' on range 0-3 is great. Note also that λ' is the relative stiffness of the pile-soil (around the shaft and at the toe) system (Massad, 1995); and d_2 is the slope of the straight line 4-5.

For the unloading ranges 6-7, 7-8, and 8-9 (Fig. 6) the equations are similar in their form, but they differ: a) in the use of the appropriate Cambeport's parameters for rebound, as shown on Figs. 5-a and 5-b; and b) if the loading stage ends further Point 4 (full mobilization of shaft friction), as assumed in Fig. 6, then $f_{res} = -f_u$ and from Eq. 14 $\mu = 2$ at $P_o = P_o^{\max}$ (see Massad, 1995).

4.2. Homothetic model for repeated loadings

Once resilient condition is reached, the following equations hold (see Fig. 5-b):

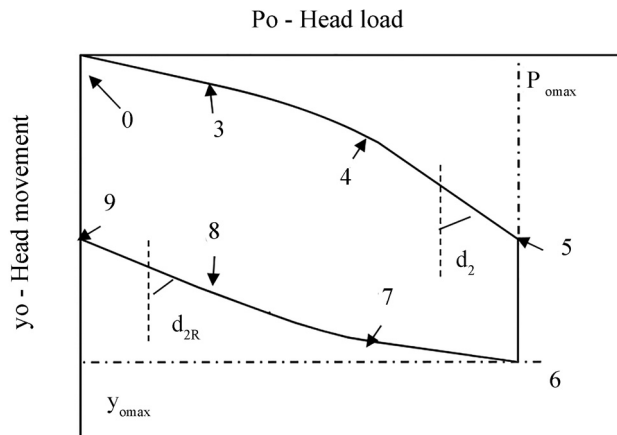


Figure 6 - Theoretical Load-movement curve.

$$B = B_{reb} \quad \text{and} \quad R' = R_{reb} \quad (20)$$

Consequently, the loading and unloading curves tend to be homothetic in the ranges 0-4 and 6-8 of Fig. 6, a conclusion that comes from an inspection of the basic equations of Table 1. Ranges 4-5 and 8-9 are excluded, unless $R = R' = R_{reb}$, which does not occur necessarily.

An indication that the resilience is achieved can be seen by graphs like Fig. 7: there is a coincidence between the two curves at least in ranges 0-3 and 6-7.

4.2.1. Center and ratio of the homothety

An analysis of the formulae given in Table 1 shows that the ratio of homothety is $\mu/2$ and its center is in Point O,

Table 1 - Basic and auxiliary equations for the ranges of Fig. 6 (homogeneous soils).

Range	Basic equation	Auxiliary equation
0-3	$P_o = \mu A_{lr} \cdot \frac{\beta_1 \cdot y_o}{z \cdot \mu y_1}$	$\beta_1 = \frac{\tanh(z) + \lambda'}{1 + \lambda' \cdot \tanh(z)} \quad \text{with} \quad \lambda' = \frac{R' \cdot S_p}{K_r \cdot z}$
3-4	$\frac{y_o}{\mu y_1} = \left(1 - \frac{\beta_2'^2}{2}\right) + \frac{k}{2} \left(\frac{P_o}{\mu A_{lr}}\right)^2$	$\beta_2'^2 - \tanh^{-1}(\beta_2'^2) = \left(\frac{P_o}{\mu A_{lr}} - 1\right) \cdot z - \tanh^{-1}(\lambda')$
4-5	$\frac{P_o - \mu A_{lr} - (R' - R) S_p \mu y_1}{y_o - c \cdot \frac{\mu A_{lr}}{K_r} - \frac{(R' - R) S_p \mu y_1}{K_r}} = d_2$	$c = 0.5 \quad \text{and} \quad d_2 = \frac{1}{\frac{1}{R S_p} + \frac{1}{K_r}}$
6-7	$P_o^{\max} - P_o = 2 A_{lr} \cdot \frac{\beta_1 \cdot (y_o^{\max} - y_o)}{z \cdot 2 y_{1R}}$	$\beta_1 = \frac{\tanh(z) + \lambda_R}{1 + \lambda_R \cdot \tanh(z)} \quad \text{with} \quad \lambda_R = \frac{R_{reb} \cdot S_p}{K_r \cdot z}$
7-8	$\frac{y_o^{\max} - y_o}{2 y_{1R}} = \left(1 - \frac{\beta_2'^2}{2}\right) + \frac{k_R}{2} \left(\frac{P_o^{\max} - P_o}{2 A_{lr}}\right)^2$	$\beta_2'^2 - \tanh^{-1}(\beta_2'^2) = \left(\frac{P_o^{\max} - P_o}{2 A_{lr}} - 1\right) \cdot z - \tanh^{-1}(\lambda_R)$
8-9	$\frac{(P_o^{\max} - P_o) - 2 A_{lr} - R_{reb} S_p \cdot 2 y_{1R}}{(y_o^{\max} - y_o) - c \cdot \frac{2 A_{lr}}{K_r} - \frac{R_{reb} S_p \cdot 2 y_{1R}}{K_r}} = d_{2R}$	$c = 0.5 \quad \text{and} \quad d_{2R} = \frac{1}{\frac{1}{R_{reb} \cdot S_p} + \frac{1}{K_r}}$

Note: The suffixes "R" and "reb" refer to the rebound condition (see Fig. 5 and 6).

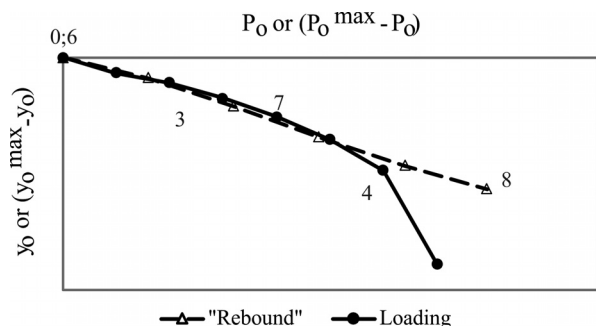


Figure 7 - An indication of homothety.

as displayed in Fig. 8. Note that μ refers to P_h at the beginning of the loading stage ($P_o = 0$).

For heterogeneous soils the auxiliary equations for ranges 0-3 and 6-7 are more complex but the basic equations are still valid; for the ranges 3-4 and 7-8, both equations, basic and auxiliaries are different. The equations of ranges 4-5 and 8-9 continue to be valid, with an appropriate c value, the parameter of Leonards and Lovell. In all of them the homothety is preserved.

Next the notable points of the homothety will be highlighted and its properties will be presented, using Fig. 8 as a reference.

4.2.2. Properties of the notable points

a) Consider the Point 4, associated to the full mobilization of lateral friction and toe reaction up to $y_p = y_3 = \mu y_1$. It has the coordinates:

$$P_{o4} = \mu A_{lr} + R' S_p \mu y_1 \tag{21}$$

$$y_{o4} = \mu y_1 + c \cdot \frac{\mu A_{lr}}{K_r} + \frac{R' S_p \mu y_1}{K_r} \tag{22}$$

b) Consider now Point P_s with the coordinates:

$$P_{os} = \mu A_{lr} \tag{23}$$

$$y_{os} = c \cdot \frac{\mu A_{lr}}{K_r} \tag{24}$$

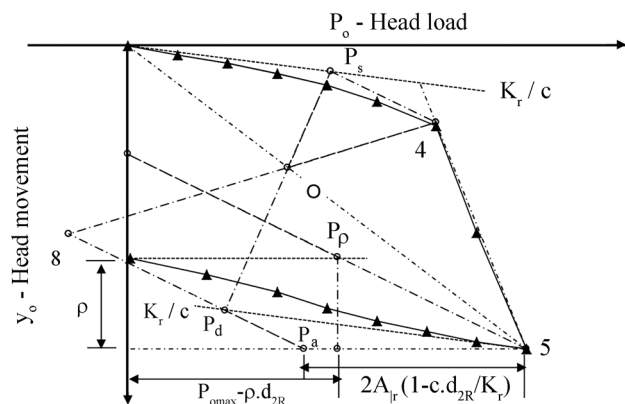


Figure 8 - Notable points of the homothety.

It is located on the line through the origin and having a slope K_r/c .

The line connecting Points 4 and P_s has a slope d_{2R} of Eq. 9, as shown below:

$$\frac{P_{o4} - P_{os}}{y_{o4} - y_{os}} = \frac{(\mu A_{lr} + R' S_p \mu y_1) - \mu A_{lr}}{\left(\mu y_1 + \frac{\mu A_{lr}}{K_r/c} + \frac{R' S_p \mu y_1}{K_r} \right) - \frac{\mu A_{lr}}{K_r/c}} = \tag{25}$$

$$\frac{R' S_p \mu y_1}{\mu y_1 + \frac{R' S_p \mu y_1}{K_r}} = \frac{1}{\frac{1}{R' S_p} + \frac{1}{K_r}} = d_{2R}$$

because $R_{reb} = R'$, expression 20.

c) The Point $P_{d'}$ homothetic to P_s , has coordinates:

$$P_{o d'} - P_{od} = 2A_{lr} \tag{26}$$

$$y_{o d'} - y_{od} = \frac{2A_{lr}}{\left(\frac{K_r}{c} \right)} \tag{27}$$

It lies on the line passing through the point of maximum load ($P_o^{\max}; y_o^{\max}$) with a slope K_r/c .

d) The Point 8, homothetic to Point 4, has coordinates:

$$P_o^{\max} - P_{o8} = 2A_{lr} + R' S_p \cdot 2y_1 \tag{28}$$

$$y_o^{\max} - y_{o8} = 2y_1 + c \cdot \frac{2A_{lr}}{K_r} + \frac{R' S_p \cdot 2y_1}{K_r} \tag{29}$$

again because $R_{reb} = R'$, expression 20. The line connecting the Points P_d and 8 has an inclination d_{2R} , as can be proved similarly to expression 25. Moreover, this line intercepts the horizontal line passing through the point of maximum load ($P_o^{\max}; y_o^{\max}$) as indicated by the point P_a in Fig. 8. It is easy to prove that the abscissa of this point is given by:

$$P_o^{\max} - P_a = 2A_{lr} \cdot \left(1 - \frac{d_{2R}}{K_r/c} \right) \tag{30}$$

e) The point P_p of ordinate $y_o^{\max} - \rho$ and belonging to the line passing through the point of maximum load ($P_o^{\max}; y_o^{\max}$) with a slope d_{2R} , that is, parallel to the lines P_s-4 and P_d-8 (see Fig. 8), has an abscissa equals to $P_o^{\max} - \rho \cdot d_{2R}$, as it can be proved easily. This allows the estimation of μ_{reb} at the end of unloading or rebound ($P_o = 0$) using Eq. 17, i.e.:

$$\mu_{reb} = \frac{P_o^{\max} - \rho \cdot d_{2R}}{A_{lr} \left(1 - c \cdot \frac{d_{2R}}{K_r} \right)} \tag{31-a}$$

4.2.3. Another way to determine μ_{reb} at the end of unloading (rebound)

In the mentioned parametric study, Massad (2001) showed that for soils with $f_u = \text{const}$ along depth, *i.e.* $c = 0.5$, the following relations hold at the end of rebound ($P_o = 0$):

$$\mu_{reb} = 2 - \frac{2-Q}{1 + \frac{2 \cdot (1-c) \cdot k \cdot (r-1)}{2-Q}} \leq r \text{ for } Q < 2 \quad (31-b)$$

If $Q \geq 2$, $\mu_{reb} = 2$

where Q is given by Eq. 18 and:

$$r = \frac{P_o^{\max}}{A_{lr}} \quad (31-c)$$

It can be proved that Eq. 31-b is also valid for $c = 2/3$ and it is postulated its soundness for any other c value in the range 0.4 to 0.8. Figure 9 is a plot of Eq. 31-b.

5. Practical Applications

To illustrate the potentiality of the homothetic model, application will be made using experimental field data related to the driven piles presented in Table 2. The piles were arranged in groups, according to the type of test, *i.e.*: I)

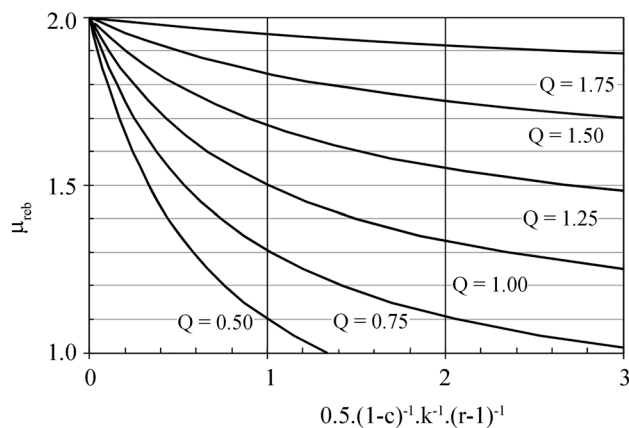
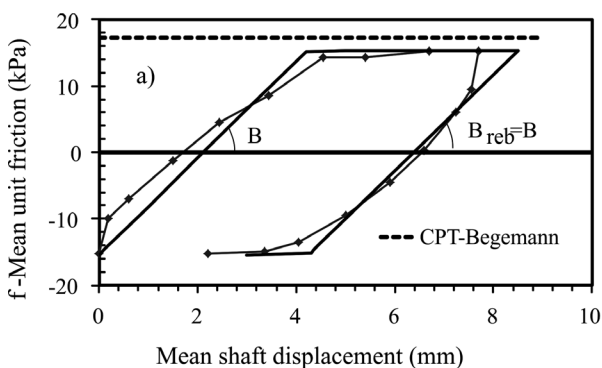


Figure 9 - μ_{reb} from Eq. 31-b as a function of c , k , r and Q .



Static Cyclic Loading Test and Dynamic Loading Tests with Increasing Blow Energy; II) Static Loading Tests; and III) Dynamic Loading Tests with Single Blow Energy.

The application of the homothetic model assumes as initial known parameters:

- a) the pile structural stiffness (K_r), given by Eq. 3;
- b) the maximum applied load ($P_{o\max}$);

5.1. Piles of Group I

It is assumed that for the piles of Group I the Van Weele's Equation (expression 17) is available, which means also that the shaft load was fully mobilized in the last cycles. It allows the determination of $\mu_{reb} \cdot A_{lr}$ and d_{2R} directly and of $R' \cdot Sp/K_r$ using Eqs. 9 and 20. For the Van Weele pile, Fig. 3 and Eq. 17 with $c = 0.75$, estimated with the Begemann CPT, led to $d_{2R} = 148$ and $\mu_{reb} \cdot A_{lr} = 621$ kN.

Next, it will be assumed that $\mu = \mu_{reb} = 2$, *i.e.*, the value of μ is the same, for the beginning of loading ($P_o = 0$) and at the end of unloading (rebound) ($P_o = 0$). This hypothesis may be validated using Fig. 10, built up with the results of measurements with electric extensometers installed in the Amsterdam Pile by Van Weele (1957). Moreover, the results of the Dutch cone (CPT) fitted with a skin-friction jacket developed by Begemann revealed a total shaft load at failure (A_{lr}) of 85 kN, which implies an average $f_u = 17.2$ kPa, a value very close to the one indicated in Fig. 10-a. The use of $\mu = 2$ in these conditions is not new: Massad (2001) and Fellenius (2001) did the same, in different ways, to estimate the true shaft resistance of a pile influenced by residual loads.

In this way, besides P_s and its homothetic Point P_d , the coordinates of Point 4 are also known (see Fig. 8): it is the interception of line 4-5 with line P_s -4, that has a known slope d_{2R} , as shown by Eq. 25. Using the homothetic relation, Point 8 is also known.

Applying Eqs. 15 and 16, with $c = 0.75$, the following values may be obtained: $C_2 = 3.41$ and $C_3 = 3.71$. Then $\rho = C_2 + C_3 = 7.11$ and $Q = C_3 / (\mu \cdot y_1) = 2$. And finally, from Eq. 31-a results $\mu_{reb} = 2$, validating the assumed initial

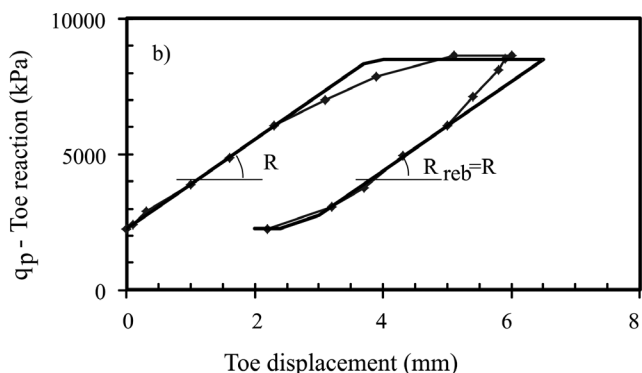


Figure 10 - Van Weele's pile: f and q_p caused by loading up to 1500 kN and unloading.

Table 2 - General information of the piles.

Group	Type of test	Local	Designation	Type of pile	Shaft soil (SPT)	D_s or L (cm)	D_i (cm)	h (m)	K_r (*) (kN/mm)	Source		
I	Static Cyclic Loading Test	Amsterdam, Netherland	VW	Reinforced Concrete Solid Pile	Alternated layers of soft clay and sand, with peat	38x38	-	14.05	394	Van Weele (1957)		
	Dynamic Loading Tests with Increasing Blow Energy	São Paulo	201	Reinforced Concrete Solid Pile	? (10)	23	-	8.80	125	Aoki (1989)		
			BR-1	Reinforced Concrete Pipe Pile	Porous Clay (3-4)	50	32	11.1	308	Machado (1995); Massad (2001)		
			BR-2			60	40	11.0	373			
			BR-3			50	32	11.0	275			
BR-4			50	32	11.0	275						
		São Paulo City (USP)	PRE-2 D	Reinforced Concrete Solid Pile	Sandy Silt (Residual Soil) (16)	50	32	8.7	333	Niyama and Aoki (1991)		
II	Static Loading Tests	Santos Plain (Cosipa)	6	Steel Pipe Pile	SFL (0-1)	35.6	33.7	31.5	69	Rottmann (1985); Ghilardi <i>et al.</i> (2006)		
			9						33.9	64		
			10							26.0	83	
			13	Steel Pipe Pile Fille with concrete	SFL and AT Clays (3-5)	46	-	45.0	134	Massad (1995)		
			P	Steel Pipe Pile	Clay and Sand (17 to 19)	34.3	32.3	20.6	107	-		
III	Dynamic Loading Tests with Single Blow	Santos Plain (Vicente de Carvalho)	PRE-2 S	Reinforced Concrete Solid Pile	Sandy Silt (Residual Soil) (16)	50	32	8.7	333	Niyama and Aoki (1991)		
			K11	Reinforced Concrete Pipe Pile, coated with bitumen (23 m) (**)	Layers of clay with sand lenses (1-6), overlying sands with gravel (10-20) (**)	80	50	34.6	223	-		
			O11	Reinforced Concrete Pipe Pile, coated with bitumen (30 m) (***)	Layers of clay with sand lenses (1-6), overlying sands with gravel and residual soil (10-20) (***)	80	50	42.4	212	-		

Notes: See attached list of symbols. (*) For composite sections (for instance, concrete and steel), area-length weighted average is used. (**) 10 m Open Steel pipe at the toe, with section reducer ($\phi = 20$ cm). (***) 10 m Open Steel pipe at the toe.

value. The value of ρ may also be found using Van Welle Equation.

A graphical construction may also be done, as illustrated in Fig. 8. The values of the expressions $2A_{lr} \cdot (1 - c \cdot d_{2R} / K_r)$ and $P_o^{\max} - \rho \cdot d_{2r}$ may be determined and so that of μ_{reb} by means of Eq. (31-a). For the Amsterdam pile one can get $\mu_{reb} = 446 / [(1500 - 1054) / 2] = 2$, confirming again the assumption made at the start.

The results of these computations are summed up on Table 3 and presented in Figs. 11-a and 11-b. Although

there is no coincidence between the two curves in Fig. 11-a, a close similarity exists between them. Figure 11-b shows that the homothety does occur, with the definition of its center (Point O).

The same procedure was used for the other piles of Group I. The Van Weele's Equation could be set for all of them, as displayed on Fig. 12 and in Table 3, which allow a rigorous determination of μA_{lr} and d_{2r} . In all of these cases the value of c was estimated using the SPT and its relation with f_u of the soil layers. Table 3 and Figs. 13 to 18 display

Table 3 - Results of the analysis of Group I.

Data	Parameter	Pile						
		Van Weele	201	BR-1	BR-2	BR-3	BR-4	Pre-2 dinamic
Input	μ (load)	2.0	2.0	2.0	2.0	2.0	2.0	2.0
	K_r (kN/mm)	394	125	308	373	275	275	333
	c	0.75	0.50	0.55	0.55	0.55	0.55	0.50
	P_o^{\max} (kN)	1500	930	2080	2640	1850	1870	3470
	Van Weele's Equation	$446 + 148\rho$	$550 + 40\rho$	$386 + 173\rho$	$591 + 225\rho$	$521 + 118\rho$	$681 + 115\rho$	$1015 + 248\rho$
	Eq. of line 4-5 $P_o = d_1 + d_2 \cdot y_o$	-	$695 + 14y_o$	$693 + 105y_o$	$1186 + 74y_o$	$787 + 55y_o$	$1086 + 50y_o$	$2314 + 44y_o$
Output	ρ (mm)	7.2	9.5	9.8	9.1	11.1	10.2	9.9
	μA_{lr} (kN)	621	655	559	884	682	884	1617
	μy_1 (mm)	3.70	2.01	1.55	1.05	1.63	2.60	1.01
	k	0.4	2.6	1.2	2.3	1.5	1.2	4.8
	P_{o4} (kN)	1482	773	1172	1478	1019	1398	2594
	y_{o4} (mm)	7.0	5.6	4.5	3.9	4.2	6.2	6.4
	$R \cdot S_p$ (kN/mm)	237	15.8	160.2	92.3	68.8	61.1	50.7
	$R' \cdot S_p$ (kN/mm)	237	59	395	567	207	198	972
	μ_{reb}	2.0	2.0	2.0	2.0	2.0	2.0	2.0
	C_2 (mm)	3.4	4.8	5.9	6.0	5.6	5.3	8.0
	C_3 (mm)	3.8	4.7	3.9	3.1	5.5	4.9	1.9
	Q	2.0	4.7	4.9	5.9	6.8	3.8	3.8

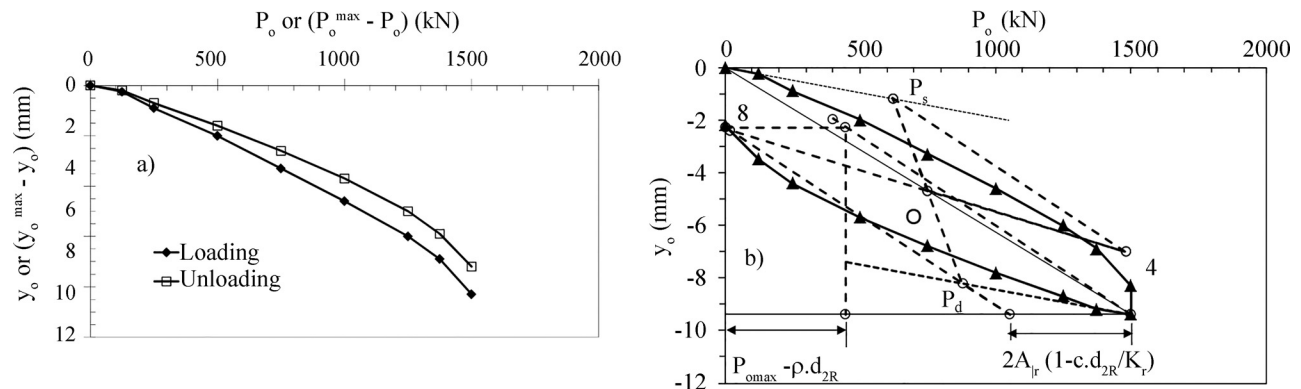


Figure 11 - Van Weele's Pile: load-movement curves, loading up to 1500 kN and unloading.

the results obtained. Note that $\mu = \mu_{reb} = 2$ for all these piles. The values of $R' \cdot S_p$ and $R \cdot S_p$ were found using, respectively, the Eq. 9 and the equation of line 4-5 (see Tables 1 and 3).

Table 4 shows that the values of f_u inferred by this analysis are consistent with those provided by the Brazilian Method of Décourt-Quaresma (1978), based on SPT values. The closeness of the assessments is remarkable.

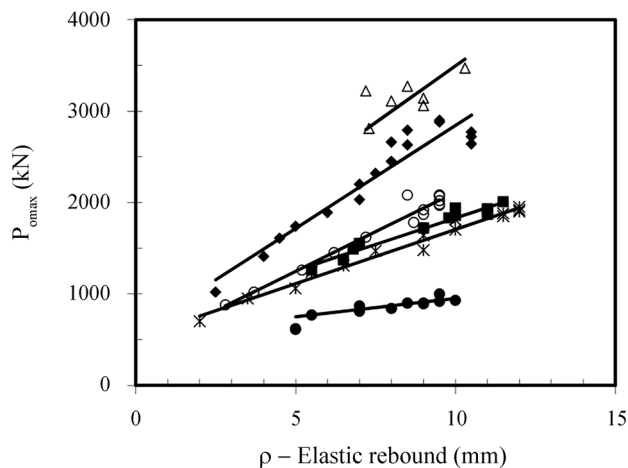


Figure 12 - Van Weele's Equation for piles of Group I.

5.2. Piles of Group II

The piles of Group II were tested at some time after driving. The post driving residual forces may decrease in value due to creep and stress relaxation or to load history, although it is difficult to know to what extent. Rieke & Crowser (1987) suggested that 12 to 72 h are not sufficient to change the residual forces. It is worth mentioning, in this context, that the installation of additional piles may lift the

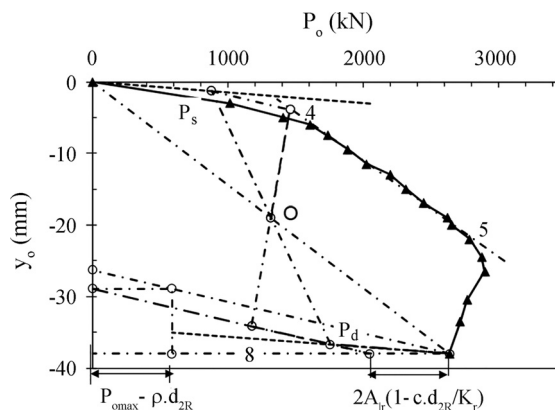


Figure 15 - Pile BR 2 - Group I.

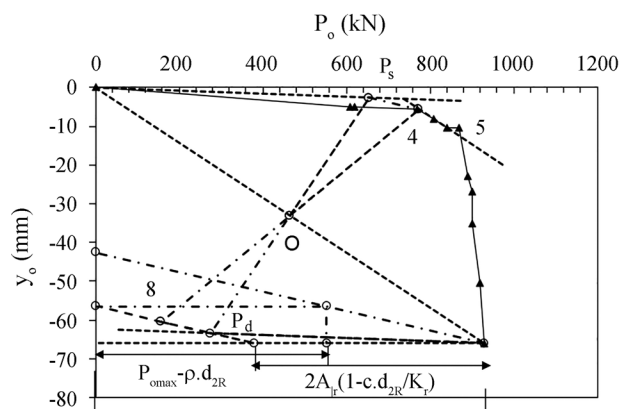


Figure 13 - Pile 201 - Group I.

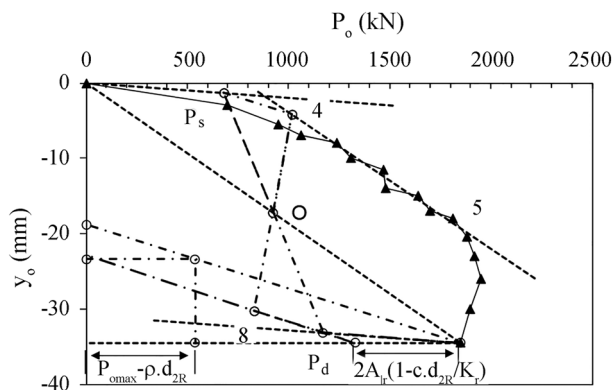


Figure 16 - Pile BR 3 - Group I.

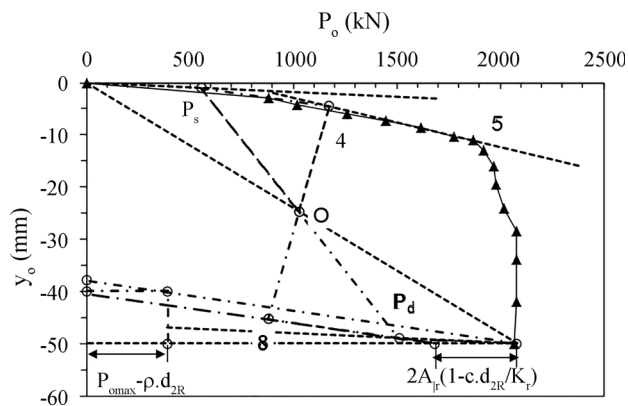


Figure 14 - Pile BR 1 - Group I.

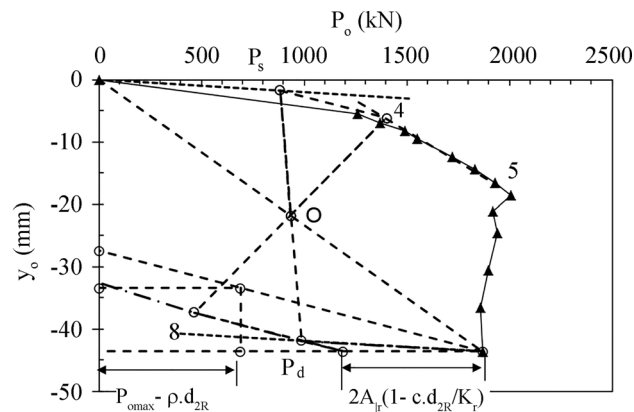


Figure 17 - Pile BR 4 - Group I.

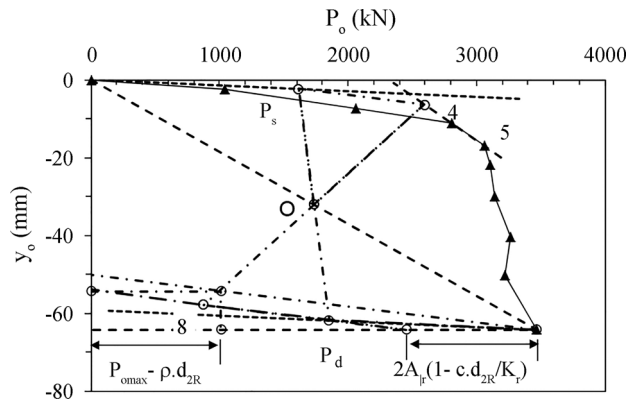


Figure 18 - Pile PRE 2 D – Group I.

piles already in position, decreasing their residual forces (Cooke *et al.*, 1979).

For the Static Loading Tests of Group II, besides the initial parameters listed above, *i.e.* K_r and P_{omax} , it is supposed to know:

- a) the elastic rebound (ρ) at pile head; and
- b) the coordinates of Point 4 ($P_{o4}; y_{o4}$);
- c) the equation of the straight line 4-5, *i.e.*, $P_o = d_1 + d_2 y_o$; and
- d) the parameter d_{2R} .

To help determining Points 4 and 5 a plot of y_o as a function of $(P_o)^2$ may be drawn, as illustrated in Fig. 19 for 2 piles of Group II. For long piles, this relation turns to be a straight line in the range 3-4, because, as observed above, the curve $P_o - y_o$ approaches a parabola.

As a consequence, Point P_s may be set as the intersection of the line passing through Point 4 with a slope d_{2R} , and the line passing through the origin with a slope K_r/c (Fig. 8).

Most of the piles of Group II were installed in Santos Plain (Table 2), comprising two different soil layers, fluvial-marine SFL clay overlying sandy silts (residual soils form Gneiss). For this soil profile, local experience reveals a value of c around 0.65. Using the Leonards and Lovell's Nomograms or Fellenius Equation the values of the ratio between f_u of the first layer and f_u of the second layer were found, as indicated on Table 5. The case of Cosipa 10 was an exception, because the residual soil layer was missing: the toe of the pile was in contact with the rock and a value of $c = 0.50$ was taken. Finally, for the other 2 piles from São Paulo City (see Table 2) the soil was supposed to be homogeneous, with $c = 0.5$.

The calculation is iterative in μ (in the beginning of loading). Therefore, a value of μ between 1 and 2 is adopted initially.

In this way, the following parameters may be determined, in sequence:

- i) $A_{lr} = \mu A_{lr} / \mu$ because μA_{lr} is the abscissa of Point P_s (Eq. 23);
- ii) soil toe stiffness $R.S_p$, computed by the equation $R.S_p = (1/d_2 - 1/K_r)^{-1}$;
- iii) $R'.S_p = R_{reb}.S_p$ using the known value of d_{2r} and Eq. 9;
- iv) $\mu_{reb} A_{lr}$ using expression 31-a;
- v) Q determined iteratively by means of Eqs. 15, 16, 18 and either Eq. 31-a or Fig. 9 and then the values of μ_{reb} , C_2 and C_3 ; and
- vi) $A_{lr} = \mu_{reb} A_{lr} / \mu_{reb}$.

Step *i* is compared with step *vi*. If the resulted A_{lr} values are different, another interaction in μ is done until convergence is achieved.

Table 4 - Comparison between f_u assessments.

Piles of group I	SPT average (Shaft)	f_u (Décourt-Quaresma)	f_u (Present analysis)
201	10.0	43	54
BR-1 to BR-4	3.8	23	20
PRE-2	16.0	63	59

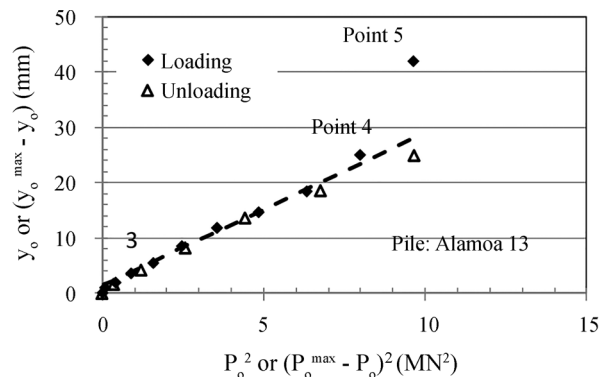
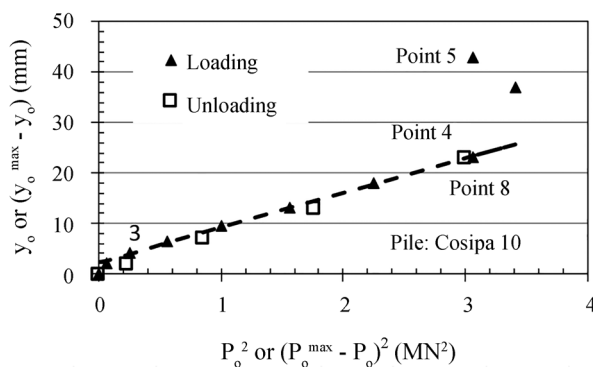


Figure 19 - Illustrations on the determination of point 4.

Table 5 - Values of f_u inferred from the analysis, supposing $c = 0.65$ – Piles of Group II.

Local	Pile	Shaft	Toe	h (m)	h_1 (m)	h_1/h	$f_s(1)/f_s(2)$	$f_u(1)$ (kPa)	$f_u(2)$ (kPa)
Santos Plain	Cosipa-6	SFL Clay (SPT \cong 0)	Sandy Silt (SPT = 15 to 35) (Residual Soil)	31.5	24.0	0.76	0.25	17	69
	Cosipa-9	SFL Clay (SPT \cong 0)	Sandy Silt (SPT = 15 to 35) (Residual Soil)	33.9	28.0	0.83	0.28	15	53
	Cosipa-10	SFL Clay (SPT \cong 0)	Soft Rock (Gnaiss)	26.0	23.3	0.90	1.00	15	-
	Alamoia 13	SFL (SPT \cong 0)+ AT (SPT \cong 3)	Sand (SPT = 55)	45.0	30.0	0.67	0.30	14	47

Legend: (1) SFL clay layer. (2) Residual Soil (Cosipa) and AT (Alamoia). h_1 : width of soft SFL Clay.

- Reporting to Fig. 8, a graphical solution is presented for the piles of Group II. It consists of the following steps:
- i) plotting Point P_s as the intersection of the line passing through Point 4 with a slope d_{2R} , and the line passing through the origin with a slope K_r/c ;
 - ii) choosing an arbitrary Point O as the center of homothety on the line that connects the origin with the point of maximum load ($P_o^{max}; y_o^{max}$);
 - iii) plotting Point P_d as the intersection of the line passing through Points P_s and O and the line drawn from the point of maximum load ($P_o^{max}; y_o^{max}$) with a slope K_r/c . Therefore, the ratio of homothety $\mu/2$, the values of μ (at the start of loading) and A_p are determined; Point 8 is easily plotted;
 - iv) projecting the point of coordinates $P_o = 0$ and $y_o = y_o^{max} - \rho$ in the line passing through the point of maximum load (P_o^{max}) and is parallel to the line P_s-4 . In this way, Point P_ρ is established and the value of $P_o^{max} - \rho.d_{2r}$ is settled;
 - v) drawing the line P_d-8 , that is parallel to the line P_s-4 and intercepts the horizontal line through the point of maximum load ($P_o^{max}; y_o^{max}$) in point P_a and so coming to the value of $2A_{pr}(1 - c.d_2/K_r)$ and of μ_{reb} using Eq. 31-a;
 - vi) determining Q iteratively by means of Eqs. 15, 16, 18 and either Eq. 31-a and then the values of μ_{reb} , C_2 and C_3 ; and
 - vii) comparing the values of μ_{reb} of steps v and vi and carrying out another interaction in μ , changing the position of Point O , up to convergence.

Application of this procedure was done for the piles of Group II, indicated in Table 2. The results are presented in Table 6 and in Figs. 20 to 25.

For the cases of Cosipa 9 and 10 it was necessary to correct the curves of the rebound, as illustrated in Figs. 21-a and 22-a. This shows the need to get the unloading curve with the same care required for the loading, which does not always happen in practice. Table 5 shows values of f_u of layers 1 and 2 for these cases plus Cosipa 6 and Alamoia-13. For the SFL clays in the Cosipa Area the values of $f_u(1)$ averages 15, agreeing with previous experience (Massad, 2009).

For the pile of Penha there was also a need to correct the curve of the rebound, as illustrated in Fig. 24-a. In this case, the toe reached the maximum resistance $q_u = P_h/S_p$ and $R' = R \cong 0!$ This means that resilience is controlled only by the friction reaction. The value of $f_u = 75$ kPa, derived from the data of Tables 2 and 6, coincides practically with the assessment by the already mentioned Décourt-Quaresma Method, *i.e.*, $f_u = 10.(SPT/3 + 1) = 10.(18/3 + 1) = 70$ kPa!

Figures 18 and 25 and Tables 3 and 6 allow comparing the static and dynamic tests on PRE-2 Pile (USP). It should be noted initially that it was necessary to correct the curve of the “rebound” of the Static Load Test, as shown in

Table 6 - Results of the analysis of Group II.

Data	Parameter	Pile					
		Cosipa-6	Cosipa-9	Cosipa-10	Alamoia 13	Penha P	Pre-2 static
Input	μ_{load}	1.4	1.9	2.0	1.6	1.8	2.0
	K_r (kN/mm)	69	64	83	134	107	333
	P_{omax} (kN)	2000	1860	1750	3104	3000	3200
	ρ (mm)	25.5	26.5	23.0	25.0	16.8	8.8
	P_{o4} (kN)	1547	1740	1750	2827	3000	2611
	y_{o4} (mm)	21.7	25.1	23.0	25.0	18.6	6.5
	d_{2R} (kN/mm)	10.3	20.8	50.1	16.2	0.0	247.3
	Eq. of line 4-5 $P_o = d_1 + d_2 \cdot y_o$	$1388+7.3y_o$	$1229+20.8y_o$	1750	$2421+16.2y_o$	3000	$2398+33.1y_o$
	c	0.65	0.65	0.50	0.65	0.50	0.50
Output	μA_{tr} (kN)	1466	1544	857	2629	3000	1596
	$R \cdot S_p$ (kN/mm)	8.2	30.9	0.0	18.5	0.0	36.8
	$R' \cdot S_p$ (kN/mm)	12.1	30.8	126.4	18.4	0.0	960.8
	μy_1 (mm)	7.00	6.4	7.1	10.8	4.6	1.1
	μ_{reb}	1.76	2.00	2.00	1.78	1.80	2.04
	k	3.2	3.8	1.5	1.8	6.1	4.5
	C_2 (mm)	19.2	20.0	15.9	15.51	14.0	7.2
	C_3 (mm)	6.3	6.5	7.1	9.49	2.8	1.6
	Q	1.3	1.9	2.0	1.41	1.1	3.1

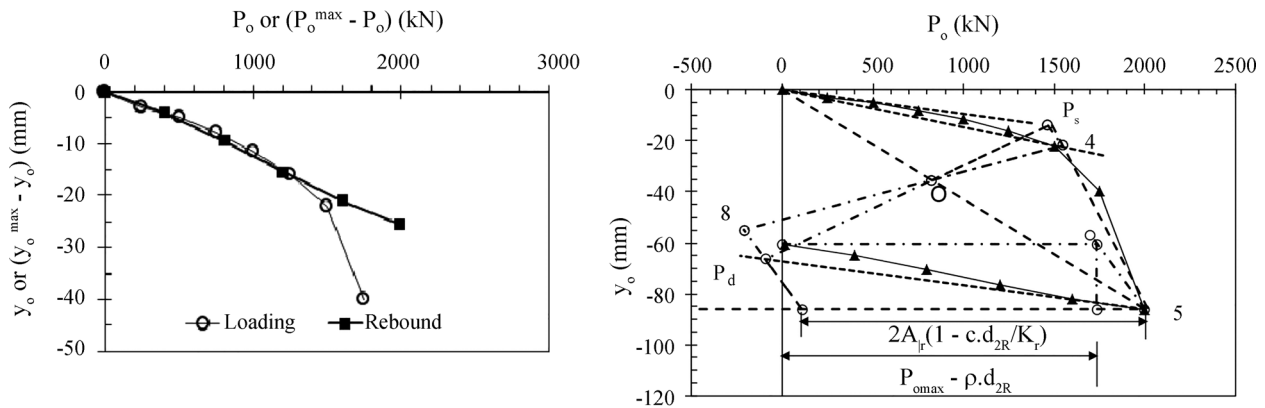


Figure 20 - Pile COSIPA 6 – Group II. Static loading tests.

Figs. 25-a, in order to “adjust” the value of the elastic rebound (ρ), an estimate based on the Van Weele’s Equation indicated in Table 3, related to the Dynamic Load Test in the same pile. Moreover, the values of μA_{tr} and d_{2R} adopted for Static Load Test were the same of the Dynamic Load Test. It can be seen that the results were identical. Niyama & Aoki (1991) had already arrived to the same conclusion, in another context.

5.3. Piles of Group III

For the Dynamic Loading Tests with a Single Blow record (Group III), it is assumed that μ (at the beginning of loading) = μ_{reb} (at the end of rebound) = 2, $B = B_{reb}$ and $R = R' = R_{reb}$ (Eqs. 20). As a matter of fact, Eqs. 20 correspond to a basic assumption of the Smith Wave Equation Model, as has been described in papers and manuals, for example, GRL (1998) and Rausche (2002). Another assump-

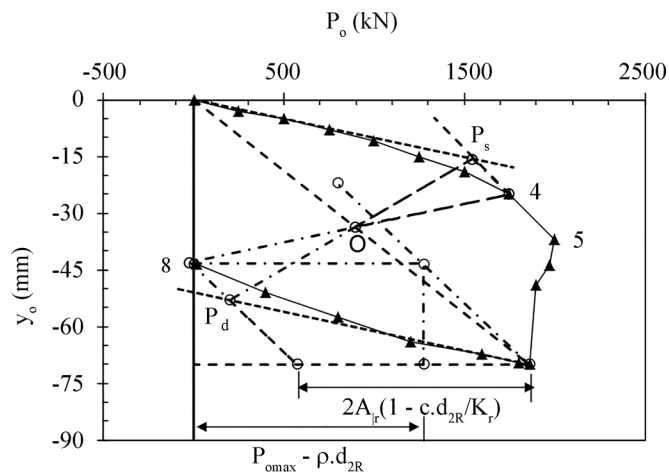
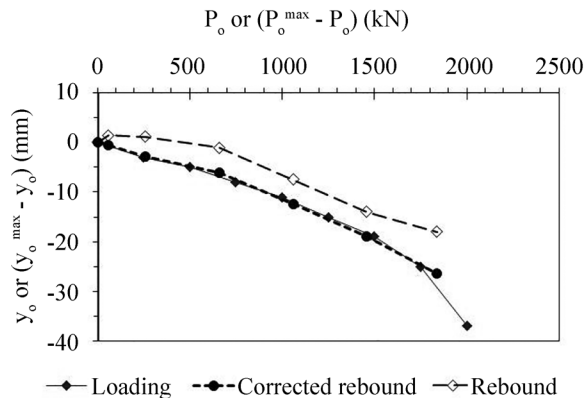


Figure 21 - Pile COSIPA 9 – Group II. Static loading tests.

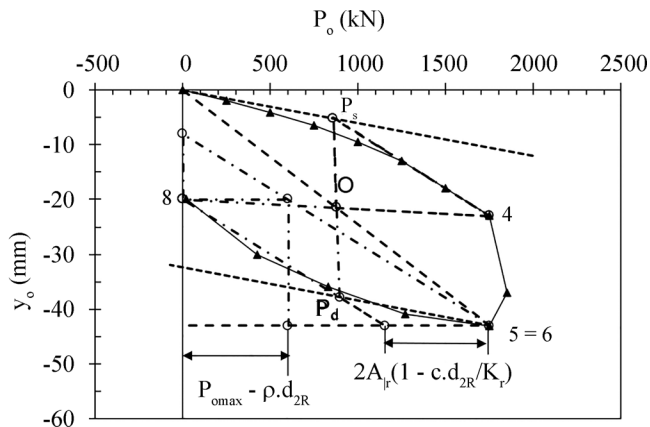
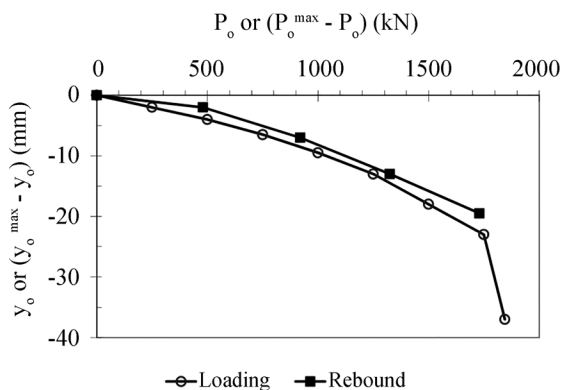


Figure 22 - Pile COSIPA 10 – Group II. Static loading tests.

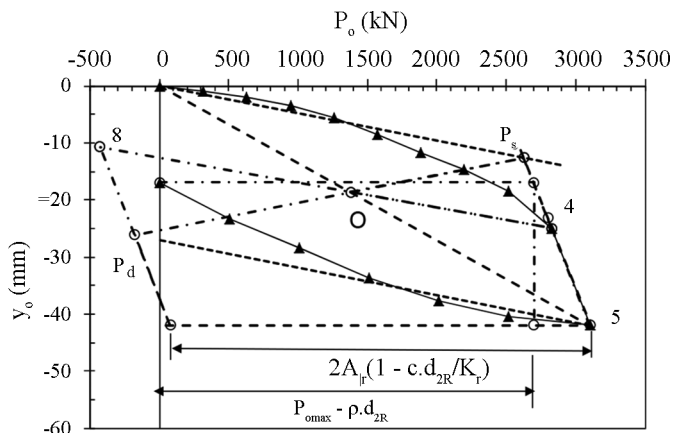
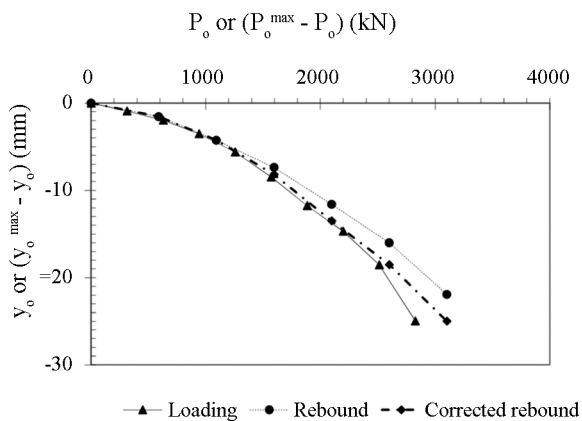


Figure 23 - Pile Alamoia 13– Group II. Static loading tests.

tion is that the shaft load at failure (A_r) has been fully mobilized.

The following initial parameters are supposed to be known from CAPWAP (Case Pile Wave Analysis Program):

- i) P_o^{max} ; y_o^{max} ; K_r and μA_r and, therefore, the coordinates of Point P_s , Eqs. 23 and 24;
- ii) $R'Sp$, given by:

$$R' \cdot S_p = \frac{\text{Toe Load (PDA)}}{\text{Toe Quake}} \quad (\text{Toe Quake} = y_2) \quad (32)$$

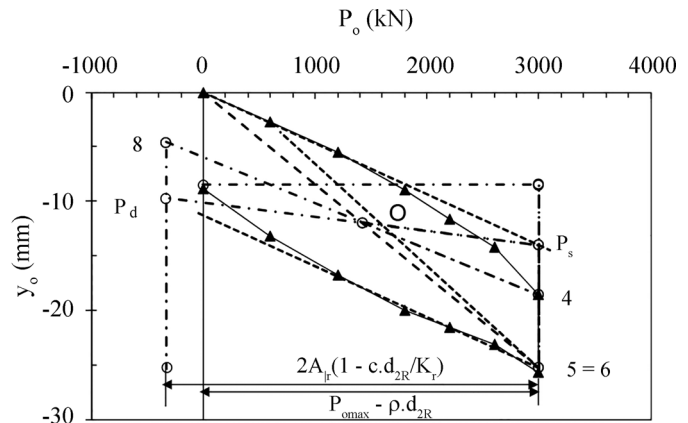
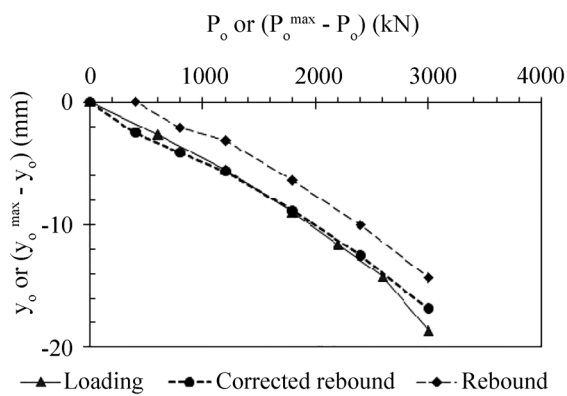


Figure 24 - Pile P (Penha) – Group II. Static loading tests.

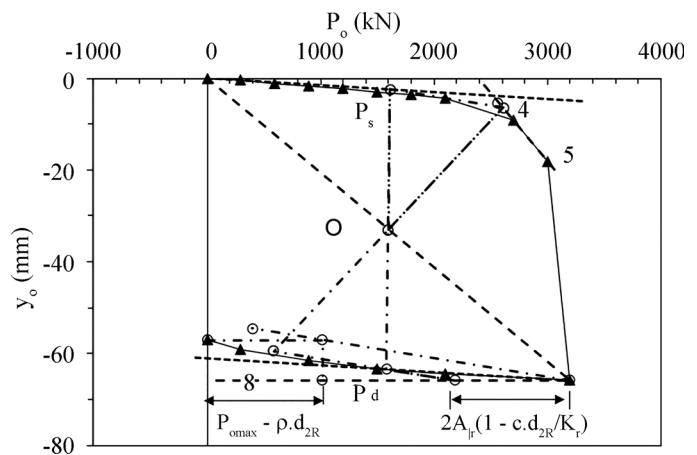
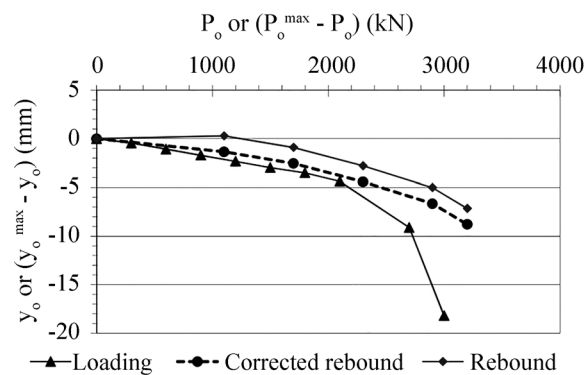


Figure 25 - Pile PRE 2 S (USP) – Group II. Static loading tests.

- iii) μ_y , taken equal to the average shaft quake; and
- iv) the distribution of the load mobilized along the shaft, which allows the estimation of the Leonards and Lovell's parameter c .

Next, computations are carried out to determine:

- a) P_{o4} and y_{o4} by means of Eqs. 21 and 22;
- b) d_{2R} , given by Eq. 9 ($R' = R_{reb}$);
- c) ρ (elastic rebound) using Eq. 17 (Van Weele's Equation); wanting, the parameters C_2 and C_3 may be estimated by means of Eqs. 15 and 16. This step allows to overcome the difficulty of estimating the set (s) using the CAPWAP (Uto *et al.*, 1989).

A graphical solution is at hand, because Points P_s (Eqs. 23 and 24) and P_d (Eqs. 26 and 27) are known and so the center of homothety, in this case, center of symmetry. The users of CAPWAP have familiarity with this symmetry. From Eqs. 21 and 22 Point 4 is settled and, by symmetry, Point 8.

The long piles K11 and O11 of Table 1 were also driven in Santos Plain, with the subsoil described above. The CAPWAP was applied during pile installation, 3 and

15 days later. The results are presented in Table 7 and in Figs. 26 to 32.

Comparing Figs. 26, 27 and 28 (pile K11) and 29, 30, 31 and 32 (pile O11) it is noticeable that Point 4 is moving to the right as the set up increases. That is, "the hammer did not fully mobilize the pile capacity, notably the toe capac-

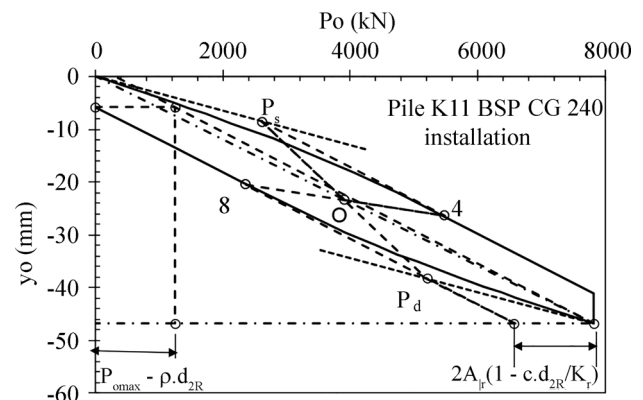


Figure 26 - Dynamic loading test.

Table 7 - Results of the analysis of Group III.

Data	Parameter	Pile K11			Pile O11			
		Installation (*)	Restrike 3 days (*)	Restrike 15 days (**)	Installation (*)	Restrike 3 days (*)	Restrike 15 days (**)	Restrike 15 days (*)
Input	μ	2.00	2.00	2.00	2.00	2.00	2.00	2.00
	μ_{reb}	2.00	2.00	2.00	2.00	2.00	2.00	2.00
	K_r (kN/mm)	223	223	223	212	212	212	212
	P_{omax} (kN)	7825	6538	6834	3882	4747	5758	6466
	μA_{lr} (kN)	2614	3627	4710	1206	2117	4832	4493
	$R'.S_p$ (kN/mm)	572.7	485.3	506.7	145.8	216.8	122.0	463.1
	μy_1 (mm)	5.00	4.80	4.30	3.80	2.85	5.50	4.46
	c	0.73	0.65	0.65	0.57	0.57	0.60	0.59
Output	P_{o4} (kN)	5478	5957	6889	1760	2735	5503	6559
	y_{o4} (mm)	26.4	25.9	27.9	9.7	11.5	22.4	26.7
	k	2.3	3.4	4.9	1.5	3.5	4.1	4.8
	d_{2R} (kN/mm)	160.3	152.6	154.6	86.4	107.2	77.4	145.4
	ρ (mm)	41.0	29.7	27.5	34.3	30.2	25.7	26.0
	s (mm)	6	0.1	5	10	10	5	4
	C_2 (mm)	31.9	23.7	23.3	15.9	18.1	18.2	21.8
	C_3 (mm)	9.1	6.0	4.2	18.4	12.1	7.6	4.2
	Q	3.6	2.5	2.0	9.7	8.5	2.8	1.9

Notes: (*) Hydraulic Hammer BSP-CG 240, (**) Hydraulic Hammer HH-JUNTTAN.

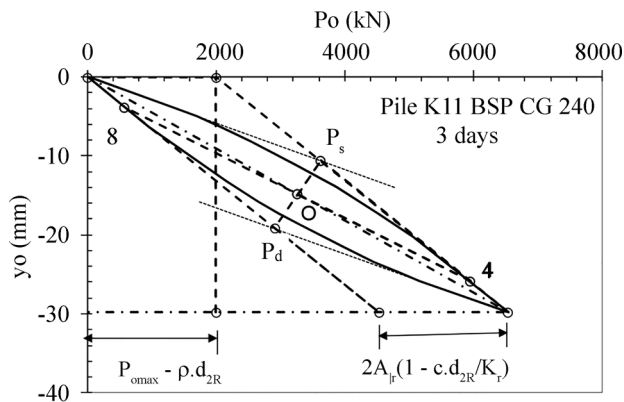


Figure 27 - Dynamic loading test.

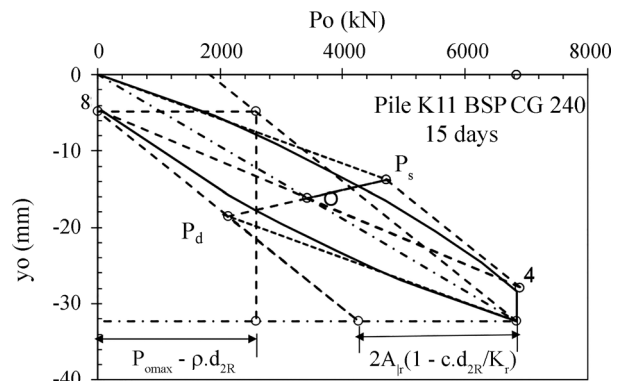


Figure 28 - Dynamic loading test.

ity”, quoting Fellenius (1998), which had arrived to this conclusion earlier, in a similar context.

This statement can be further developed in the light of the results obtained so far. In fact, considering that $\mu A_{lr} = A_{lr} + P_h$, Eq. 21 may be rewritten as:

$$P_{o4} = A_{lr} + (P_h + R'.S_p \mu y_1) \quad (33)$$

where the amount in parenthesis is the mobilized toe reaction up to Point 4. In other words, the toe reacts with the-

sidual load $P_h = A_{lr}$ (since $\mu = 2$) plus $R'.S_p \mu y_1$ along the pseudo elastic range of Fig. 5-b. Figures 33-a and b show how the two parcels of Eq. 33 vary with the time of restrike.

For both piles Fig. 33-a reveals that the total shaft friction increases with time due to set up effects. But the mobilization of the toe reaction is different. Reporting to Fig. 33-b and Table 7, for Pile K11 the toe reaction amounts 8 to 9 MPa, as the set (s) decreases from 6 to 4 mm; and for Pile O11 it increases from 2 to 9 as the set (s) varies from 10 to 4 mm.

In these cases, the hammer did mobilize the toe capacity, perhaps not fully: Ghilardi & Massad (2006) found values from static load tests ranging from 8 to 14 MPa for piles embedded in residual soils in Santos Plain. Note that the transferred energy (Fig. 34) remained almost constant for 3 and 5 days restriking of Pile K11. Figure 35 shows that the maximum displacement ($\rho + s$) reached a constant value of 30 mm, confirming that at 15 days of restriking the piles reached a firm substratum.

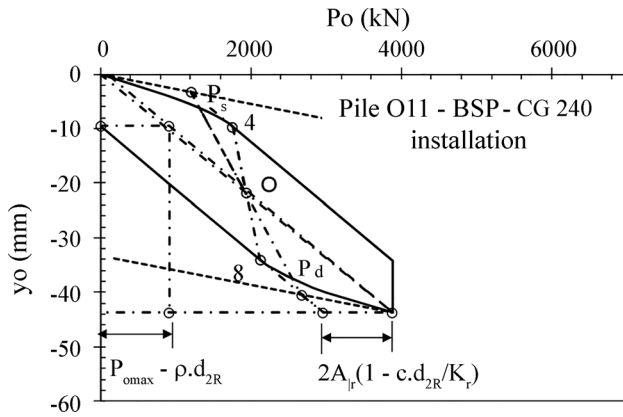


Figure 29 - Dynamic loading test.

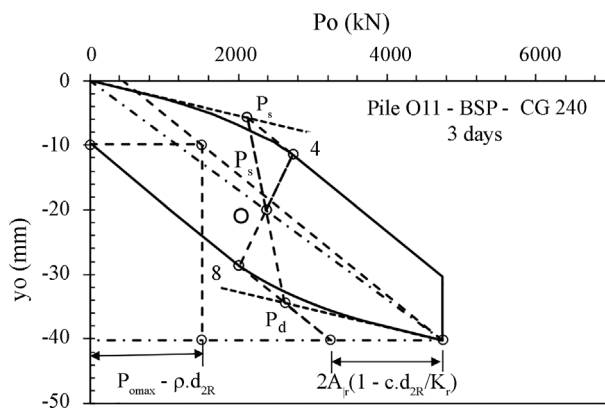


Figure 30 - Dynamic loading test.

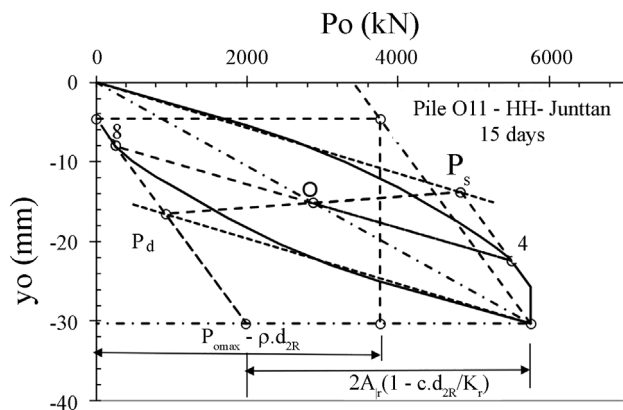


Figure 31 - Dynamic loading test.

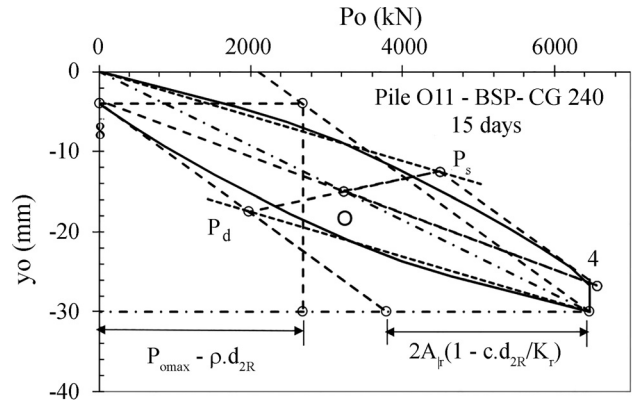


Figure 32 - Dynamic loading test.

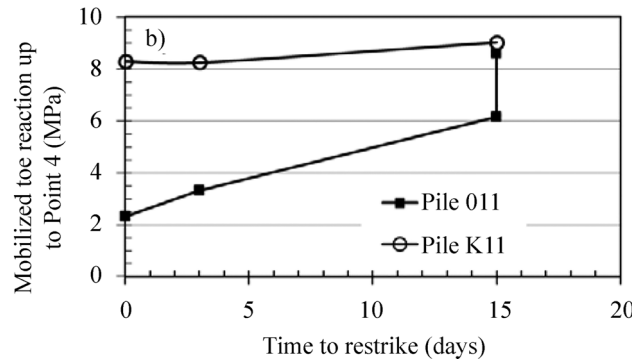
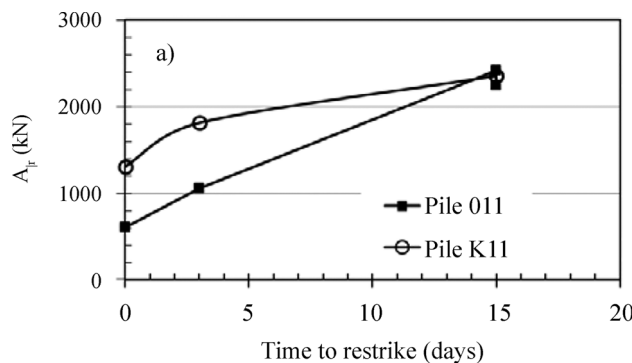


Figure 33 - Separation of loads during restriking.

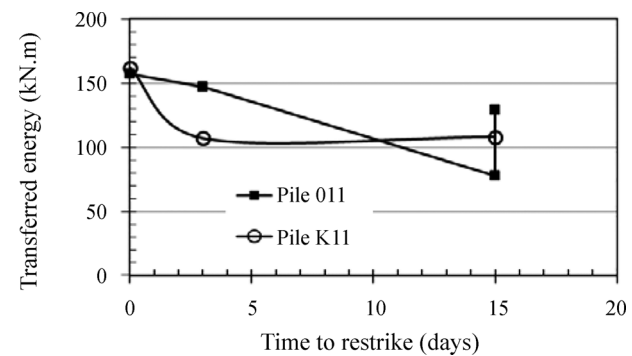


Figure 34 - Transferred energy and time to restrike.

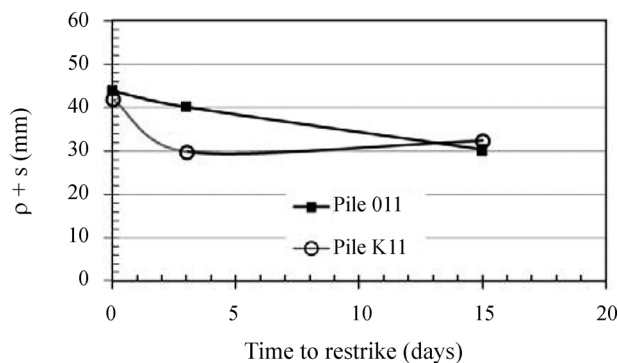


Figure 35 - Max. displacement and time to restrike

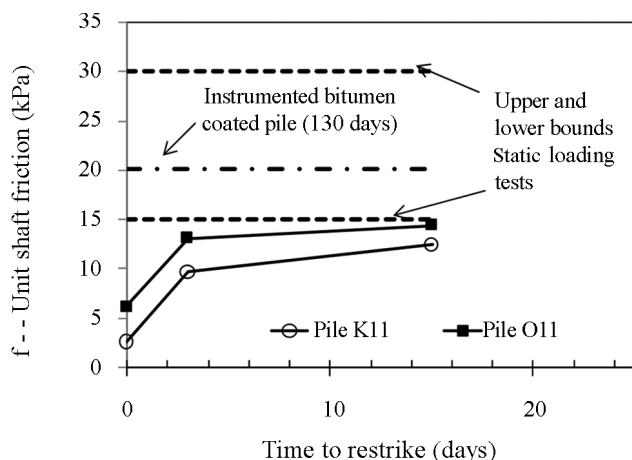


Figure 36 - Unit shaft friction and time to restrike.

Other results are shown in Table 8. The mobilized unit shaft friction (f) of the SFL clays were plotted in Fig. 36, taking $\mu = 2$. In this figure the dash-dot line represents the value obtained in an instrumented bitumen coated pile subjected to static loading test in Santos Plain, 130 days after installation. Considering that the Piles K11 and O11 were also coated with bitumen, the agreement is reasonable due to expected scatter of values. The scatter of f values in Santos Plain is shown in Fig. 36: the dashed lines represent the upper and lower bounds of the mobilized unit shaft friction (f) derived from static loading tests in piles without bitumen. These results validate the assumption made before that the shaft load at failure (A_{iv}) has been fully mobilized.

6. Conclusions

This paper showed that a resilient condition may be reached during pile driving or under static cyclic and even monotonic loading. This fact was confirmed by Van Weele's data on an instrumented precast concrete pile submitted to static cyclic loading test. Under this condition, the loading and unloading movement curves at pile head are homothetic.

Table 8 - Other results of the analysis - Piles of Group III.

Group	Local	Pile	Subsoil description	h (m)	h_1 (m)	h_1/h	c	μf (1)	μf (2)
III	Santos Plain (Vicente de Carvalho)	K11 (Installation) BSP-CG-240	Up to 19 m: SFL Clay 19 to 34.6: Alternate layers of Sand and Clay Toe embedment: Sand	34.6	19	0.55	0.73	5.0	60.5
		K11 (Restrike 3 days) BSP-CG-240		34.6	19	0.55	0.65	19.3	69.4
		K11 (Restrike 15 days) HH-JUNTTAN		34.6	19	0.55	0.65	24.8	91.3
	O11	O11 (Installation) BSP-CG-240	Up to 30.4 m: SFL Clay 30.4 to 42.4 Residual silty soil from Gneiss Toe embedment: Residual silty soil from Gneiss	42.4	30.4	0.72	0.57	9.0	17.2
		O11 (Restrike 3 days) BSP-GG240		42.4	30.4	0.72	0.57	15.9	30.0
		O11 (Restrike 15 days) HH-JUNTTAN		42.4	30.4	0.72	0.60	32.1	79.0
		O11 (Restrike 15 days) BSP-CG-240	42.4	30.4	0.72	0.59	32.0	68.0	

Note: (1) SFL clay layer, (2) Alternate clay-sand layers (K11) and residual soil (O11).

The notable points of the homothety were set based on a mathematical model that incorporates, as load transfer functions, the modified Cambeftort's Relations, considers pile compressibility, the residual stresses and matches the Cambeftort parameters for loading and unloading (re-bound).

A graphical construction was developed along with a numerical procedure – the Homothetic Model - allowing determining the notable points together with significant parameters of pile-soil interaction like the unit shaft friction, the toe stiffness and resistance besides the shaft and toe shakes. In particular, the mobilization of shaft and toe plus residual loads was clarified with the concept of resilience.

The application of the Homothetic Model to several piles allowed improving the understanding of their behavior under static or driving loadings. In particular, a new procedure was developed to analyze dynamic loading tests with a single blow record, considering the residual load at the toe. Underlying this approach is the need to get the unloading curve with the same care required for the loading, which does not always happen in practice.

Acknowledgments

The author acknowledges the support given by EPUSP – Escola Politécnica of University of São Paulo and is grateful to the disposal of data by ODEBRECHT INFRAESTRUTURA and EMBRAPORT S.A.

References

- Aoki, N. (1989) A new dynamic load test concept. In: *Drivability of Piles*, Proc. 12th International Conference of Soil Mechanics and Foundation Engineering, August 13-18, Rio de Janeiro, Brazil, v. I: p. 1-13.
- Baguelin, F. & Venon, V.P. (1971) Influence de la compressibilité des pieux sur la mobilisations des efforts résistant. *Bulletin des Liaison Laboratoire des Ponts et Chaussées*. Num. Especial. Paris, Mai, p. 308.
- Cooke, R.W.; Price, G. & Tarr, K. (1979) Jacked piles in London Clay. *Géotechnique*, v. 27:1, p. 121-157.
- Décourt, L. & Quaresma, A.R. (1978) Load capacity of piles from SPT. In: *VI Brazilian Conference on Soil Mechanics and Foundation Engineering*, Rio de Janeiro, ABMS, p. 45-53 (In Portuguese).
- Fellenius, B.H. (1980) The analysis of results from routine pile load tests. *Ground Engineering*, v. 13:6, p. 19-31.
- Fellenius, B.H. (1998) Recent Advances in the Design of Piles for Axial Loads, Dragloads, Downdrag and Settlement. *ASCE and Port of NY& NJ Seminar*, p. 1-19.
- Fellenius, B.H. (2001) Determining the true distribution of load in piles. In: M.W. O'Neill, & F.C. Townsend (eds) *American Society of Civil Engineers, ASCE - International Deep Foundation Congress, Geotechnical Special Publication No. 116*, Orlando, v. 2, p. 1455-1470.
- Fellenius, B.H. (2002) *Basic of Foundation Design*. Electronic Edition, p. 106, <http://www.fellenius.net/papers.html>.
- Ghilardi, M.P. & Massad, F. (2006) Considerations about the behavior of plugged steel pipe piles in Santos Plain, Brazil. In: *Proc. XIII Brazilian Conference on Soil Mechanics and Geotechnical Engineering*, Curitiba, v. 2, p. 873-878 (In Portuguese).
- GRL, Goble Rausche Likins and Associates, Inc. (1998) *GRLWEAP, Wave Equation Analysis Program*. 4535 Renaissance Parkway, Cleveland, OH, 96 p.
- Leonards, G.A. & Lovell, D. (1979) Interpretation of Load Tests in High Capacity Driven Piles. *Behavior of Deep Foundations*, ASTM STP 670, Raymond Lundgren (ed) ASTM, p. 388-415.
- Machado, J.R.A (1995) Evaluation of the Load Capacity of Piles Based on the Elastic Rebound Measured at the End of Driving. MSc. Thesis, Escola Politécnica, São Paulo, 270 p (In Portuguese).
- Massad, F. (1995) The analysis of piles considering soil stiffness and residual stresses. In: *Proc. 10th. Pan-American Conference on Soil Mechanics and Foundation Engineering*, Guadalajara, México, v. II, p. 1199-1210.
- Massad, F. (2001) On the use of the elastic rebound to predict pile capacity. In: *Proc. 15th International Conference of Soil Mechanics and Geotechnical Engineering*, 2001, Istanbul. Balkema, London, v. 2, p. 1100-1104.
- Massad, F. (2009) *The Marine Clays of Santo Plain – Characteristics and Geotechnical Properties*. Oficina de Textos, São Paulo, 247 p. (In Portuguese).
- Niyama, S. & Aoki, N. (1991) Dynamic and Static Loading Tests in the Experimental Field of EPUSP. II Seminar on Special Foundation Engineering, S. Paulo, p. 285-293.
- Randolph, M.F. & Wroth, C.P. (1978) Analysis of deformation of vertically loaded piles. *Journal of the Geotechnical Engineering Division*, v. 104:GT12, p. 1465-1488.
- Rausche, F. (2002) Modeling of vibratory pile driving. In: *Vibratory Pile Driving and Deep Soil Compaction*. Balkema Publishers, Lisse, p. 123-131.
- Rieke, R.D. & Crowser, J.C. (1987) Interpretation of pile load test considering residual stresses. *Journal of the ASCE*, v. 113:4, p. 319-334.
- Rottmann, E. (1985) *Theoretical Predictions and Results of Pile Instrumentation as a Basis for Design*. MSc Thesis, Escola Politécnica, São Paulo, 209 p (In Portuguese).
- Uto, K.; Fuyuki, M. & Miyaji, A. (1989) Measuring cases of phenomena of pile driving using accelerometer. In: *Proc. 12th International Conference of Soil Mechanics and Foundation Engineering, Drivability of Piles*, Rio de Janeiro, Brazil, v. I, p. 83-86.
- Van Weele, A.F. (1957) A method of separating the bearing capacity of a test pile into skin-friction and point resistance. In: *Proc. 4th. International Conference of Soil*

Mechanics and Foundation Engineering, v. II, Division 3b/16, p. 76-80. London.

List of Symbols

- A_t : Total lateral (shaft) load
 $A_{t,f}$: Total lateral (shaft) load at failure
 A'_t : Average value of lateral (shaft) load
 $B; B_{reb}$: Cabefort Parameters (see Fig. 5-a)
 c : Ratio of the average value of the transferred lateral load and A_t (see Eq. 4)
 C_2 : shaft quake
 C_3 : Toe quake
 $d_2; d_{2R}$: Stiffness of the set pile-toe soil
 D : Diameter of solid pile
 D_e and D_i : Outside and inside pile diameters
 E : Modulus of elasticity of the pile
 f : Unit skin friction
 f_u : Maximum (ultimate) unit skin friction
 f_{res} : Residual unit skin friction
 G_b : Shear modulus of the soil at the pile toe
 h : Pile length embedded in soil
 h_1 : Width of upper layer of the subsoil
 k : Relative stiffness of the pile-soil (shaft)
 K_p : Pile stiffness, as a structural piece
 L : Dimension of a square pile
 P_h : Residual toe load
 P_h^{reb} : Residual toe load at the end of rebound
 P_o : Vertical load at the pile head
 P_{o4} : P_o associated to full lateral friction mobilization
 $P_s; P_d$: Notable points of Fig. 8.
 P_o^{max} or $P_{o,max}$: Maximum value of P_o
 q_p : Toe pressure
 Q : C_3 / y_1 (Eq. 18)
 Q_p : Toe load
 $Q_{p,max}$: Maximum value of Q_p
 r : See Eq. 31-c
 $R; R'; R_{reb}$: Soil stiffness at the pile toe (see Fig. 5-b)
 s : Pile set
 S : Cross sectional area of the pile shaft
 S_p : Cross sectional area of the pile toe
 SPT : Standard Penetration Test blow count
 y : Pile movement
 $y_o; y_p$: Movements of the pile at head and bottom
 $y_1; y_2; y_{2R}$: See Figs. 5-a and 5-b
 z : Square root of k
 Δe : Pile shortening or lengthening
 μ : Magnifier factor of shaft load due to P_h
 ν : Poisson's ratio
 ρ : Elastic rebound measured at the pile head

Suggested Methodology for Rehabilitation of Ancient Masonry Castles and Forts on Rock Hills

A. Viana da Fonseca, L. Ribeiro e Sousa, A. Arêde, J. Guedes, E. Paupério,
K. Karam, A. Costa, J.E.Q. Menezes

Abstract. Forts, including in this designation military castles, present high complexity due to their nature. Methodologies followed in the rehabilitation of forts are briefly presented, with the emphasis on characterization of materials and rock masses and on tests and numerical models developed for ancient forts. Studies concerning forts with Portuguese legacy are presented. The first case is related with rehabilitation of foundations and walls of the Guimarães Castle, Portugal. The causes of the appearance of holes or torn threads in the exposed face of the wall and the tower of the extreme southwest of the castle were assessed. The intervention performed was focused on the stabilization of the rock mass and careful sealing of discontinuities in the high strength rock mass and consolidation of the most weathered fractured rock mass. The second case is related to forts existing at Muscat, Oman. The protection of the Jalali Fort is studied in detail. During 2007, cyclone Gonu caused substantial damage to the seawall adjacent to the fort. The study addresses the redesign of the seawall.

Keywords: masonry forts, rehabilitation, rock mechanics, Guimarães Castle, Jalali Fort.

1. Introduction

The analysis of historical masonry forts is a complex task. Relatively limited resources have been allocated to the study of the mechanical behavior of masonry, which includes nondestructive *in situ* testing, adequate laboratory experimental testing and development of reliable numerical tools. Despite this, significant contributions have been made in these research fields. The difficulties in using the existing knowledge are inherent to the analysis of historical structures.

Conservation and restoration of historical monuments and their surrounding areas, both urban and rural, are disciplines that require specific training and a multidisciplinary approach. The continuous changes in materials and construction techniques, and the challenging technical and scientific developments, make new possibilities available for the preservation of the architectural heritage, and are key aspects in the division between the science of construction and the art of restoration. These aspects add an intrinsic dimension and character to the field and it seems extremely difficult to appreciate historical buildings without a broad knowledge. The necessary knowledge includes a wide variety of non-traditional fields that are usually not

covered by most university curricula in civil engineering and architecture.

Forts, including in this designation military castles, are among these monuments that are high complexity due to their frequent location in high hills. Each fort has distinctive engineering and architectural features that make its study a challenge. This paper deals with the methodologies for the rehabilitation of ancient forts with focus on forts with Portuguese legacy. These forts are frequently on high elevated natural rock that hinders their access, which adds a dimension of difficulty to their study. An example of the foundations for a medieval fort is indicated in Fig. 1. Forts with Portuguese legacy are disseminated in all the continents. Several good examples are forts in Oman such as the Muttrah Fort constructed in the 17th Century (Fig. 2), and the Hormuz Fort in Iran, as represented in Fig. 3. These forts are made by sectioned walls built over rock outcrops overlapping the walls that tend to adapt to these erratic weathered profiles sweetening the foundations to these geologies.

In this paper, the methodologies in the field of rock mechanics studies and investigations on forts are briefly presented in section 2, with emphasis placed on the charac-

A. Viana da Fonseca, PhD, University of Porto, Faculty of Engineering, Department of Civil Engineering, Dr. Roberto Frias Street, 4200-465 Porto, Portugal, e-mail: viana@fe.up.pt.

L. Ribeiro e Sousa, PhD, University of Porto, Faculty of Engineering, Department of Civil Engineering and China University of Mining and Technology, Dr. Roberto Frias Street, 4200-465 Porto, Portugal, e-mail: sousa-scu@hotmail.com.

António Arêde, PhD University of Porto, Faculty of Engineering, Department of Civil Engineering, Dr. Roberto Frias Street, 4200-465 Porto, Portugal, e-mail: aarede@fe.up.pt.

João Guedes, PhD, University of Porto, Faculty of Engineering, Department of Civil Engineering, Dr. Roberto Frias Street, 4200-465 Porto, Portugal, e-mail: jguedes@fe.up.pt.

Esmeralda Paupério, Engineer, University of Porto, Construction Institute, Dr. Roberto Frias Street, 4200-465 Porto, Portugal, e-mail: pauperio@fe.up.pt.

Karim Karam, PhD, Sarooj Construction Company, P.O. Box 1413, Postal Code: 112 Ruwi, Oman, e-mail: karim.karam@gmail.com.

Aníbal Costa, PhD, University of Aveiro, Department of Civil Engineering, Campus Universitário de Santiago, 3810-193 Aveiro, Portugal, e-mail: agc@ua.pt.

J.E. Quintanilha de Menezes, PhD, University of Porto, Faculty of Engineering, Department of Civil Engineering, Dr. Roberto Frias Street, 4200-465 Porto, Portugal, e-mail: menezes@fe.up.pt.

Submitted on April 2, 2014; Final Acceptance on Jul 25, 2014; Discussion open until December 31, 2014.



Figure 1 - Foundations of the medieval Algozo Fort.



Figure 2 - Muttrah Fort, Oman.

terization of materials and rock masses in section 3 and on tests and numerical models developed for ancient forts in section 4. The paper also presents specific studies concerning forts with Portuguese legacy. The first case is related to the rehabilitation of foundations and walls of the Guimarães Castle in Portugal in section 5, where the intervention consisted of stabilizing the foundation by the careful sealing of discontinuities in the high strength rock mass,

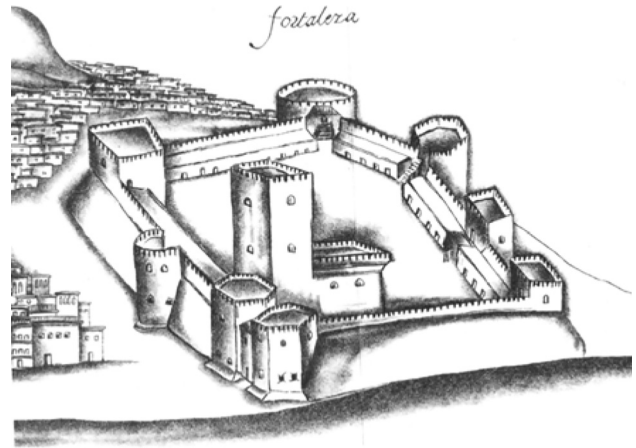


Figure 3 - Fort of Hormuz: drawing of Gaspar Correia (16th Century) (Couto & Loureiro, 2008).

and consolidation of the most weathered and fractured rock mass. The second case is presented in section 6 and is related to forts existing at Muscat, Oman. The protection of the Jalali Fort is studied in detail. During 2007, Cyclone Gonu caused substantial damage to the seawall adjacent to the fort, and the study addresses the redesign of the seawall. Finally, section 7 ends with conclusions.

2. Rock Mechanics Activities

The analysis of ancient structures is faced with several challenges that include the complexity of the geometry and construction details, the variability of the properties of the materials and rock masses of the foundations, and the pathologies induced over time. Thus, one of the major difficulties encountered when attempting to simulate of these structures is related to a detailed characterization of the properties of the materials and the rock masses involved. These studies have particular interest when they are located in areas of high probability of occurrence of earthquakes. A great effort has been made to gain a better knowledge of the behavior of structures to seismic action and how this affects the type of damages, especially when dealing with ancient masonry structures, which exhibit complex and unpredictable behavior when subjected to dynamic loads. Finally, important Rock Mechanics activities are related with the characterization of the masonry materials and of the foundation geotechnical formations, normally rock formations.

The methodologies for the rehabilitation of ancient forts requires a detailed analysis of the behaviour of these structures, comprising of several rock mechanics activities, numerical modelling and monitoring of the structures during the rehabilitation process.

The analysis of ancient forts must not be made without careful consideration to the historical changes that have occurred during the lifetime of the forts, and this has to be included in any structural analysis (Betti *et al.*, 2006). The genesis of the geological materials that make up the foun-

dations on which the forts are built is also a very important factor. The fracture patterns are greatly influenced by tectonics, stratigraphy, hydrology, rock formations, weathering, and faults, filling material of discontinuities, shear surfaces and heterogeneities. In order to map the rock mass beneath and around the forts, digital photogrammetry can be adopted using high quality digital cameras in different systems. These cameras are simple to use and have a high degree of performance and automation that make it accessible (Birch, 2006; Pötsch & Gaich, 2007).

The use of appropriate in situ and laboratory tests are described in detail in the next section. For the calibration of numerical models it is essential to perform tests for geometrical identification, evaluation of deformability and strength characterization.

In general, the activities involve the following phases:

- Knowledge phase – In this phase, information on the structure is collected. This information includes, but is not limited to geologic, geotechnical, construction history and the evolution of the structural transformations.
- Analysis phase – In this phase, the structure is modeled using appropriate tools and models. The modelling should consider: type of model (limit analysis, finite element models and discontinuity models using discrete element models); and type of analysis (static linear, static non-linear, dynamic, and 2D and 3D modelling).
- Rehabilitation phase – In this phase, the design and implementation of rehabilitation works is performed. This should include proper monitoring of the rehabilitation works, which includes human supervision, and monitoring systems.

The flowchart of Fig. 4 summarizes the methodologies that should be followed for the rehabilitation of ancient masonry forts on rock hills indicating the need to assess to historical documentation and the existing information, and to have a detailed site characterization of the fort and its foundations.

3. Characterization of Materials and Rock Masses

The characterization of structural materials and rock masses that form the foundations of such ancient structures through in situ experimentation is one of the fundamental steps in any rehabilitation process. The methodologies that should be implemented for rock mass and masonry characterization are summarized in Figs. 5 and 6, respectively.

Foundations of ancient forts, which are frequently in rock masses, are first characterized using standard rock mechanics procedures (Wyllie, 1992; Hudson & Harrison, 1997; Wyllie & Mah, 2004). Natural cavities are detected using seismic techniques such as high resolution seismic reflection, by boreholes in the areas where major cavities are expected. If necessary, P and S waves seismic cross-hole (CH) techniques, complemented with tomographic

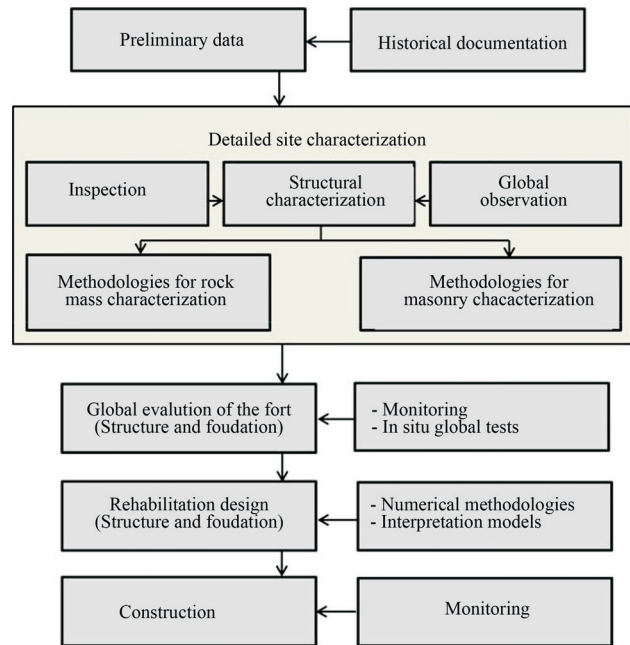


Figure 4 - Flowchart for rehabilitation of ancient masonry forts.

(RT) refraction, can also be used, giving tomographic images that can show to a very good resolution the spatial distribution of VS, which in turn indicates the presence of weak zones where attention may be addressed (Carvalho *et al.*, 2008). Logging of the core should be when possible done during all drilling operations and digital photographs of the core as each box is filled up. The selection of the cores for laboratory tests can be done at the core storage area. Sonic logging and/or televiewer scanning is often better, faster and cheaper than recovery of oriented core (Sousa, 2009). Finally, for the selection of the optimal position of boreholes appropriate virtual Bayesian preposterior analysis should be used (Sousa, 2010; Einstein & Sousa, 2012).

The materials that make up forts masonry are normally rocky, with few cases existing in some countries where masonry is made of ceramic or earth materials. There are several tools, procedures and techniques that enable the qualitative and the quantitative characterization of these materials. Such techniques include the use of sonic wave propagation tests and flat jack tests at the location of the site, followed by broader characterization techniques, such as load tests and identification dynamics tests (Guedes *et al.*, 2010). In addition, classical rock mechanics tests can also be used to characterize the masonry.

A laboratory prototype for discontinuity shear behavior was developed at University of Porto to perform tests on stone masonry joints as illustrated at Fig. 7. The shear box is 200 x 200 x 150 mm³ with a capacity of 500 kN in normal and shear loads. Shear displacement is mechanically imposed up to a maximum 25 mm/hour rate. Normal displacements are measured for dilatancy characterization. The

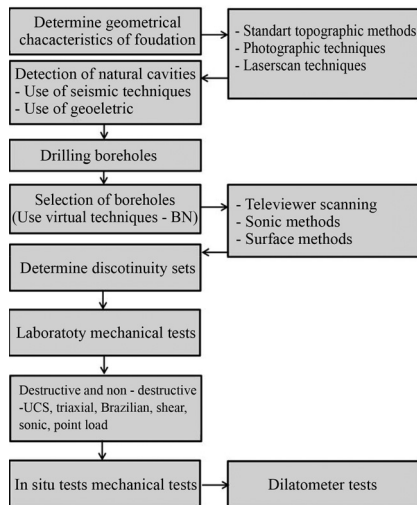


Figure 5 - Methodologies for rock mass characterization.

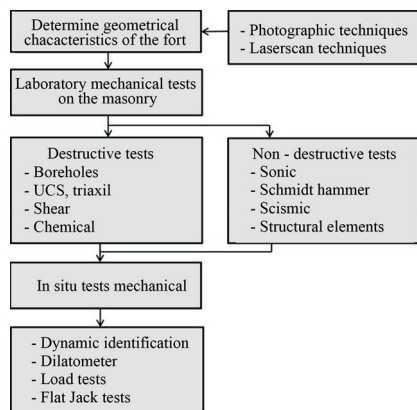


Figure 6 - Methodologies for masonry characterization.



Figure 7 - Discontinuity shear tests.

equipment also allows cyclic testing of joints for residual shear strength determination. Masonry samples are specially cut to fit the shear box volume with the mean joint plane at 75 mm from base. When mortar is used in masonry

its thickness is included in the 150 mm sample height. If a shear test of rock over soil (tout-venant) is performed, the upper half of joint sample is always of rock. An example of studies performed using this equipment is described in Costa *et al.* (2012) for the bulwark of Chaves.

Local sonic wave tests are non-destructive techniques that can be applied in situ and measure the velocity of propagation of a sonic wave between two points, which depends on the characteristics of the medium the wave is travelling through (Guedes *et al.*, 2010; Lopes *et al.*, 2010).

In ancient masonry structures this technique can be applied to determine the mechanical properties of the materials that make up walls for example. In Fig. 8 results of application of this sonic technology to the Caminha tower are presented (Silva *et al.*, 2009).

Another local non-destructive technique to evaluate mechanical properties of a masonry wall is using flat jacks. This is a common technique in rock mechanics that allows one to evaluate the in situ state of stress as well as the deformability of the rock mass materials. Testing procedures for stone masonry structures are standardized in ASTM and RILEM. In particular, these standards define the dimensions of the jacks in function of the main stone elements and define the minimal dimensions of the jacks. This implies to use adapted jacks to the different types of masonry.

The technique of flat jacks, when applied to walls, allows one to perform two types of tests for different purposes; simple test and double test. These two procedures turn out to be complementary. The simple test uses one horizontal slot and one flat jack and can be considered as the first phase of a double test (Fig. 9a). The test permits one to evaluate the state of stress on the wall, which in turn allows one to determine the existing loads on the wall. Since this value can be estimated by considering the various elements discharging on the structure, comparison between the estimated value and the value determined by tests can be made. The eventual difference between values may indicate the existence of anomalies (Miranda *et al.*, 2010). Figure 10 illustrates results of a single flat jack test.

After a single test is performed, and with the flat jack still positioned in the slot, a second slot is made, above and parallel to the first one (Fig. 9b). After it is placed, displacement measuring apparatus between the two flat jacks, often four vertically and one horizontally, is installed. The flat jacks are supplied from the same pump, so that they convey the same pressure. The double test may be considered as an in situ compression test performed on a stretch of the wall that lies within the area bounded by the two flat jacks. Figure 9b illustrates the double flat jack test.

To calibrate numerical models of ancient forts, it is essential to perform dynamic tests which identify the dynamic behavior of the structure (frequencies and shape modes). An example of this for the Caminha tower is in Silva *et al.* (2009). The tower that dates from the thirteenth

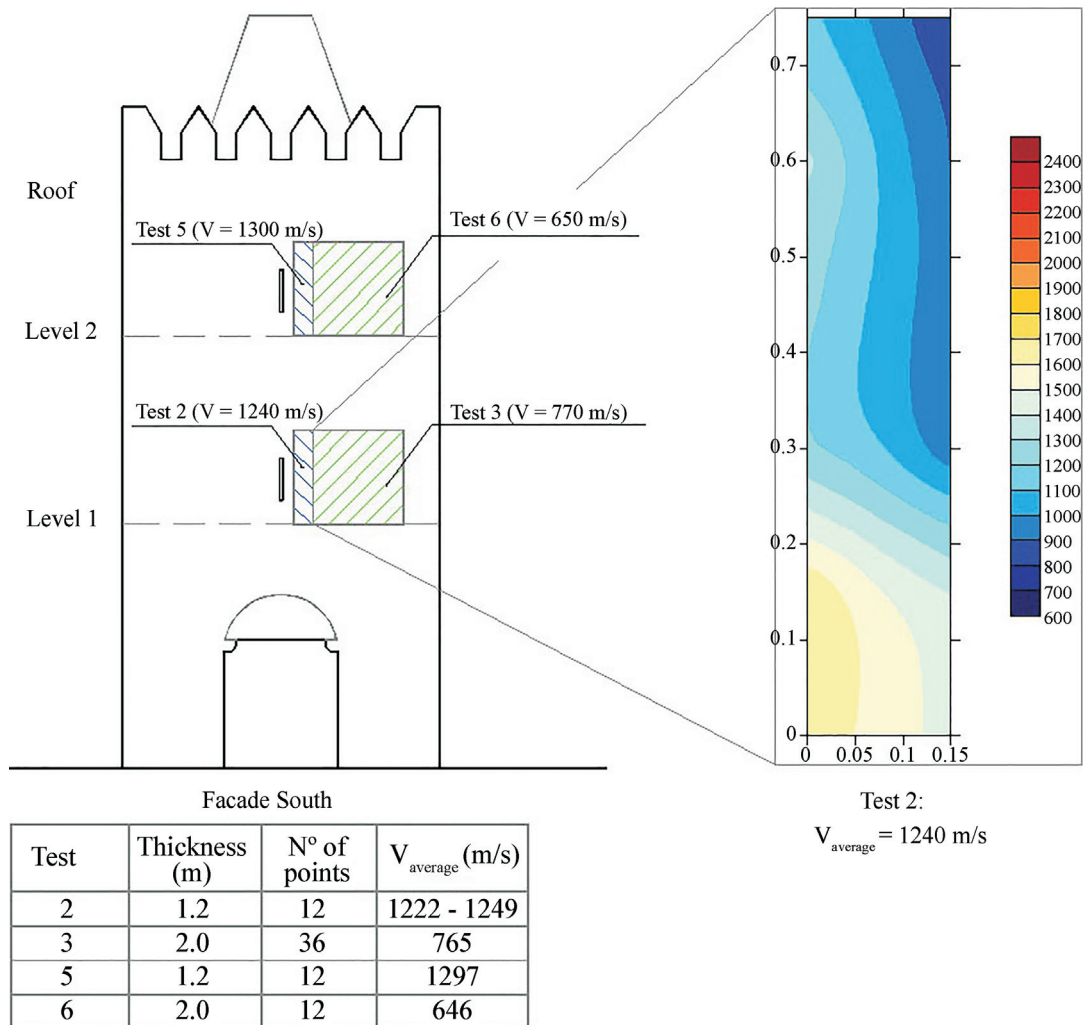


Figure 8 - Results of a sonic test for the walls of Caminha tower (Silva *et al.*, 2009).

Century is what remains of a medieval castle, with three levels and a regular plan (Fig. 11a). The study involved a geometric, exterior and interior, survey using the laser scanner technique, and the mechanical characterization of the stone masonry using dynamic identification and sonic wave tests. Figure 11b shows the detail of a laser scan image, the control points and the positioning of the accelerometers for the vibration tests (Figs. 11c and d), and the hammer for the sonic tests (Fig. 11e). Details of the dynamic identification of the tower are analysed in Lopes *et al.* (2010).

The position of the accelerometers shown in Fig. 11c was chosen to identify a large number of possible modes. The analysis of the testing results showed 28 peaks (Fig. 12). However, not all correspond to vibration modes of the tower, and out of these, 10 were associated with the tower vibration. The remaining peaks are local modes associated with the structure that exists on top of the tower to sustain the tower bell. The main dynamic identification modes are illustrated at Fig. 13 (Lopes *et al.*, 2010).

In seismically prone areas, it is important to study the response of ancient monuments during earthquakes, particularly during the process of rehabilitation. Figure 14 illustrates shaking table tests of a model simulating the fort that was severely damaged during the earthquake at Abruzzo, in 2009, after being strengthened (Miranda *et al.*, 2010).

Other tests in the laboratory can be performed for masonry using samples of rock and of joints (UCS, triaxial tests, Brazilian tests, shear tests, etc.). Load tests at the laboratory can also be conducted on models or panels of ancient monuments (Costa *et al.*, 2010). In situ tests, like ultrasound surveys or dilatometer tests can also be performed (Costa *et al.*, 2010; Paupério *et al.*, 2010).

4. The Role of Numerical Modeling

Numerical modeling forms an essential part of the study of ancient forts and structures. A practical numerical analysis implies great simplifications and assumptions and must evaluate what is important and what can be neglected in the analysis. Geometric idealizations can and should be

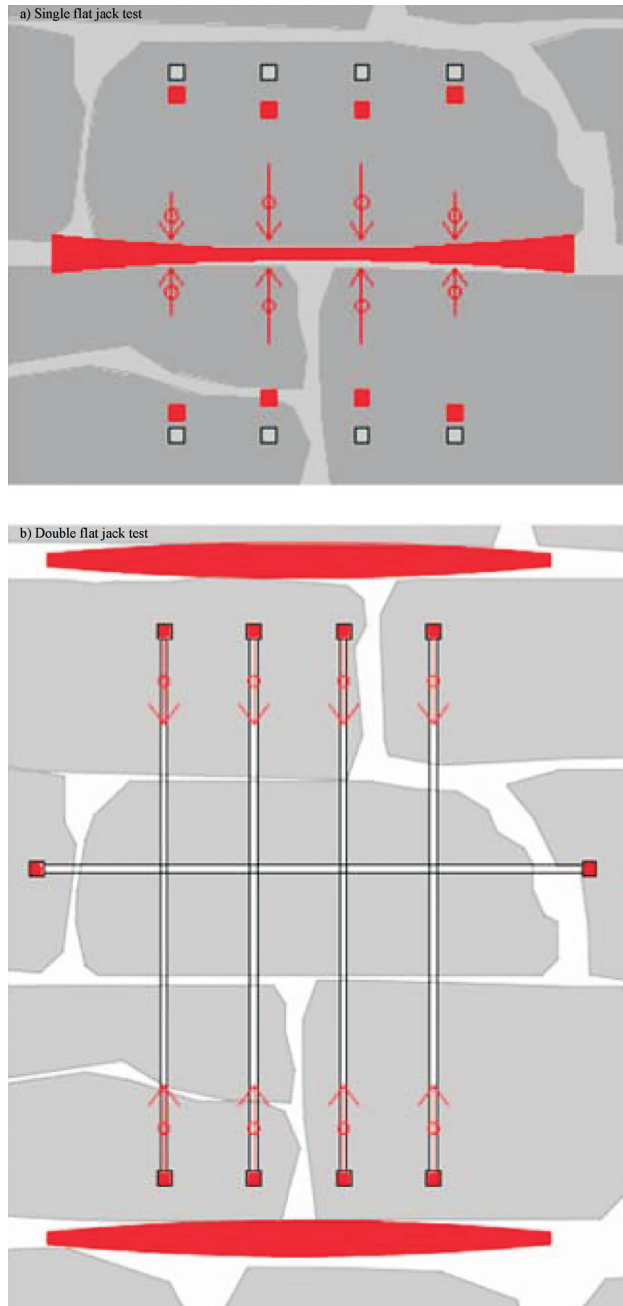


Figure 9 - Type of flat jack tests: single and double test (Miranda *et al.*, 2010). a) Single flat jack test. b) Double flat jack test.

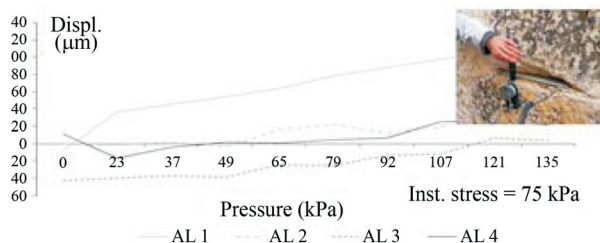


Figure 10 - Results of a single flat jack test (Guedes *et al.*, 2010).

kept as simple as possible, while still being appropriate to solve the problem. While technological and scientific advances allow increasing complexity in numerical models, often the increase in size and detail of a model may yield too much information that can complicate the analysis and make it difficult to interpret the behavior of the structure.

Figure 15 summarizes different types of numerical models that can be used for the numerical modeling of ancient forts in masonry.

The Finite Element Method (FEM) is one of the most frequently used models in numerical analysis of structures (Silva *et al.*, 2010). The modelling can be done at the micro level, considering the material batch, or at the macro level. Hybrid models can also be created when modelling a specific structural element within in a more complex structure.

Some studies have used strategies with micro simplified modeling characterized by the combination or omission of certain constituents, allowing for a drastic reduction in computation time without significant loss of accuracy. For example, Lourenço (2001) considers joints and filling as a single material with characteristics equivalent to their individual components. Other studies have used macro models, also known as continuous or homogeneous models, in which all the elements of an assembly of materials are incorporated into a continuous medium, and a relationship between extensions and average stresses of masonry is established. Damage models with distributed scalar cracking are often used in modeling macro masonry. Such models, in which damage is defined at each point by a scalar value that defines the level of degradation of the material, are commonly used in modeling of reinforced concrete structures (Silva *et al.*, 2009).

The Discrete Element Method (DEM) of modeling is important for modeling the discrete behavior of discontinuous rock masses (Lemos, 2012). DEM is also useful in modeling materials such as masonry. Applications of DEM to stone masonry structures are based on rigid or deformable blocks. Models based on deformable blocks can be used in a finite element mesh based on contact conditions in which the deformations are obtained from the relative displacement between blocks, taking into account normal and tangential stiffness. This type of contact model allows a slight overlap of blocks in compression, and uses explicit solutions for the resolution of static and dynamic problems.

Other models can be formulated as presented by Silva *et al.* (2010). This is the case for volume models (Fig. 15), which allow one to reproduce in a more realistic way the areas of intersection of elements. When using volume models it is possible to evaluate the stresses in the thickness of a wall. However, the models must be used with more than one element to discretize the thickness, otherwise errors may be high.

An example of the application of numerical models is for Caminha tower, which was analysed using FEM. The mesh developed using the software Cast3M is illustrated in

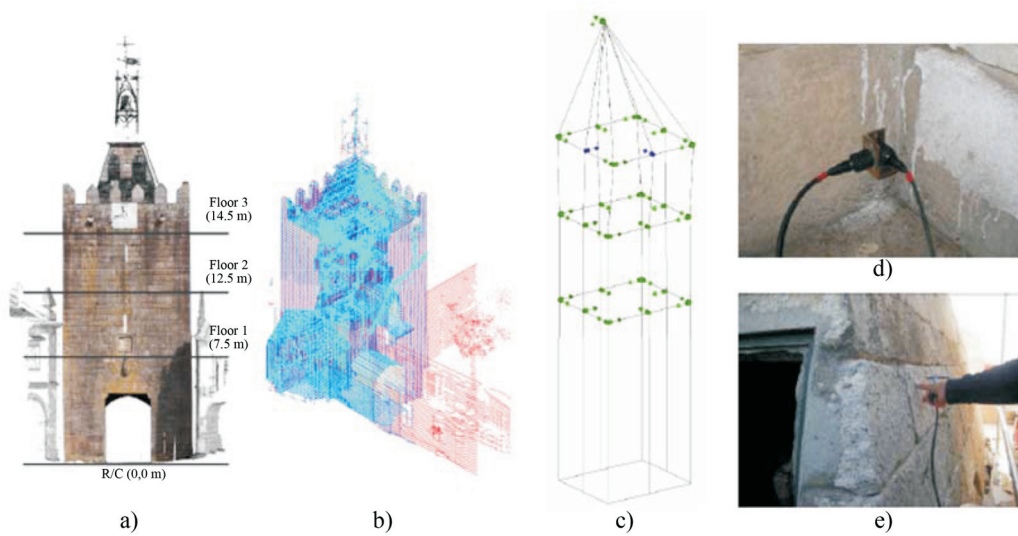


Figure 11 - Studies for the Caminha tower (Silva *et al.*, 2009). a) image of tower; b) laser scanning; c) points for vibration tests; d) colocation of accelerometers; e) hammer.

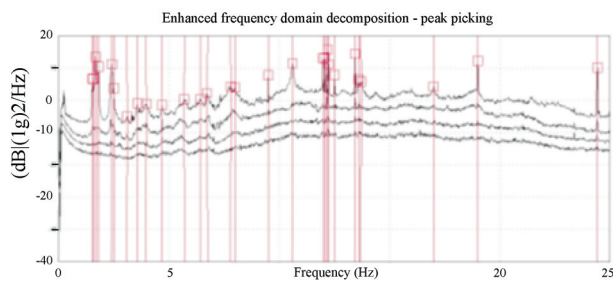


Figure 12 - Frequency peaks of the identified vibration modes for the Caminha tower (Lopes *et al.*, 2010).

Fig. 16 (Lopes *et al.*, 2010). Since the tower is connected with several buildings, these connections were taken into consideration. The calibration of the mechanical properties was done using the results of dynamic tests, to adjust the

values of the modal frequencies and the obtained modal deformations using a parameter MAC (Lopes *et al.*, 1982). The deformability moduli obtained were: masonry of the tower – $E = 1.4$ GPa; masonry of the neighbor walls – $E = 2.0$ GPa. These values can be considered within the expected range for this type of fort.

5. Rehabilitation of Foundations and Walls of Guimarães Castle

The Guimarães Castle was founded in the 10th Century (Fig. 17). In the last gothic phase, the southwest corner of the fence was reviewed, advancing on the walls of the village. The castle was rebuilt between 1265 and 1318. In the last century, starting in 1936, several restoration works on the monument were made. The works consisted of consolidation of the walls, restoration of the main door, re-

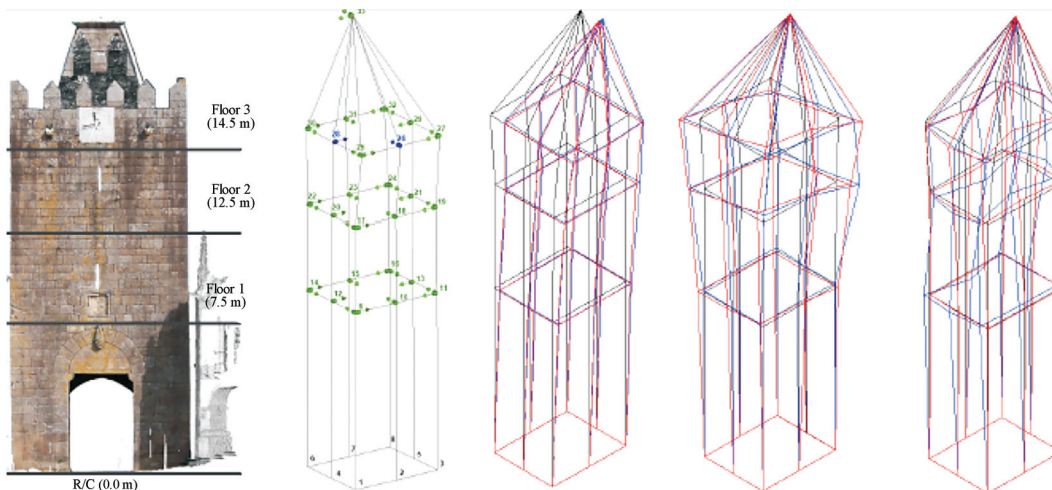


Figure 13 - Mode shapes identified from dynamic tests on Caminha tower (Lopes *et al.*, 2010).

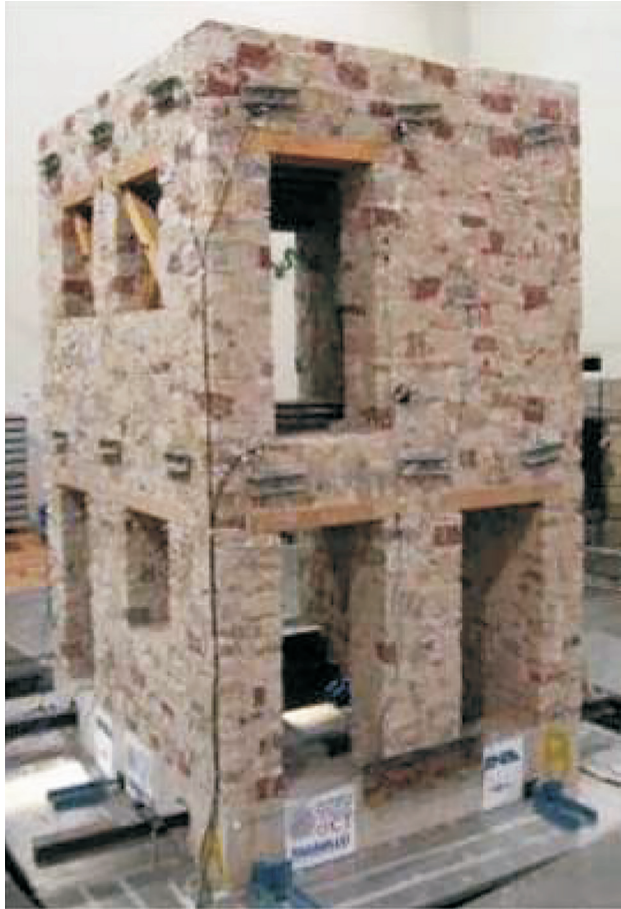


Figure 14 - Shaking table tests in a masonry model reinforced using injections (Modena *et al.*, 2010).

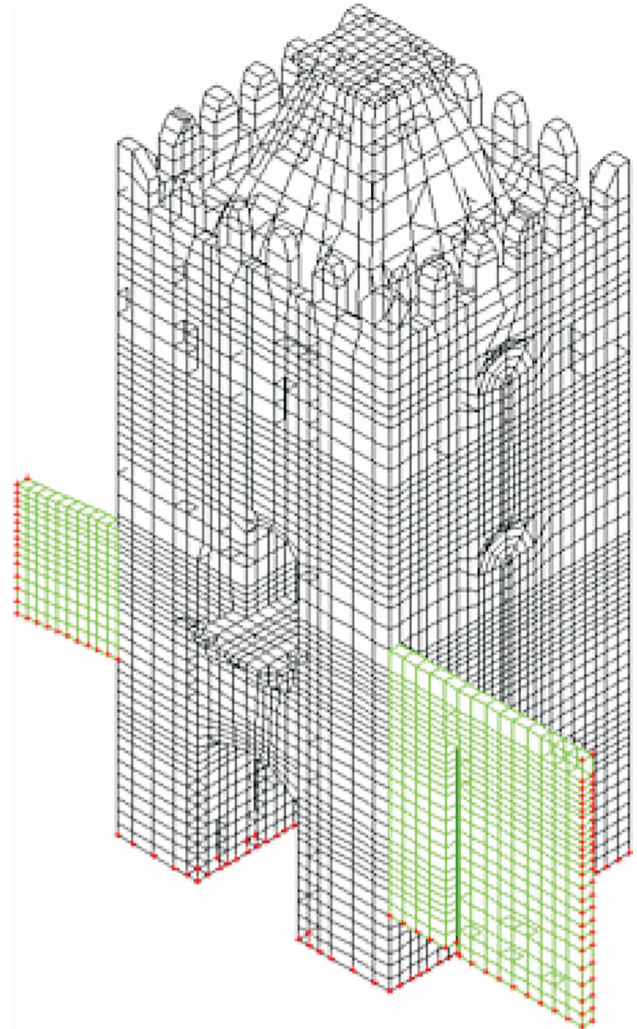


Figure 16 - Numerical discretization of Caminha tower using volume elements (Lopes *et al.*, 2010).

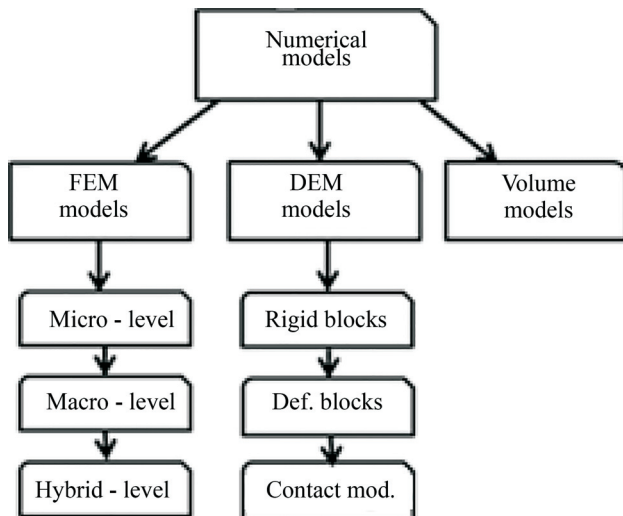


Figure 15 - Numerical models for masonry forts.

placement of masonry, demolition of elements ‘newly built’, and the reconstruction of the battlement stairs, parapets and battlements, reconstruction of wall panels, etc. These operations ended in 1971.



Figure 17 - A general view of the medieval Guimarães Castle.

In November 2008, an intervention was commissioned to evaluate the causes of the development of fissures and fractures in the exposed in face of the main wall and tower in the Southeast of the castle. A solution for these problems should be arisen from it, namely for the contention of these damages (Fig. 18). The tower presents an

opening of the joints with a development in the vertice on the base of the wedge, reflecting a rotation in the base. On the North face, together with the opening of the joint, a singular fracture was observed with some losses of stone masonry indicating a crushing by compression, as a consequence of the increase in stress resulting from the rotation of the wedge.

The foundation of the wall, and specifically of this wedge, is a rocky system with an outcrop of around 3.5 m above the surface and presents a clear fracturing system and a high degree of weathering, more intense in the base. The position and orientation of the discontinuity sets explains fairly well the orientation of the fissuring in the masonry, especially along vertical joints in the North side of the fort, as illustrated in Fig. 19. Therefore, from the performed analysis, where the geological-geotechnical studies have played an important role for the understanding of the structural mechanisms, it was concluded that an early cutting of the rock outcrops, executed in the decade starting on 1940, to enlarge the view of the fortified masonry in a urbanistic arrangement, might have been responsible for the instability verified in some of these outcrops. (Viana da Fonseca *et al.*, 2006).

The presence of granite blocks is related to geological structures such as fractures, foliation or faults, where water can easily flow into and through, accelerating chemical weathering processes. They can be reasonable determined when a careful and rigorous geological-geotechnical site investigation campaign, involving the all excavated volume, is carried out into the boreholes net, in order to construct a reliable geological-geotechnical model.

The study area is characterized by granite formations, whose matrix corresponds to a calcalkaline granite two-mica biotite with predominant porphyritic texture. An emphasis is due to the importance of masses of rounded blocks, consisting of granites low weathering levels (W2), included in sound granitic masses.

The characterization of discontinuities contained in the unstable blocks was first made in a field survey and

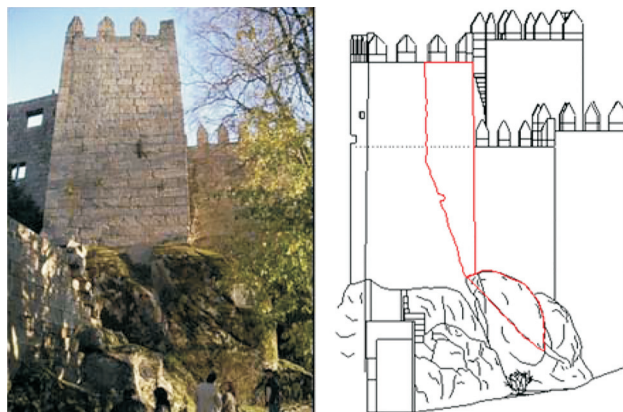


Figure 18 - Perspective of the instabilized foundations.

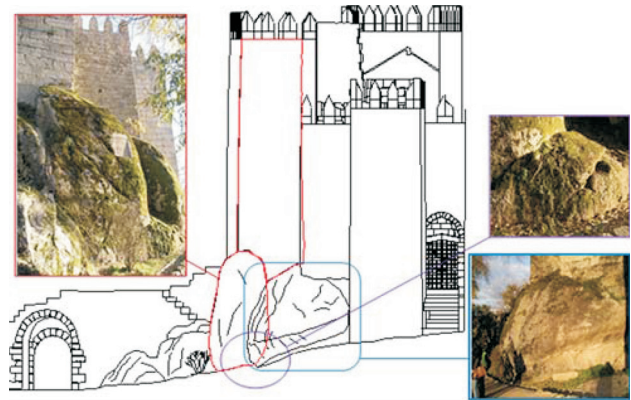


Figure 19 - Perspective of the granite massif that supports the foundation of the tower.

drilled cores. Table 1 presents the characteristics of the discontinuity sets at the foundation. Three sets were obtained, being F2 subdivided in two (F2A and F2B with a small variation in the orientation), using the software DIPS from Rocscience (Fig. 20). FT and LT represents the average planes of the main families.

Strength parameters were evaluated through discontinuity shear tests or through the combination of tilt tests and the use of Schmidt hammer (Rocha, 1971; Barton & Choubey, 1977). In Table 2 are represented the obtained results with tilt and Schmidt hammer tests, where D1 and D2 are addressed, respectively, to the higher and lower values. The value of r varies between 25 to 35, R equal to 46, JRC equal to 11 and JCS between 40 to 60 MPa. The friction angles calculated varies (Barton, 1976; Hoek, 2007): basic (ϕ_b) 35-45°; peak (ϕ_p) 55-65°; and residual (ϕ_r) 34-36°.

After the geological-geotechnical characterization, it became evident the need for adopting measures to stabilize the large block that supports the foundation of the tower, in particular the west corner, dominated by an inclined fracture with an unfavorable tilt angle, and where, apparently, there had been a very recent movement that evolved to the foundation of that part of the structure which leaned partially. Figure 21 outlines the most likely mechanism of instability, and illustrates photos of areas of weakness.

Table 1 - Characteristics of the discontinuities at the foundation.

Discontinuity set	Average dip/direction	JRC
FT	90/070	10-12
LT	90/320	10-12
F1	71/333	10-12
F2A	30/250	10-12
F2B	10/250	10-12
F3	30/140	1-12

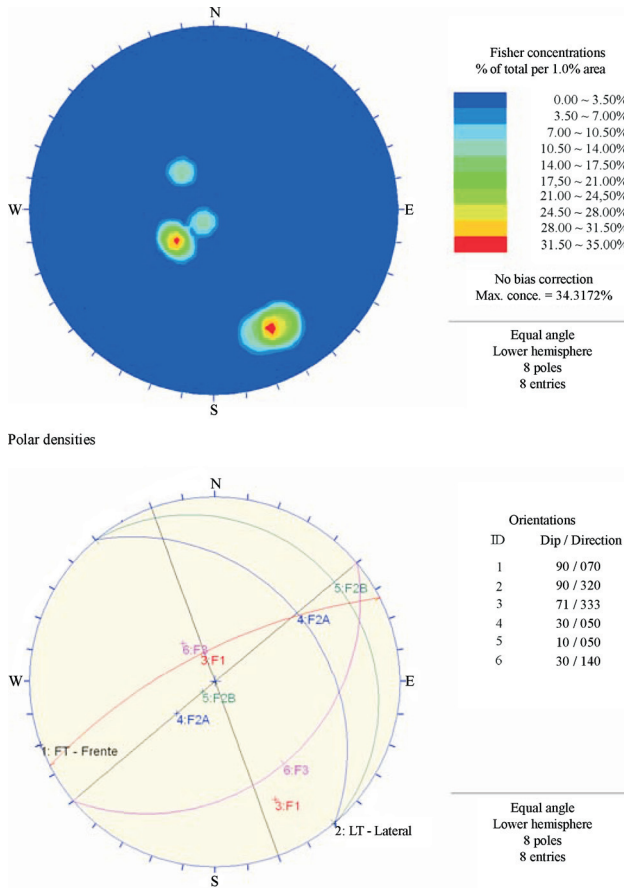


Figure 20 - General aspects of the discontinuities (Mota Engil, 2009).

The stabilization measures were intended, as a principle, to “sew” the two sides of the block and prevent future relative movements. Figure 22 presents a scheme of stabilization - absolutely indicative and preliminary.

After studying various solutions that could be implemented in this case and taking into account the constraints of the site, a set of stabilization measures were proposed that, at first glance, would ensure the stabilization of the rock mass above the large fractured block by bolting the passive feature. These high resistance steel bolts would be sealed with selective and repetitive injections in the area of fractures and faults, but also in the rest of the involved areas, looking to fill other discontinuities which would be identified in drilling process for installation of the bolts. To

Table 2 - Results with tilt test and Schmidt hammer.

Sample	φ_b (°)	UCS (MPa)	
		Average	σ^2
Not weathered	-	123.5	39.3
D1	40	64.0	22.9
D2	35	41.4	24.7

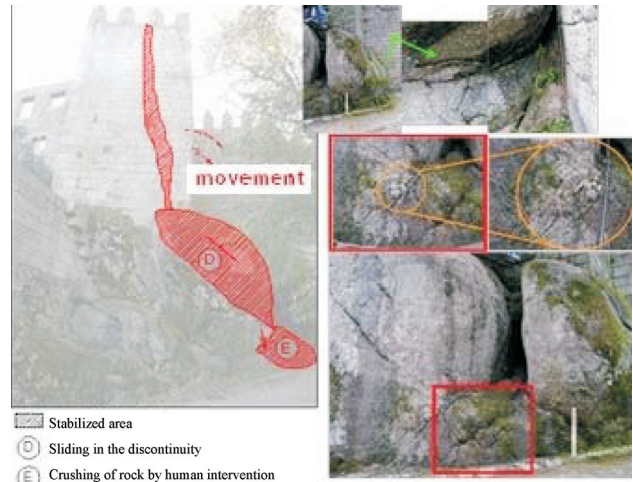


Figure 21 - Instability mechanism explaining the observed damage.



Figure 22 - Plan of nailing positioning and drilling.

this end the drilling procedure that has been prescribed would have to enable an integral sampling for characterization and classification of the underlying rock mass, in particular the foundation of the wall itself. The integral rotary technique that was used to execute the holes for the inclusion of the steel bars had the advantage of not transmitting significant vibrations to the structure. This drilling was extended deep enough so that the lengths of sealing guaranteed a safe embeddedness in the sound rock (W2 to W3). This was complemented with enough drilling extend to assure the nailing of the contiguous block, to ensure its attachment to the base, and finally, the mass sealed with micro-cement underlying the two major granite balls (identified in Fig. 21 as zone E). The space between the two blocks would still be filled with structural material cemented due to capping of the original stone material. Finally a thorough monitoring system was installed to evaluate a possible structural reinforcement of the tower and adjacent walls.

It is considered that bolts subject to cutting forces should be introduced through the upper surface of the block, near the area of the foundation close to the walls, and that drilling openings should be spaced at 1.5 m from the edge line, looking for a layout that was as orthogonal as possible to the gap plane (diagram in Fig. 22). The bolting elements to be adopted should consist of steel bars of high resistance so that they could establish the safety levels imposed by design criteria in a number compatible with the available space. The injection procedure and inspection criteria are described below.

The design model used a limit equilibrium analysis with the following expression for the safety factor (Viana da Fonseca & Cruz, 2010):

$$FS = \frac{[(1 \pm k_v)W_n - V - k_h W \sin(\alpha)] \tan(\delta) + T}{W_t + U + K_n W \cos(\alpha)} \quad (1)$$

where W_n and W_t are, respectively, the normal and tangential projection at the failure surface of the weight of the block; V and U uplift forces that are equal to zero in this situation; T force applied by bolts; δ friction angle of the failure surface; k_v and k_h the seismic coefficients that were not relevant in this case. The strength capacity of the bolts is given by:

$$T = \frac{0.9f_{yd}A_s}{2} \quad (2)$$

The value of f_{yd} was equal to 913 MPa for a bolt with a diameter of 45 mm, being the strength capacity of the bolts equal to 653 kN (Viana da Fonseca & Cruz, 2010).

The solution proposed required continuous monitoring, needed to adjust the solution in terms of length of the bars, arrangement and number depending on the recognition of the solid and weathered rock zones. Figure 23 shows a monitoring scheme with clinometers for tower T1 (Arêde *et al.*, 2010).

The construction phases are illustrated in Fig. 24. The work should be started from injection upwards defining two injection steps: a first run by gravity purge tube up to the mouth; the second - performed immediately - by injection under pressure with the volume control (accompanied by a careful check upwelling). Two different types' injections should be considered: injections in rock masses of good quality and injections in rock masses very weathered and soils. The injections were performed with cement grout to achieve the pressures defined in paragraph below, which ensured the consolidation of land and good sealing of the armor. The first hole injection would be used to assess the type of solution to be used and method of implementation of the injections. In the treatment of mass for the foundations and in the presence of soils areas and highly weathered rock masses, selective and repetitive injections would be necessary in some specific sections.

Finally, all the mouths of the holes were closed with cores that were cut with a diameter of 200 mm and that had been removed on the starting of the execution of the holes.

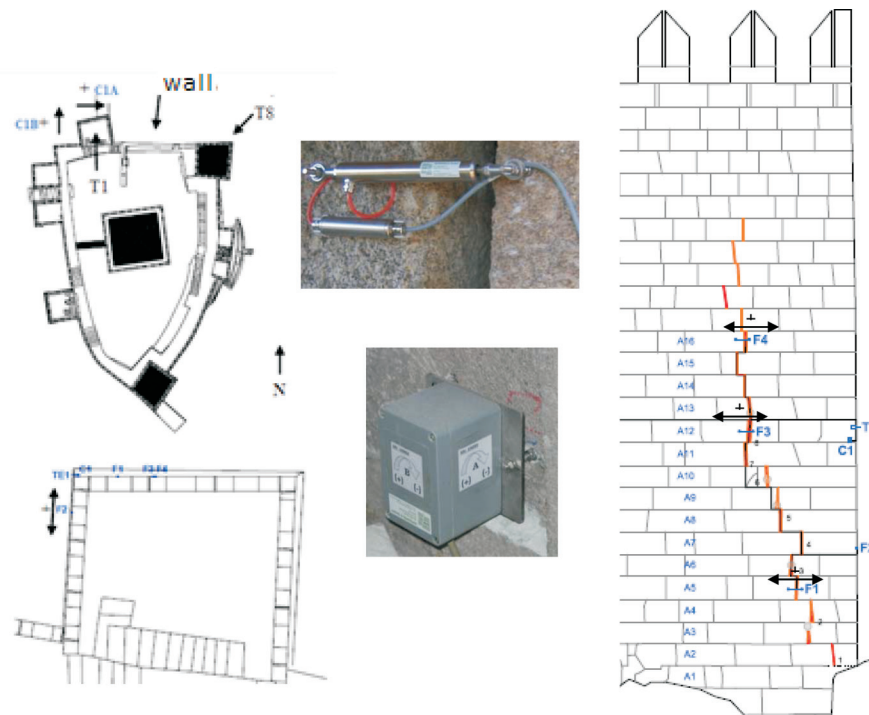


Figure 23 - Guairães Castle. Instrumentation on tower T1 for structural monitoring with relative displacement (crackmeter) and rotation monitoring (tiltmeter) (Arêde *et al.*, 2010).



Figure 24 - Arrangement of nailings and consolidation zone with micro-cement.

The space in between was filled with cemented large stone blocks and a dry stone masonry similar to the wall was built faceting that fill. At the base of the second block, where consolidation had been made with very fluid mortar and micro-cement it was proceeded similarly (Fig. 25).

6. Forts in Muscat, Oman. Protection of the Jalali Fort

The fortifications in the region of Muscat with Portuguese legacy are very complex consisting of several forts and bastions arranged according to the nature of the mountainous terrain and were constructed to defend the bay. Figure 26 is a schematic of the fortification system from the 17th Century (Garcia, 2009). The Jalali and Mirani forts, which were built in the 16th Century, are the most famous forts and are located at the entrance of the Muscat Bay. The Jalali Fort in particular is the finest of Omans historical fortifications in the capital area and its environment (Fig. 27).

The fort went through a series of transformations in design and fortification. The Mirani Fort was completed in 1587, and is located at the opposite side of the bay of the Jalali Fort. It currently overlooks the Sultan's Palace, in the old city of Muscat.

As part of a major rehabilitation and restoration program for forts around the Muscat area, the rocky slopes on which both the Jalali and Mirani forts are constructed were studied. For the Jalali Fort, a detailed geotechnical investigation was carried out including a topographic survey, plotting engineering geological data and collecting geotechnical information from the faces of the hill. Reference is made to the two watching towers protecting the entrance of the bay, as well as to the magnificent Mutrah Fort in a bay very near the Jalali and Mirani forts (Fig. 2). It is interesting to note that there is a small chapel located in one of the watching towers which is still preserved to this day. The Mutrah Fort lies on a rocky formation over the Sultan Qaboos harbour near the city of Muscat. The rocky slopes were studied in detail and a geological map was prepared. The topographic map was done by a total station where the geological structures were located. The cavities were also studied in detail and suitable measures were suggested for reducing their enlargement.

The geology of the old Muscat area is described in detail in a geotechnical report from Chaterjee (2007). The geology comprises mainly of dunite and peridotite (Hurzburgite). Therefore, the forts are founded on hard and tough ultra-basic rock stratum. The weathering effect of the rock masses, which is extensive, and the nature of the rocks have affected the strength of the rock masses, with the existence of significant discontinuities, sometimes with significant aperture, zones with marked heterogeneity, and the occurrence of natural cavities. Also relevant weak regions were identified which have important consequences on the stability of slopes upon which the forts are built. Figures 28 and 29 illustrate the occurrence of natural cavities, and dis-



Figure 25 - Stabilized situation of the castle.



Figure 26 - Forts around Muscat (Garcia, 2009).



Figure 27 - Jalali Fort.

continuities with significant aperture and major shear surfaces (Sousa, 2009).

In the Muttrah Fort area, the rock is mainly peridotite and in the Mirani Fort area mainly dunite. There is a profuse quantity of olivine intruded by serpentine veins and dykes which maintain parallelism with prevailing joints. The dykes vary in thickness from about 2 to 50 cm. The rocks may be described as greenish grey occasionally met with black spots. Under the microscope the rocks may be classified as indicated in Table 3, taking into consideration their mineralogical composition, grade of alteration and strength. Special mention is made to cavities and holes and their influence in the stability of the forts.

A detailed structural analysis of the joint systems has been carried out by plotting several types of diagrams. From the analysis of these diagrams, five predominant sets of joints were established (Chaterjee, 2007): 1) dipping northerly; 2) dipping towards N 30° E; 3) dipping towards S 20° E; 4) dipping towards S 30° W; and 5) dipping towards westerly. Only 3 sets were considered vulnerable, namely sets 1, 2 and 5. Geological structures like fault/shear zones,

Table 3 - Microscopic study of rocks below Forts Muttrah and Mirani (Chaterjee, 2007).

Rock	Main minerals	Texture	Texture	Texture
Peridotite Muttrah Fort	Olivine (55%) Orthopyroxene (40%) Chromites (5%)	Interlocking texture with jacketed look due to alteration to serpentine	Massive more than 75% of olivine are altered to serpentine as well as iddingsite (brown)	Very strong, crystalline
Dunite Mirani Fort	Olivine (95%) Phlogopite(2%) Chromites (2%) Carbonates(1%)	Interlocking texture with vigorous (> 75%) alteration of olivine along fractures to serpentine produces a jacketed look	Massive with increased porosity, highly fractured (regular and irregular)	Crystalline, weakened by fracturing and increased porosity
Dunite Mirani Fort	Olivine (> 90%) Clinopyroxene (5%) Phlogopite (3) Chromites (2%)	Interlocking texture with vigorous alteration of olivine produces a jacketed look	Massive with increased porosity	Crystalline, weakened by recrystallization, increased content of secondary mineral and porosity

disposition of different joint planes and other features were evaluated.

The initial phase of the protection and rehabilitation works on the fortifications comprised of protecting the entire rocky hill and surrounding area from further erosion from the action of sea waves. Protection works started with Jalali Fort (Karam, 2007) while rehabilitation works for the foundations were only performed until now for the Muttrah Fort.

The eastern side of the Jalali Fort is particularly prone to large waves caused by high winds, and this is especially the case during cyclones that occasionally hit the Muscat coast. The eastern side of the fort is open to the Indian Ocean, and is characterized by a very steep sea bed. On 6 June, 2007, cyclone Gonu hit the coastline of Oman causing extensive damage to many coastal areas including the cities of Muscat, Sur and Ras al Hadd at the easternmost point of the Omani mainland. The cyclone killed 49 people, with 27 reported missing. Around 20,000 people were affected and damage in the country was estimated at around



Figure 28 - Rock mass in the vicinity of Jalali Fort.



Figure 29 - Discontinuities in the rock mass.

\$4 billion, ranking it as the worst natural disaster on record in Oman.

In Muscat, Cyclone Gonu caused significant damage to the 300 m long seawall protecting the Jalali Fort (Fig. 30). The damage included destruction of 200 m of the Shed concrete armor units, collapse of numerous 160 ton concrete crest blocks and failure of the slope (Bentika *et al.*, 2010). It was therefore necessary to redesign the existing seawall for protection against the occurrence of cyclones as the first step in protecting these historically significant structures.

As an initial assessment of the impact of the Gonu cyclone on the seawall, track and wind speed information was reviewed and used to model the storm as it crossed the Indian ocean and approached the site using the 3rd generation SWAN wave model driven by moving wind fields as boundary conditions (Bentika *et al.*, 2010).

The seawall was originally constructed in 1980, and was about 265 m long. The armor was provided by Dolos units in two layers with total thickness of 2.6 m at a slope of 1:1.5 (V:H) laid on stone. The potential causes of failure included armor unit structural failure, toe failure and loss of underlayer leading to undermining of the units. Figure 31 shows a view of the fort during construction of the new seawall.

The seawall was redesigned using appropriate hydraulic models for simulating the extreme conditions for the waves and scale tested in a random wave flumes to optimize the design. The new seawall is shown in Fig. 32, and the final configuration is shown in Fig. 33.

The construction works included dredging the debris field at the toe from the failed slopes of the old seawall; lifting the large, and oddly shaped 180 ton concrete crest units, splitting them into two 90 ton concrete blocks and then lifting them into position to form the new toe for economic



Figure 30 - Jalali Fort. Location of the new seawall.



Figure 31 - Jalali Fort during construction of the seawall.

purposes; re-profiling the slope and laying the 2.4-4.8 ton underlayer rock; and placing over 900 16 m³ Accropode™ units on the slope. The 16 m³ Accropode™ units weigh about 40 tons each, and represent the largest sized 16 m³ Accropode™ units used in the Middle East, and are amongst the largest used in the world. The quantities of different materials used in the construction are shown in Table 4 (Karam, 2007).

The rocks were sourced from a quarry about 70 km from Muscat and were sorted and tested at the quarry prior to transporting to site. Standard rock tests included shape ratio tests, hardness, and abrasion tests, as well as others. The Accropode™ units were cast at a batching plant located about 100 km away from site. While transportation costs would be higher since trailers can only carry a single Accropode™ unit, the casting process could be better monitored and testing ensuring quality control. Geotextile was placed under toe blocks to create an impermeable



Figure 33 - View of the new protection of Jalali Fort.

membrane. A bedding layer was immediately placed to ensure that the membrane stays in place. To ensure the stability of the new toe, a series of boreholes were performed in order to identify the geotechnical formations. The surface layer to the depth of 2.5 to 4.0 m was identified as man-made ground with basalt origin; between 2.5 to 19.0 m, dense light grey clayey sand with occasional shell fragments; and at depths greater than 19.0 m, black fractured basalt. Slope stability analyses with shallow and deep rotational failure surfaces were performed with the geotechnical profile, and the revetment was found to be stable.

The newly constructed seawall successfully stood up to cyclone Phet, albeit it is noted that Phet was much milder than cyclone Gonu.

7. Conclusion

The analysis of historical masonry structures such as forts and castles on rock hills is a complex task, and the

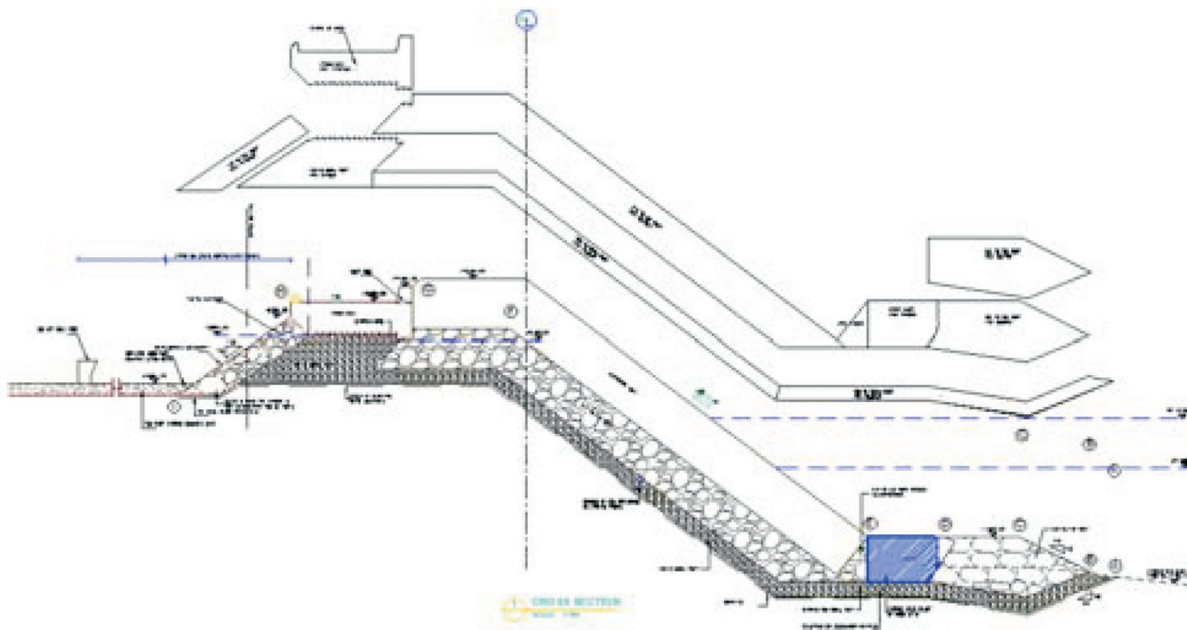


Figure 32 - Final design typical section.

Table 4 - Quantities in the new design of the revetment.

Item	Quantity
100-500 kg bedding rock	20,000 m ³
2.4-4.8 T underlayer rock	25,000 m ³
5-7 T scour rock	10,500 m ³
Total Rock	58,750 m ³
Crown wall concrete	4,250 m ³
Accropodes (901 x 16 m ³)	14,400 m ³
Total concrete	18,650 m ³
Geotextile	7,750 m ²

conservation and restoration of these monuments and its rock foundations in historical areas are disciplines that require specific training. Each fort and castle has distinctive engineering and architectural features that make it a physical challenge.

Emphasis was made to the methodologies followed in studies and investigations on ancient forts and castles. A flowchart was presented that summarized the methodology that should be followed for the rehabilitation of ancient masonry forts on rock hills indicating the need to assess to historical documentation and the existing information, and to have a detailed site characterization of the fort and its foundations. Also the methodologies that should be implemented for rock mass characterization and masonry characterization were detailed. In situ and laboratory tests as well numerical modelling were discussed.

Difficulties in the analysis of historical forts are mainly related to missing information related to geometry, characterization of mechanical properties of materials, and the large variability of mechanical properties, the significant changes in the core and constitution of structural elements, and the unknown construction sequence and the existing damage in the structure.

The solution for the rehabilitation of foundations and walls of the Guimarães Castle is an excellent example of application of rock mechanics concepts for the stabilization of the foundation and of the walls. The empirical knowledge used was important in all the design process. The importance of the monitoring activities during the rehabilitation works has been also emphasized

The fortifications in the region of Muscat with Portuguese legacy are very complex consisting of several forts and bastions. The redesign and construction of a new seawall to protect the Jalali Fort and its surroundings constitutes a complete study combining issues regarding the influence of the occurrence of severe cyclones, and the geotechnical issues related to the needs of rock materials. The rehabilitation of the foundation of Jalali Fort has not yet started but the nature of the rocks, the existence of significant discontinuities and the occurrence of detected natural cavities imply to do that in the future.

Acknowledgments

The authors thank the Department for the Cultural Heritage of DRCN (IGESPAR), in Portugal, in the persons of Mrs. Paula Silva and Anabela Carvalho, for creating the best conditions for the execution of the stabilization solution of the Guimarães Castle and the authorization for the publication of this work.

References

- Arêde, A.; Guedes, J.M.; Paupério, E.; Vila-Pouca, N. & Costa, A. (2010) Experimental evaluation and monitoring of structures as a support tool for the decision in patrimony rehabilitation (in Portuguese). Proc. Congress of Patrimony, Porto, 30 p. (CD-ROM).
- Barton, N.R. (1976) The shear strength of rock and rock joints. *Int. J. Mech. Min. Sci. & Geomech. Abstr.*, v. 13:10, p. 1-24.
- Barton, N.R. & Choubey, V. (1977) The shear strength of rock joints in theory and practice. *J. Rock Mech.* v. 10:1-2, p. 1-54.
- Bentiba, R.; Crickshank, I. & Khalili, S. (2010) Failure during cyclone Gonu and reconstruction of the fort Jalali revetment, Oman. 2nd Int. Conf. on Coastal Zone Engineering and Management, Arabian Coast 2010, Muscat, p. 21.
- Betti, M.; Orlando, M. & Vignoli, A. (2006) Modelling and analysis of an Italian castle under earthquake loading: Diagnosis and strengthening. *Structural Analysis of Historical Constructions*, New Delhi.
- Birch, J. (2006) 3DM Analyst Case Study. Adam Technology, Brochure, 4 p.
- Carvalho, J.M.; Viana da Fonseca, A. & Almeida, F. (2008) Signal treatment techniques of seismic cross-holes for modeling ISC'2 experimental site. In: *Geotechnical and Geophysical Site Characterization*, Taylor & Francis Group, p. 799-805 (CD-Rom).
- Chatterjee, B. (2007) Rock slope stabilization and structural restoration work at Muttrah Fort & Mirani Fort. *Constell Consultants Pvt. Ltd., Kolkata*, 79 p.
- Costa, A.; Delgado, R.; Arêde, A.; Guedes, J.; Vila Pouca, N.; Romão, X. & Paupério, E. (2010) Patrimony interview - The experience of NCREP/IC from University of Porto (in Portuguese). Proc. of Congress of Patrimony, Porto, 16 p. (CD-ROM).
- Costa, A.; Viana da Fonseca, A.; Miranda Guedes, J.; Paupério, E. & Raposo, N. (2012) Reconstruction of the knight bulwark of the defense wall of the City of Chaves (in Portuguese). *Ingenium*, no. 3, p. 96-100.
- Couto, D. & Loureiro, R. (2008) Revisiting Hormuz. *Portuguese Interactions in the Persian Gulf Region in the Early Modern Period*. Maritime Asia 19, Calouste Gulbenkian Foundation, Harrassowitz Verlag, Wiesbaden, 280 p.

- Einstein, H. & Sousa, R.L. (2012) Risk in slopes. In: Innovative Numerical Modeling in Geomechanics. Sousa, Vargas, Fernandes and Azevedo (eds), Taylor & Francis, London, p. 201-210.
- Garcia, J.M. (2009) Cities and Forts in the State of India (in Portuguese). Ed. QuidNovi, Lisbon, p. 224.
- Guedes, J.M.; Arêde, A.; Paupério, E. & Costa, A. (2010) Mechanical characteristics evaluation of construction materials through *in situ* experimentation (in Portuguese). Proc. of Congress of Patrimony, Porto, 16 p. (CD-ROM).
- Hoek, E. (2007) Practical Rock Engineering. 17 Chapters, available at <http://www.rocsience.com>.
- Hudson, J.A. & Harrison, J.P. (1977) Engineering Rock Mechanics. An Introduction to the Principles. Pergamon Press, London, p. 444.
- Karam, K.S. (2007) The Construction of the seawall at the Fort Jalali. Sarooj Construction Company Internal Report SCC028, p. 75.
- Lemos, J.V. (2012) Explicit codes in geomechanics - FLAC, UDEC and PFC. In: Innovative Numerical Modelling in Geomechanics. Sousa, Vargas, Matos Fernandes e Azevedo (eds) Francis and Taylor, London, p. 299-315.
- Lopes, V.; Guedes, J.M.; Arêde, A.; Milheiro, J. & Costa, A. (2010) Dynamic identification of structures (in Portuguese). Congress of Patrimony, Porto, 21 pp. (CD-ROM).
- Lourenço, P.B. (2001) Analysis of historical constructions: from thrust lines to advanced simulations. 3rd Int. Seminar on Structural Analysis of Historical Constructions, Guimarães, p. 91-116.
- Miranda, L.; Cantini, L.; Guedes, J.; Binda, L. & Costa, A. (2011) Applications of sonic tests to masonry elements. The influence of joints on the velocity of propagation of elastic waves. Int. Journal of Materials in Civil Engineering (accepted for publication) - Ref.: Ms. No. MTENG-1011R2.
- Miranda, L.; Guedes, J.M. & Costa, A. (2010). Non-destructive tests in masonry buildings (in Portuguese). Proc. of Congress of Patrimony, Porto, 13 p. (CD-ROM).
- Modena, C.; Porto, F.; Casarin, F.; Munari, M.; Silva, B. & Bettiol, G. (2010). Emergency actions and definitive intervention criteria for the preservation of cultural heritage constructions subjected to seismic actions - Abruzzo 2009. Congress of Patrimony, Porto, 12 p. (CD-ROM).
- Mota Engil (2009) Geotechnical characterization. Guimarães Castle (in Portuguese). Technical Report AT.008. Porto, p 14.
- Paupério, E.; Costa, A.; Arêde, A.; Guedes, J. & Vila Pouca, N. (2010) Inspection and diagnosis (in Portuguese). Proc. of Congress of Patrimony, Porto, 24 p. (CD-ROM).
- Pötsch, M. & Gaich, A. (2007) Rock mass characterization for geotechnical analyses using 3D computer vision. ISRM Congress, Specialized Session S9, Paper 1, Lisbon, 6 p. (CD-ROM).
- Rocha, M. (1971) Rock Mechanics (in Portuguese). LNEC, Lisbon, p. 445.
- Silva, B.; Guedes, J.M. & Costa, A. (2010) Numerical modeling strategies in the study of historical structures. Experience of NCREP (FEUP) (in Portuguese). Proc. of Congress of Patrimony, Porto, 20 p. (CD-ROM).
- Silva, B.; Lopes, V.; Miranda, L.; Guedes, J.; Paupério, E. & Costa, A. (2009) Geometric and mechanical characterization of Caminha tower through visual inspection and NTD techniques (in Portuguese). 3rd Meeting on Pathology and Rehabilitation of Buildings, Porto.
- Sousa, L.R. (2009) Works for the forts in Oman. Report to Sarooj, Muscat, 25 p.
- Sousa, R.L. (2010) Risk Analysis for Tunneling Projects. PhD Thesis, Massachusetts Institute of Technology, Cambridge, 589 p.
- Viana da Fonseca, A.; Carvalho, J.M.; Ferreira, C.; Santos, J.A.; Almeida, F.; Pereira, E.; Feliciano, J.; Grade, J. & Oliveira, A. (2006) Characterization of a profile of residual soil from granite combining geological, geophysical and mechanical testing technique. Geotechnical and Geological Engineering, v. 24:5, p. 1307-1348.
- Viana da Fonseca, A. & Cruz, N. (2010) Geotechnical interventions in Patrimonium with reinforcement of foundations. The Castle of Guimarães (in Portuguese). Proc. of Congress of Patrimony, Porto, 31 p. (CD-ROM).
- Wyllie, D.C. (1992) Foundations on Rock. E & FN Spon, New York, p. 401.
- Wyllie, D.C. & Mah, C.W. (2004) Rock Slope Engineering. Civil and Mining. Spon Press, London & New York, p. 431.

List of Symbols and Acronyms

- δ : friction angle of the surface failure
- ν : Poisson's ratio
- φ_c : peak friction angle
- φ_r : residual friction angle
- ρ : density
- A_s : area of the bolt transversal section
- E : modulus of deformability
- k_v, k_h : seismic coefficient in vertical and horizontal directions
- r : Schmidt rebound number wet and weathered fracture surfaces
- R : Schmidt rebound number on dry unweathered sawn surfaces
- T : strength capacity of bolts
- U and V : uplift forces

w_n and w_t : normal and tangential projections of the weight at failure surface	IPPAR/IGESPAR: Institute for Buildings and Natural Monuments in Portugal
2D: two dimensional	JCS: Joint wall Compressive Strength
3D: three dimensional	JRC: Joint Roughness Coefficient
Accropode TM : units for the protection revetment	MAC: Correlation coefficient for modal vector analysis
ASTM: American Society for Testing and Materials	RILEM: Reunion Internationale des Laboratoires et Experts des Materiaux
CH: P and S wave seismic cross-hole technique	RMR: Rock Mass Rating
DEM: Discrete Element Method	RT: Tomographic refraction
DRCN: North Regional Direction of Culture in Portugal	Q: Q system index volume
FEM: Finite Element Method	UCS: Uniaxial Compressive Strength
FS: Safety Factor	W: ISRM weathering level
GSI: Geological Strength Index	

Influence of the Fibre Component of Soft Plastic on Shear Strength Parameters of Pre-Treated Municipal Solid Waste

A.V.A. Borgatto, C.F. Mahler, K. Münnich, A.D. Webler

Abstract. For an appropriate stability analysis of pre-treated MSW landfill, the shear strength parameters of the material should be well defined in order to have a more realistic assessment of its geomechanical behaviour. As is well known, the shear strength of the material can be determined using two distinct components: friction (between the granular particles) and apparent cohesion. Unlike soil, where tensile strength is very low, in the case of pre-treated and fresh waste, the tensile forces are high and have a relevant participation in landfill stability due to the presence of fibres and foil material. The apparent cohesion is also called the reinforcing component, and consists basically of a wide range of substances: paper/cardboard, soft plastic, hard plastic and wood. Soft plastic is the most representative reinforcement component and due to its increasingly high volumetric concentration in the overall pre-treated MSW composition, its influence on the shear strength parameters was chosen for study. Laboratory tests were carried out with a sample of pre-treated MSW material in its original composition and modified composition (without soft plastic material). The results showed the influence of this group of materials on the strength properties of the pre-treated MSW, especially on the apparent cohesion parameter.

Keywords: pre-treated municipal solid waste, fibre component, soft plastic, shear strength parameters, landfill stability.

1. Introduction

The stability of pre-treated MSW landfills has become one of the most challenging topics in geo-environmental engineering. The shear strength parameters of pre-treated MSW should be well defined in order to provide a more realistic assessment of landfill geotechnical behaviour and stability. So, the use of appropriate laboratory tests and calculation methods is relevant for investigation and analyses of pre-treated MSW and landfills. Simple methods of geotechnical engineering are not suitable to obtain the usual shear strength parameters of pre-treated MSW and determine the landfill slope stability. It is well known that pre-treated and fresh MSW have different geomechanical behaviour from soil material. Pre-treated and fresh municipal solid wastes differ clearly in the strength characteristics from soil material due to their fibrous components.

Pre-treated and fresh waste landfill stability can be separated into two components: the friction between the granular particles and the apparent cohesion caused by the fibre effect, *i.e.*, the tensile forces that appear in the fibrous components, such as textiles, foils, paper/cardboard, soft plastic, hard plastic and wood. However, each of these materials has different physical and mechanical properties. In other words, each one of the listed materials influences the reinforcement in different ways.

According to Kölsch (1993, 1996), separate tests should be conducted for the study of pre-treated and fresh MSW shear strength, distinguishing the friction and tensile part by performing direct shear and tensile tests, respectively. In this way, tests with the same type of waste composition were carried out using medium-scale tensile box equipment in order to separately investigate the influence of the soft plastic material on the shear strength properties of pre-treated MSW (Borgatto, 2010). The results of tensile tests will be presented in another paper.

In particular, soft plastic material is the most representative reinforcement component due to its higher volumetric concentration in the overall pre-treated MSW composition. In Brazil, for instance, the percentage by weight of soft plastics in the composition of MSW can be higher than 30%. On the other hand, a higher percentage of soft plastic in MSW (or fibrous materials) leads to an extremely high strength, even enabling the construction of vertical temporary slopes in a landfill (Kölsch *et al.*, 2005). Laboratory tests were carried out in order to investigate the influence of soft plastic on pre-treated MSW strength in the way of reinforcement or due to reduction of its final emplacement density.

In Germany, no landfill can be constructed today with fresh waste. Mechanical-biological treated (MBT) material (Münnich *et al.*, 2006) was chosen for this investigation; The results showed that even with visibly reduced amount

A.V.A. Borgatto, D.Sc., COPPE, Universidade Federal do Rio de Janeiro, Coordenador de Fiscalização na Concremat Engenharia Recife, Pernambuco, Brazil. e-mail: aborgatto@gmail.com.

C.F. Mahler, D.Sc., Associate Professor, Programa de Engenharia Civil, Universidade Federal do Rio de Janeiro, 21941-596, Rio de Janeiro, RJ, Brazil. e-mail: cfmahler@gmail.com.

K. Münnich, Dr., Ing. T.U. Braunschweig, Alemanha. e-mail k.muennich@tu-br.de.

A.D. Webler, M.Sc., D.Sc. Student, Programa de Engenharia Civil, Universidade Federal do Rio de Janeiro, 21941-596 Rio de Janeiro, RJ, Brazil.

Submitted on April 19, 2013; Final Acceptance on July 25, 2014; Discussion open until December 31, 2014.

of soft plastic in its composition compared to untreated waste, the remaining part still influences pre-treated MSW strength properties.

So, the results obtained in these studies concern a landfill constructed with pre-treated MSW by a mechanical biological or equivalent process.

As indicated by the name, the mechanical biological process for pre-treatment of municipal solid waste is basically divided into two steps: (i) a mechanical procedure to remove items with large dimensions and/or special characteristics (batteries and other hazardous materials, tyres, recyclable materials), including opening of trash bags, and reduction of the size of the material not removed; and (ii) biological treatment with or without revolution, involving aerobic degradation of the material. After this process, the material is considered to be inert.

2. Material and Methods

2.1. Test material

The pre-treated waste material used in this investigation was obtained from Blankenhagen sanitary landfill, in the district of Northeim, Germany. It is an output material of mechanical biological treatment (MBT) with maximum particle size of 60 mm after screening. Approximately 300 kg of this material was collected from a static pile after the biological stabilization period (windrow system) and taken to the laboratory. This pre-treated waste was characterized in accordance with GDA E 1-7 DGGT (1994), a technical recommendation issued by the German Society of Geotechnics. This recommendation entails waste identification and description according to waste mechanics. The waste is classified according to type, identification and its condition (Borgatto *et al.*, 2006).

From the determination of the waste type, the indications for analysis into groups of substances (gravimetric composition) are obtained in a second stage. Afterwards, the morphological characterisation (dimensions and shape of waste particles) was performed considering size, length and volume. In this way, materials with one significant dimension (*e.g.*, rope), two significant dimensions (*e.g.*, foil), three significant dimensions (*e.g.*, boxes) and small particles (*e.g.*, grains) were identified and separated (Borgatto *et al.*, 2006). Likewise, further analyses were carried out, such as determining water content, particle size distribution and chemical analyses.

The segregation into groups of substances consists of separating pre-treated MSW samples in such a way that each group of substances presented similar characteristics with respect to mechanical behaviour and biochemical stability.

The groups of substances were: large pieces; paper/cardboard - waste substances consisting basically of paper or paper-similar fibres, such as cardboard, paper packaging, carpets, diapers, etc.; soft plastics - waste consisting

basically of soft synthetic substances or with similar characteristics, such as soft plastic, packaging, plastic foil, textiles, soft rubber, soft leather, etc.; hard plastics - waste composed basically of hard synthetic substances, such as rigid plastic packaging, PET bottles, rigid plastics, rigid leather, hard rubber, etc.; metals - ferrous and non-ferrous metal; minerals - waste consisting basically of mineral substances or with similar mechanical or biological behaviour (inert) such as glass, pottery, etc.; wood; and organic matter - waste of natural origin, organic, *e.g.*, vegetables, grass cuttings, plants, dry leaves.

The morphological classification of pre-treated MSW in terms of shape and size according to relevant mechanical characteristics comprised the following groups associated with geometric shape: Dimension 0 - grains (no significant dimension, *i.e.*, ≤ 8 mm); Dimension 1 - Fibre (one significant side compared to the others); Dimension 2 - Foil (two significant sides compared to the third side); Dimension 3 - Volume (three significant sides).

With regard to the particle size distribution curve, tests were carried out according to the German standard DIN 18123. The following sieve meshes were used: large sieving equipment (#60 mm, 40 mm, 20 mm and 8 mm), and standard sieving equipment (#4 mm, 2 mm and 1 mm).

2.2. Testing procedures

Normal Proctor tests were carried out based in the German technical standard DIN 18127. These tests were performed with pre-treated waste in its original composition and, in a second step, with samples of the same material but without soft plastic material.

Direct shear tests were used in this work to investigate the pre-treated waste strength properties. Direct shear tests were carried out using medium-scale device (300 x 300 x 150 mm). This equipment consists of two metal frames: bottom and top with a height of 60 mm and 90 mm respectively. The vertical load is applied through a hydraulic cylinder placed above the metal frame with maximum capacity of about 1000 kN/m². The shear strength is measured through a load cell with maximum capacity of 500 kN. Horizontal and vertical displacements are measured by automatic reading sensors. The direct shear device is shown in Fig. 1.

First, the pre-treated waste samples were prepared and moulded into the metal frame (shear box) and compacted to the optimum water content from a Proctor test. The normal stress was applied and the pre-treated waste samples were left to consolidate for a period of 24 h. After the consolidation stage, direct shear tests were conducted as a consolidated drained test (CD) with a displacement speed of 0.05 mm/min, which is usually used for clay soils, to prevent development of excess pore water pressure.

In order to investigate the influence of soft plastic on MSW strength, direct shear tests were performed with pre-treated waste material as follows:

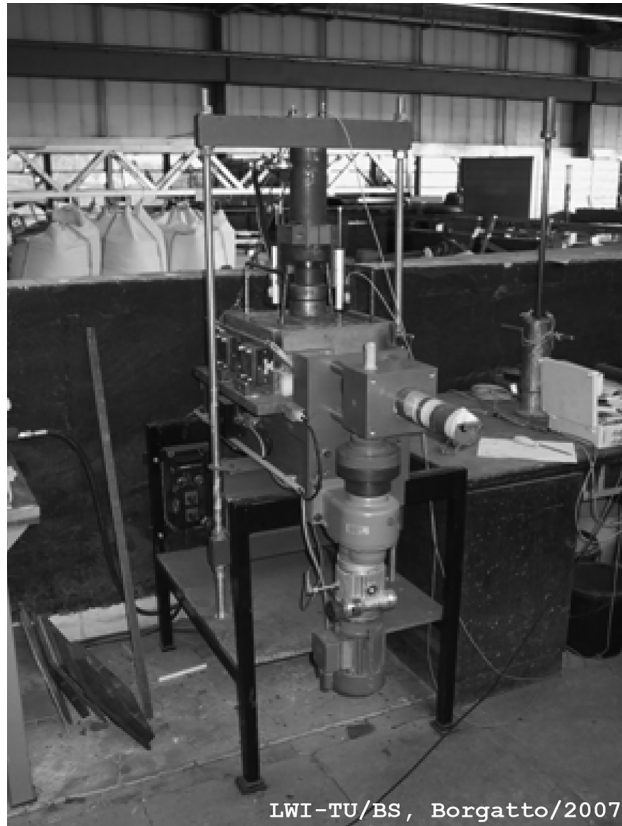


Figure 1 - Direct shear device.

- Sample A - pre-treated MSW with original composition, compacted to the maximum dry density according to the Proctor test;
- Sample B - pre-treated MSW with modified composition (without soft plastic material), compacted to the maximum dry density according to the Proctor test.

All samples were tested at normal stresses of 25, 50, 100, 200 and 300 kN/m².

3. Results and Discussion

3.1. Test material

The results of the classification into groups of substances of the pre-treated waste material under study are given in percentages of the total mass related to dry weight. The values are presented in Fig. 2.

The findings were typical for pre-treated waste material (MBT). The largest fraction corresponded to mixed materials with the particle size smaller than 20 mm, representing 83% water content dry of the total sample ($\varnothing < 8 \text{ mm} + \varnothing < 20 \text{ mm}$). Soft plastic material with 4% water content dry of the total sample corresponded to 29% water content dry of the total reinforcement material (soft plastic + paper/cardboard + textiles + wood + hard plastic = 14%wt.). Figure 3 shows the results of morphological characterization of the pre-treated material.

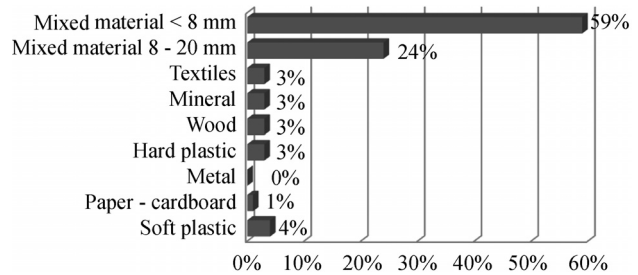


Figure 2 - Classification into groups of substances of pre-treated waste material.

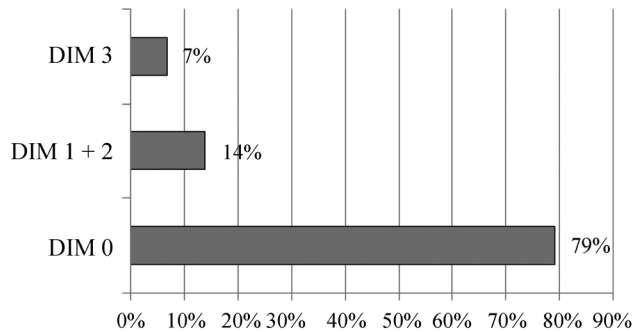


Figure 3 - Morphological classification of the pre-treated waste material.

Concerning the increases in shear strength, the percentage of fibrous components with dimension 1 and 2 are the most interesting due to the reinforcement generated. A value of 14%wt. was found in this study for materials with dimension 1+2, consisting mostly of soft plastic material (5%wt.). In tests performed by Kölsch (1996) with samples of MBT material, values of 16%wt. were found for dimension 1+2.

As a result of organic decay during pre-treatment, a large quantity of granular material was found (dimension 0).

The results of the particle size curve distribution of the pre-treated waste material under study are presented in Fig. 4. As in the previous tests, due to the mechanical biological pre-treatment (MBT), the largest fraction corresponded to particles smaller than 20 mm, representing 83%wt. of the total sample.

3.2. Testing procedures

According to the testing procedure regarding compaction tests (normal Proctor test), two types of pre-treated waste material composition were tested: original composition and modified composition (without plastic material). The results are compiled in Table 1.

The waste material sample with modified composition (without soft plastic) reached, as expected, a higher Proctor density (maximum dry density) compared to the sample with original composition. A comparison between

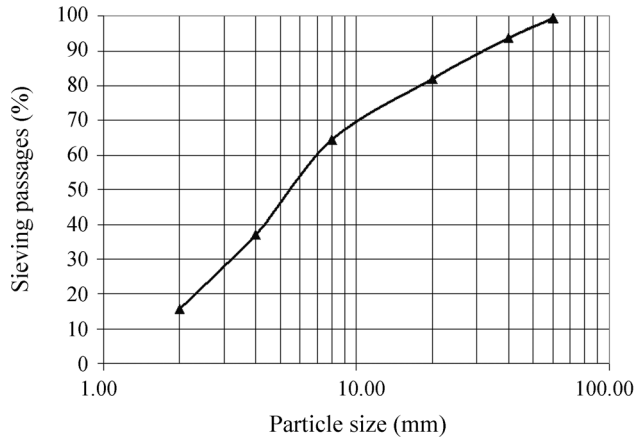


Figure 4 - Particle size curve distribution of the pre-treated waste material.

the Proctor test curves from those two types of pre-treated waste material composition is presented in Fig. 5.

The results of the medium-scale direct shear tests on the curves of shear strength vs. horizontal displacement for

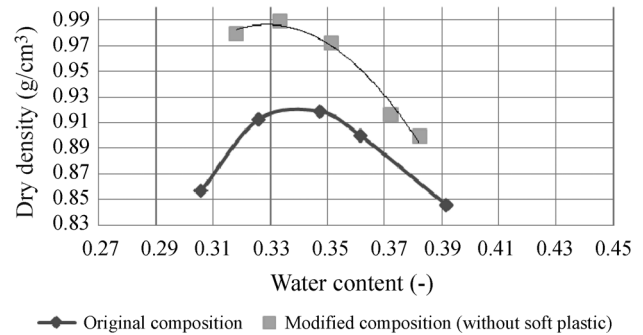


Figure 5 - Normal proctor curves of pre-treated waste material.

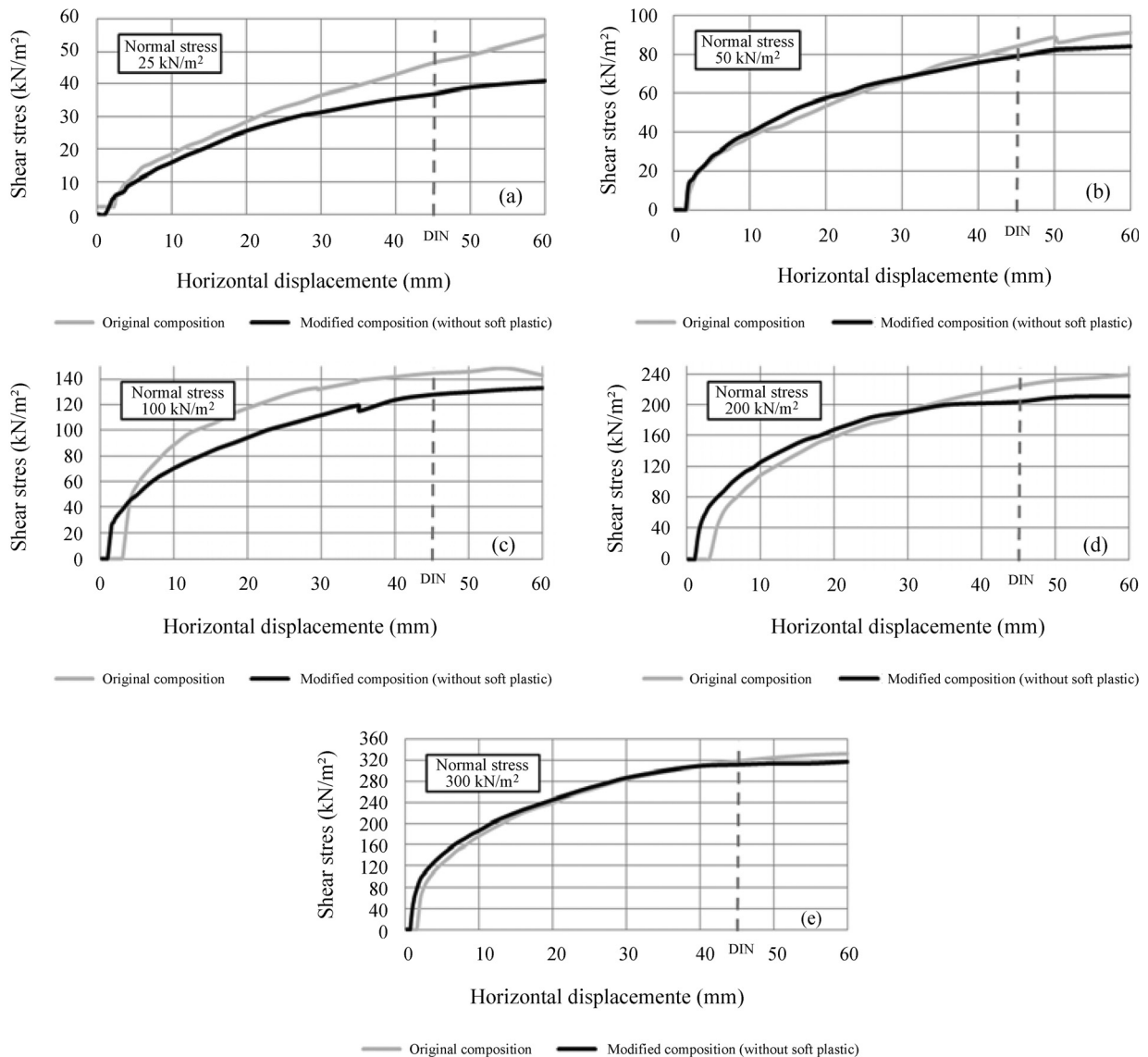


Figure 6 - Shear strength vs. horizontal displacement curves for pre-treated waste material.

Table 1 - Results of the proctor test on pre-treated waste material.

Waste material	Optimum water content (%)	Dry density (g/cm ³)	Wet density (g/cm ³)
Original composition	34	0.92	1.41
Modified composition (without soft plastic material)	33	0.99	1.48

pre-treated waste material under study are presented in Fig. 6.

First of all, according to the stress-strain curves presented, no material failure occurred during the test. As reported by Mahler & De Lamare (2006) and Bauer *et al.* (2007), that finding is common for pre-treated waste materials containing fibrous components. Consequently, deformation or displacement-dependent shear strength parameters should be used to calculate landfill stability. Based on the German soil testing standard for direct shear testing (DIN 18137-3 (2002)), deformation of 15% is stated for estimating the shear strength parameters. In the test done, this corresponds to a horizontal displacement of 45 mm.

The second point to be observed is the fact that with the increase of horizontal displacement, the mobilisation of the shear strength was always greater in the sample with original waste material composition, at all levels of normal stress. This behaviour may evidence the influence of soft plastic material on the shear strength of pre-treated MSW, mainly when the levels of horizontal displacement are high (due to fibrous components). As pointed out by Fucale *et al.* (2007), the strength properties of the pre-treated waste material are first mobilised by the friction components (basic matrix) for a low level of horizontal displacement.

Then, with the increase in displacement, the strength properties are mobilised as a result of tensile forces from fibrous components such as soft plastic.

The mobilisation of shear strength parameters of the pre-treated waste material samples (cohesion and angle of internal friction) vs. horizontal displacement are presented in Fig. 7. According to results, soft plastic material has more influence on the strength parameter cohesion than on the angle of friction. Observing Fig. 7 (b), the curves of cohesion mobilisation of the two samples are parallel to each other, at least qualitatively, up to a horizontal displacement of around 45 mm. After that point, both curves behave as mentioned previously, higher mobilisation in the sample with original waste composition (due to presence of fibrous components - soft plastic, in this case) compared to the sample with modified composition.

Assuming the Mohr-Coulomb failure criteria and considering the DIN 18137-3 (2002) (15% strain), the shear strength envelopes for the pre-treated waste material are presented in Fig. 8.

As a result, the soft plastic material has almost no influence on the angle of friction. Only a slight difference between the angle of friction for both tested samples (original waste composition and modified sample composition) was found. Despite the angle of friction, higher values for apparent cohesion parameters were found for the sample with original pre-treated waste composition compared to the sample with modified waste composition. The strength parameters are summarised in Table 2.

In comparison with strength parameter values provided in the literature on MBT waste, it is possible to affirm

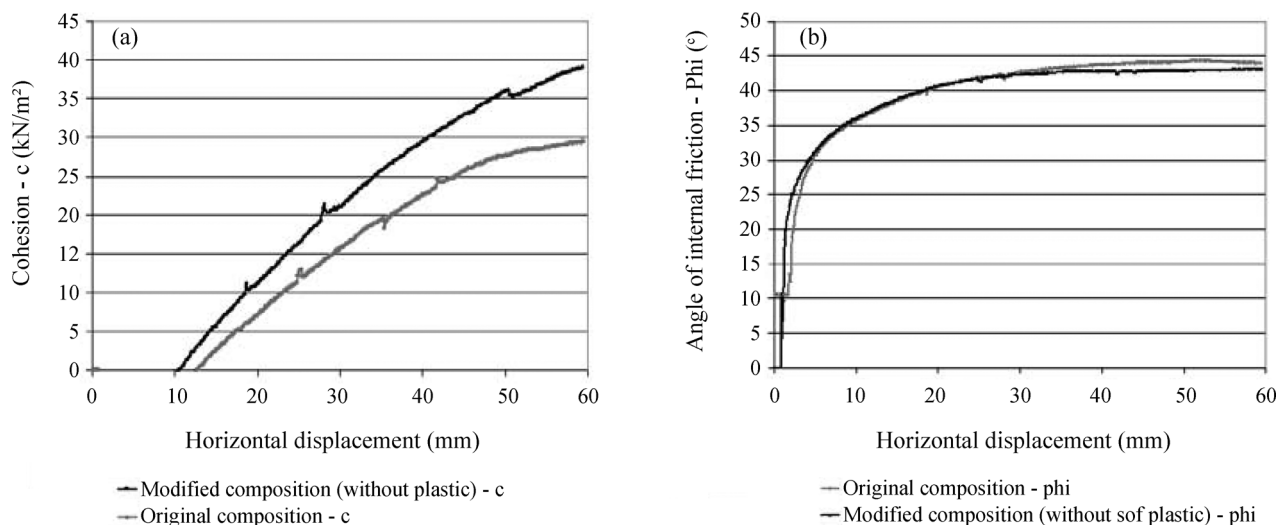
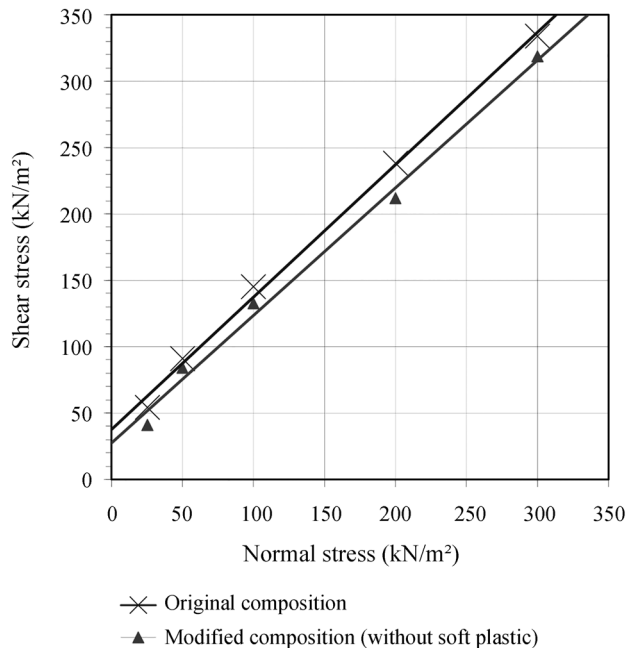

Figure 7 - Mobilisation of shear strength parameters of pre-treated waste material.

Table 2 - Strength parameters results of pre-treated waste material (for 45 mm horizontal displacement - DIN 18137-3 (2002)).

Waste material	Dry density (g/cm ³)	Angle of friction (°)	Apparent cohesion (kN/m ²)
Original composition	0.92	44.9	38.1
Modified composition (without soft plastic material)	0.99	43.9	28.0

**Figure 8** - Shear strength envelopes (Mohr-Coulomb) for the pre-treated waste material considering DIN 18137-3 (2002).

that the findings are in the same range. Klumpfer (1998) found for samples of MBT material with $\phi_{max} < 60$ mm, a cohesion value of $c = 32.7$ kN/m² and angle of friction of $\Phi = 41.0^\circ$. Fucale *et al.* (2007) reported cohesion value of $c' = 34.7$ kN/m² and angle of friction of $\Phi = 45.4^\circ$ determined in direct shear tests with MBT material. As mentioned before, when estimating the shear strength parameters of pre-treated MSW to be used in landfill stability calculation, deformation criteria must be considered. According to German soil testing standards, a limit deformation of 15% should be used to estimate the shear strength parameters. The results are presented in Table 3.

However, the finding for apparent cohesion is divided into two parts: one in terms of friction properties (ba-

sic matrix) and the other in terms of fibre cohesion (fibrous components like soft plastic).

4. Conclusion

The results obtained in these studies are relevant for landfills constructed with MSW pre-treated by a mechanical biological or equivalent process.

Even though soft plastic material corresponded only to 4%wt. of the total pre-treated waste material under study, it had a relevant influence on shear strength properties. In fact, that behaviour was more evidenced in the apparent cohesion parameters after a high level of deformation. According to the results of the tests performed in a medium-scale direct shear device, the value of apparent cohesion showed a reduction of nearly 17% in the modified sample (without soft plastic material) compared to the sample with original material. As mentioned before, the parameter angle of internal friction had almost no influence, with a value in the range of 2% reduction in the sample with modified waste composition compared to the sample with original pre-treated material.

Concerning compaction testing (Proctor test), by removing the soft plastic material from the original waste composition, there was a gain in the value of maximum attainable dry density of around 7%. On one hand, this effect looks interesting from the point of view of air space gain (larger amount of waste can be landfilled in the same area) and a lower rate of water seepage leading to lower generation of leachate. As mentioned, lower values of waste emplacement density is one of the factors responsible for triggering landfill failures. On the other hand, the absence of soft plastic in the pre-treated waste composition negatively influences the shear strength properties of the pre-treated MSW. Thus, the stability of the whole pre-treated landfill body will be greatly reduced.

Acknowledgments

To the Leichtweiss Institute of the Technical University of Braunschweig, Germany. We also thank CAPES,

Table 3 - Strength parameters results of pre-treated waste material. Estimated by Limit Deformation of 15% (According to German Soil Testing Standards - DIN 18137-3 (2002)).

Waste material	Dry density (g/cm ³)	Angle of friction (°)	Apparent cohesion (kN/m ²)
Original composition	0.92	44.0	33.4
Modified composition (without soft plastic material)	0.99	43.6	24.0

DAAD, DFG, CNPq and FAPERJ for their constant support for our research.

References

- Bauer, J.; Münnich, K. & Fricke, K. (2007) Influence of hydraulic properties on the stability of landfills. Proceedings Sardinia 2007, Eleventh International Waste Management and Landfill Symposium S. Marguerita di Pula, Cagliari, Italy, B5, p. 167-168.
- Borgatto, A.V.A. (2010) Study of The Geomechanical Properties of Pre-Treated Municipal Solid Waste. PhD Thesis, COPPE, Federal University of Rio de Janeiro, Brazil, 271 p. (in Portuguese).
- Borgatto, A.V.A.; Izzo, R.L.S. & Mahler, C.F. (2006) Classification of the municipal solid waste from Rio de Janeiro/RJ. 2nd International Workshop Hydro-Physico-Mechanics of Landfills, Southampton, UK, 7 p.
- DGGT (1997): Geotechnik der Deponien und Altlasten, GDA-Empfehlungen, Deutsche Gesellschaft für Geotechnik e.V. (Hrsg.), Ernst & Sohn, Berlin, 9 p.
- DIN 18123 (2011) Soil, Investigation and Testing - Determination of Grain-Size Distribution. German Institute for Standardization, 24 pp.
- DIN 18127 (2012) Soil, Investigation and Testing - Proctor-Test, German Institute for Standardization, 32 p.
- DIN 18137-3 (2002) Soil, Investigation and Testing - Determination of Shear Strength. Part 3: Direct Shear Test. German Institute for Standardization, 33 p.
- Fucile, S.P; Jucá, J.F.T; Münnich, K. & Bauer, J. (2007) Study of the mechanical behaviour of MBT-waste. Proceedings Sardinia 2007, Eleventh International Waste Management and Landfill Symposium S. Marguerita di Pula, Cagliari, Italy, E6, p. 631-632.
- Klumper, A. (1998) Untersuchung und Bewertung des geotechnischen Verhaltens von mechanisch-biologisch vorbehandelten Restabfällen auf Grundlage der Bestimmung ausgewählter bodenmechanischer (abfallmechanischer) Parameter. Master Thesis, University Essen, 89 p.
- Kölsch, F. (1993) Material values for some mechanical properties of domestic waste. Proceedings Sardinia 93, Fifth International Landfill Symposium. S. Marguerita di Paula, Cagliari, Italy. pp 1393-1410.
- Kölsch, F. (1996) Der Einfluss der Faserbestandteile auf die Scherfestigkeit von Siedlungsabfall. PhD Thesis. Mitt. Leichtweiss-Institut TU Braunschweig, H. 133/96, 185 p.
- Kölsch, F.; Fricke, K. & Mahler, C.F. (2005) Stability of landfills - failures and projects, Intern. Tenth International Waste Management and Landfill Symposium, S. Marguerita di Pula, Cagliari, Italy. B6, p. 179-180.
- Mahler, C.F. & Lamare Neto, A. (2006) Effect of fibre on shear strength of residue from mechanical-biological pre-treatment of waste. Int. J. Environmental and Waste Management, v. 1:1, p. 85-93.
- Münnich, K.; Mahler, C.F. & Fricke, K. (2006) Pilot project of mechanical-biological treatment of waste in Brazil. Waste Management (Elmsford), v. 26:2, p. 150-157.

Technical Notes

Soils and Rocks
v. 37, n. 2

Impacts on the Groundwater Quality Within a Cemetery Area in Southeast Brazil

A.G. Fineza, E.A.G. Marques, R.K.X. Bastos, L.S. Betim

Abstract. This article presents the results of a case study carried out in the cemetery of Tabuleiro, state of Minas Gerais, Brazil, from August 2007 to March 2008. Five sampling wells were drilled within the cemetery area, and water samples analyzed for pH, conductivity, nitrogen ammoniacal nitrogen, nitrate, total phosphorus, sodium, potassium, calcium, manganese, BOD, COD, total coliforms and *E. coli*. The results demonstrated that the groundwater is subjected to contamination from burials leakage and the most evident impacts have been observed in the sampling well located downstream of the cemetery site.

Keywords: cemetery, contamination, flooding plains, groundwater, environmental impacts.

1. Introduction

Frequently, cemeteries in Brazil have been constructed close to settlements because of religious and culture circumstances or lack of land availability in populated areas. Also, several have been sited without proper geological and hydrological assessments, therefore posing environmental impacts and public health risks (Üçisik & Rushbrook, 1998).

Typical human bodies are composed of water (64%), proteins (20%), fat (10%), mineral salts (5%), and carbohydrates (1%). The human body of a 70 kg adult male contains approximately: 16 000 g carbon, 7 000 g hydrogen, 1800 g nitrogen, 1 100 g calcium, 500 g phosphorous, 140 g sulfur, 140 g potassium, 100 g sodium, 95 g chlorine, 19 g magnesium, 4.2 g iron, and water 70-74% by weight. The elemental composition of females is between two thirds and three quarters of that for males (Üçisik & Rushbrook, 1998; Environmental Agency, 2004).

The progression of human decomposition has been described as taking place through the stages of autolysis, putrefaction and diagenesis. The process of autolysis (or self-digestion) begins rapidly after death has occurred, causing cells to rupture and releasing nutrient-rich fluids. The following process, putrefaction, is the destruction of the soft tissues of the body by the action of microorganisms (bacteria, fungi and protozoa) and results in the catabolism of tissue into gases, liquids and simple molecules. At this point in the decay cycle electrolytes are rapidly leaching out of the body. Saponification or adipocere formation (the formation of soap from fat under high pH conditions) typically occurs after the onset of putrefaction in warm, moist, environments and is seen as deposits of a yellowish white,

greasy, wax-like substance. Finally, diagenesis is a natural process that serves to alter the proportions of organic (collagen) and inorganic components (hydroxyapatite, calcium, magnesium) of bone exposed to environmental conditions, especially moisture. This is accomplished by the exchange of natural bone constituents, deposition in voids or defects, adsorption onto the bone surface and leaching from the bone. This complex pathway leads to the formation of various gases (hydrogen sulfide, carbon dioxide, methane, ammonia, sulfur dioxide and hydrogen), and the release of by-products rich in fatty acids, phenolic compounds and glycerols, indole, 3-methylindole (skatole), and toxic diamines (cadaverine and putrescine) (Vass *et al.*, 1992; Vass, 2001).

A wide variety of microorganisms are involved in the decompositional process of human corpses. Strict aerobic organisms play a role only in the very early stages of putrefaction and are rapidly replaced by anaerobic organisms which constitute the vast majority of organisms found in human tissues. Although the intestine hosts a large array of microorganisms, only relatively few groups have been implicated as major colonizers of human corpses during putrefaction, such as *Clostridium spp.*, *Streptococci* and *Enterobacteriaceae*. In addition to these, putrefactive bacteria such as micrococci, coliforms, diptheroids, *Bacillus spp.*, *Staphylococcus spp.* and *Pseudomonas aeruginosa* can also be found (Üçisik & Rushbrook, 1998; Vass, 2001). Thus, typical microorganisms known to be responsible for waterborne diseases can be present in cemeteries seepage, including micrococcaceae, streptococci, bacillus, enterobacteria (*e.g. Salmonella*), as well as viruses. Besides bacteria, other microorganisms, like saprophyte fungi and

A.G. Fineza, Civil Engineer, D.Sc. Student, Departamento Engenharia Civil, Universidade Federal de Viçosa, Campus Universitário, Viçosa, MG, Brazil. e-mail: adonaifineza@yahoo.com.br.

E.A.G. Marques, Geologist, Associate Professor, D.Sc., Departamento Engenharia Civil, Universidade Federal de Viçosa, Campus Universitário, Viçosa, MG, Brazil. e-mail: emarques@ufv.br, eagmarques1965@gmail.com.

R.K.X. Bastos, Associate Professor, D.Sc., Departamento Engenharia Civil, Universidade Federal de Viçosa, Campus Universitário, Viçosa, MG, Brazil. e-mail: rkxb@ufv.br.

L.S. Betim, Environmental Engineer, M.Sc., Departamento Engenharia Civil, Universidade Federal de Viçosa, Campus Universitário, Viçosa, MG, Brazil. e-mail: luizabetim@gmail.com.

Submitted on March 6, 2014; Final Acceptance on July 26, 2014; Discussion open until December 31, 2014.

diverse entomofauna act during putrefaction of cadavers (Üçisik & Rushbrook, 1998; Vass, 2001).

Approximately 60% of a coffined human corpse is readily degradable matter, 15% is moderately degradable, whereas 20% is slowly degraded and 5% is considered inert (Environmental Agency, 2004). The rate of decay depends on the extent of microbial growth and activity. This is influenced by (i) the availability of nutrients (carbon, nitrogen, phosphorus, sulphur) and moisture - the high water content of a corpse and the favorable carbon : nitrogen: phosphorus ratio in vertebrate bodies (about 30:3:1) encourages rapid degradation of the corpse; (ii) pH - neutral pH conditions are most favorable; (iii) climate - warm temperatures accelerate decomposition; (iv) soil lithology - well-drained soil will accelerate decomposition, whereas poorly drained soil has the reverse effect; and (v) burial practice - depth of burial and coffin construction control the ease with which invertebrates/ vertebrates may gain access to the corpse and hasten its decay (Rodriguez & Bass, 1985; Environmental Agency, 2004). A human corpse normally decays within 10 to 12 years, however it is estimated that over half of the pollutant load leaches within the first year and halves year-on-year. Less than 0.1 per cent of the original loading may remain after 10 years (Environmental Agency, 2004).

Cemeteries leakage may eventually work its way down to the groundwater underlying the site. This is influenced by rainfall and infiltration or by the direct contact of buried remains with the water table. The risk of contamination is therefore related to soil's nature and infiltration rate, types of burials, and the effect of rainfall on the groundwater level (Üçisik & Rushbrook, 1998). Pathogens may be retained in the unsaturated soil zone, mainly due to filtration and adherence to clay particles, and eventually die off due to lack of nutrients and reduced soil moisture, increased temperature, and soil pH outside the range of 6 to 7. Thus, pathogenic organisms may be prevented to reach the groundwater due to the relative immobility and attenuation in the soil (Morgan, 2004). However, decomposition of bodies in a grave site promotes soil wetness and the nutrient-rich seepage may favor pathogen survival (Engelbrecht, 1998).

Thus, it is imperative that the authorities with control over construction of cemeteries follow adequate criteria, addressing both environmental and health risks, making regulatory decisions based on available geological and hydrological studies of the area in question, and relying on construction and sanitary techniques (Üçisik & Rushbrook, 1998; Brasil, 2003; Environmental Agency, 2004.). The aim of this paper is to present a preliminary evaluation of groundwater contamination by a cemetery in southeast Brazil.

2. Material and Methods

2.1. Description of the study area

The cemetery studied is located in Tabuleiro, a small town in Minas Gerais state, southeast Brazil (Fig. 1). The total surface area of the cemetery is approximately 15,000 m² and it is located in the central region of the town, at a local river flood plain. It is surrounded by dwellings and small commercial buildings. Burial started in second half of twenty century and it is carried out mainly by inhumation or by burial in niche. The average depth of burial into soil is 3.5 m. The soil type in the cemetery area is predominantly gleysol with high clay content. Local temperatures range from 11 to 36 °C. Average annual rainfall at the closest station (Coronel Pacheco - 30 km from Tabuleiro) is approximately 1.580 mm, varying from 20-47 mm to 200-310 mm during the dry and rainy seasons, respectively (Fig. 2).

2.2. Monitoring wells

Five wells were drilled within the cemetery area for water samples collection and the groundwater level monitoring. Wells 1, 2, 3 and 5 were drilled essentially at the same topographical level, whereas well 4 was located upstream. In addition, an existent well located outside the cemetery area, and in an upper position on flow direction, was used as a control (Fig. 3). All wells were drilled up until 4.5 m depths, above water level, even during dry season, in order to allow water samples collection.

All wells were drilled using SPT percussion boring equipment and accordingly to NBR 12244/1992 (ABNT, 1992). On those wells were installed 3 inches (diameter) monitoring wells with PVC pipes with a 1.0 m long screwed section wrapped in Bidim® geotextile (filtering tips) at the end of each hole. The filtering tip was completely under water during rainy season and partially under water during dry season. The ring space between the bore-

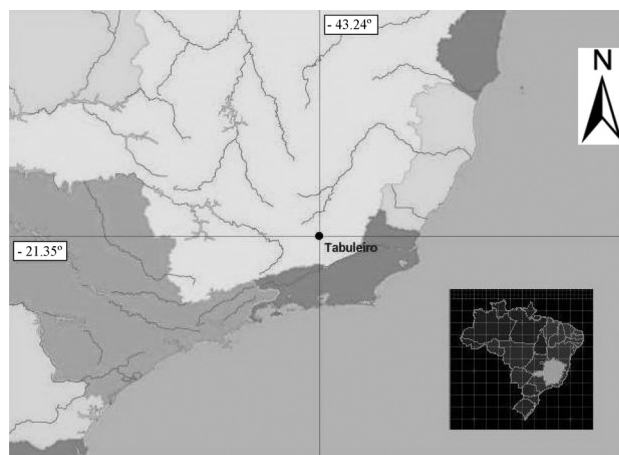


Figure 1 - Location of Tabuleiro, Minas Gerais state (highlighted in the small map), Brazil.

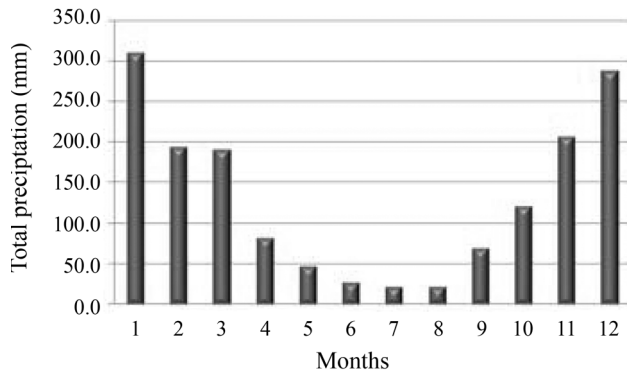


Figure 2 - Average total precipitation at Coronel Pacheco station, located 30 km from Tabuleiro cemetery.

hole cavity wall (with four inches diameter) and the PVC pipe was filled with sand up until 0.50 m above the end of each filtering tip. The remaining space was filled with soil excavated on the same borehole. The final 0.20 m were filled with cement, and a cement slab was installed around the borehole mouth, on the ground surface. At the top of the well, a locked cap was installed to avoid tampering and water leakage.

2.3. Samples collection and analysis

Samples were collected from the five monitoring wells from August 2007 to February 2008 according to the schedule shown in Table 1, thus covering both dry (August

to November) and rainy (December to February) seasons. In September 2007 and in February 2008 additional samples were also collected from the control well.

Groundwater aquifer flow was defined throughout the evaluation of water level position measured on those monitoring wells in September 2007 and in March 2008 (Fig. 4).

Bailer sampling devices were used to collect samples from all five wells. To prevent cross-contamination, different bailers were used in each sampling well. All underground water samples were collected after purging the wells. Water samples were conditioned in 500 mL polyethylene disposable bottles, stored on ice inside thermal containers and taken to the laboratory in the same day, where they were kept frozen until the chemical analysis were carried out. Microbiological analysis took place within 24 h after sampling.

Water samples were analyzed in the laboratory for biochemical oxygen demand (BOD), chemical oxygen demand (COD), potassium (K), sodium (Na), calcium (Ca), magnesium (Mg), ammonia (N-NH₃), nitrate (N-NO₃), total phosphorus (P), total coliforms (TC), and *Escherichia coli*. On-site measurement of electrical conductivity, temperature and pH were carried out at each sampling occasion. All these parameters were analyzed according to the guidelines set forth by the Standard Methods for the Examination of Water and Wastewater (APHA, 1998). TC and *E. coli* were

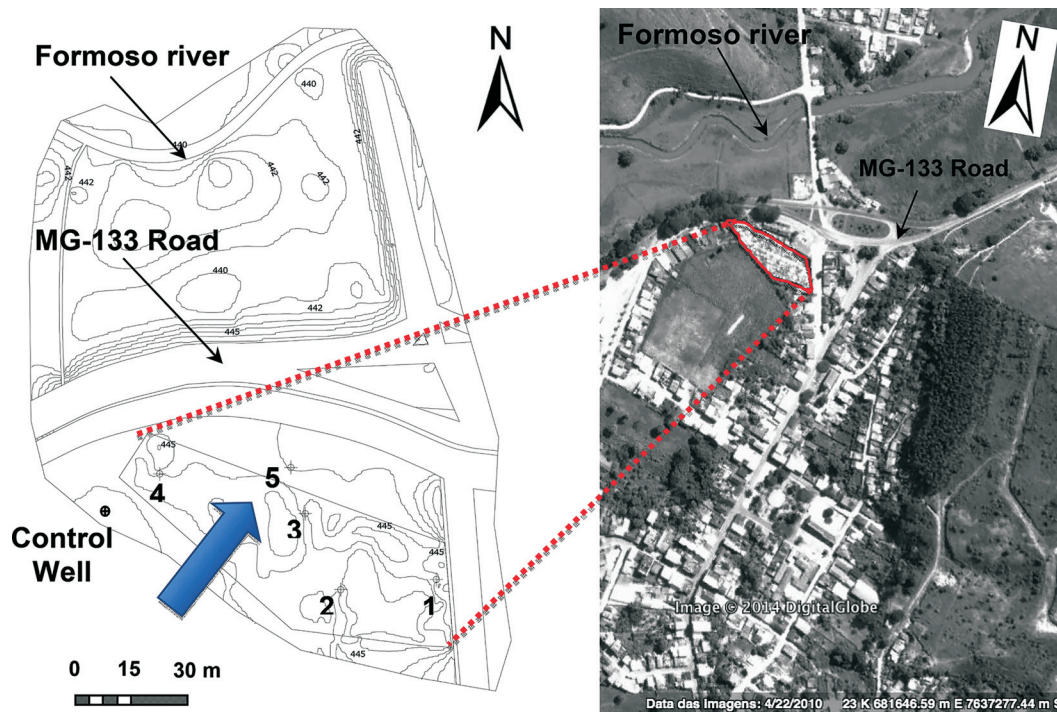


Figure 3 - On the left, the topography of the cemetery area (within straight lines on the South of the road) and its vicinities, and location of the monitoring wells, Tabuleiro-MG, Brazil. Blue dart show the groundwater flow direction. On the right, a satellite image (Google Earth, 2014) showing the cemetery (limit in red) and its vicinity.

Table 1 - Parameters analyzed in water samples from the sampling wells within the cemetery area, Tabuleiro-MG, Brazil, August 2007 to February 2008.

Parameters	Sample 1	Sample 2	Sample 3	Sample 4	Sample 5	Sample 6	Sample 7
	Aug/07	Sep/07	Oct/07	Dec/07	Jan/08	Feb/08	Mar/08
Temp.	X	X	X	X	X	X	
pH	X	X	X	X	X	X	
EC	X	X	X	X	X	X	
P	X	X	X	X	X		
N-NH ₃		X	X	X	X	X	
N-NO ₃	X	X	X	X	X	X	
Na		X	X	X	X		
K		X	X	X	X		
Ca	X	X	X	X	X	X	
Mg	X	X	X	X	X	X	
BOD		X	X	X	X		
COD	X	X	X		X	X	
Total coliforms				X	X		
<i>E. coli</i>				X	X		

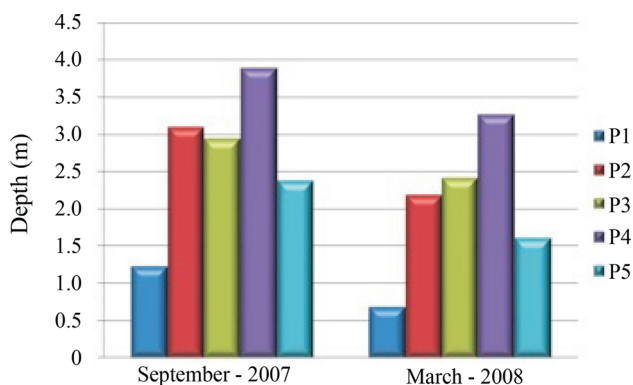


Figure 4 - Water table depth on monitoring wells on September/2007 (beginning of rainy season) and March/2008 (end of rainy season).

enumerated using the enzymatic substrate method (Colilert®).

3. Results and Discussion

3.1. Groundwater level

All groundwater levels were measured at the same day. During the dry season (September 2007) groundwater levels in wells 1 and 5 were, respectively, 1.20 m and 2.38 m below surface. Conversely, in February 2008 during the raining season, the groundwater level raised approximately 0.50 m for well 1 and 0.80 m for well 5, reaching 0.68 m and 1.60 m below surface, respectively. In the other

monitoring wells, groundwater level varied from 0.50 m (well 3) to 0.90 m (well 2) from dry to raining season. Because they were at deeper position than wells 1 and 5 during the dry season, groundwater level measured on those monitoring wells during the raining season remained at least 2 m below surface (Table 2).

3.2. Geological-geotechnical characteristics of the area

The cemetery is installed on flood plains of Formoso River. The alluvium sediments on this area are mainly composed by clay, silt and fine sand (more sparse). The geological-geotechnical profile observed up until the maximum depth excavated on the boreholes (4.5 m) is mainly composed by three layers. The first one is a landfill found close to the surface and with a thickness varying from 0.1 to 0.3 m. Below this superficial layer lays a reddish clayey soil with thickness varying from 2.0 m to 3.0 m. At the end of

Table 2 - Ground water level in the monitoring wells during dry and raining seasons, Tabuleiro-MG, Brazil, 2007-2008.

Well	Aug 2007	Feb 2008	Well depth
1	1.22	0.68	2.00
2	3.11	2.19	3.50
3	2.95	2.42	3.50
4	3.90	3.28	4.50
5	2.38	1.60	3.00

Obs.: All measures in (m).

the soil sequence observed on the boreholes there is a grey silty, locally with fine sand, soil layer with 1.5 m thickness. The main geotechnical characteristic of those soils related to the purpose of the study is the permeability. In order to determine this property, two SPT boreholes were specifically done inside the cemetery area in order to allow the realization of permeability tests. On both boreholes, three permeability tests were carried out at 1.5, 2.5 and 3.5 m depth. The average permeability for each of these depths obtained from those tests were:

- 1.5 m depth = 2.00×10^{-6} cm/s;
- 2.5 m depth = 5.50×10^{-7} cm/s; and
- 3.5 m depth = 1.05×10^{-4} cm/s;

These results are in accordance with the texture observed on the boreholes at those depths, as long as there is a more impervious material close to the surface, related to the presence of the reddish clayey soil layer; and a more permeable layer at higher depths, related to the presence of the grey silt material.

3.3. Groundwater bacteriological quality

Total coliforms and *E. coli* were measured only from samples 2 and 4 (in the end of dry season or in beginning of the rainy season), and afterwards in samples 5 and 6 (by the end of the rainy season). In wells 1 to 4 total coliforms were only occasionally detected, mostly in rather low numbers, whereas higher counts were usually found in wells 2 and 5, ranging from 2.4×10^3 organisms per 100 mL (sample 2) to 7.4 (sample 2). *E. coli* was never detected in wells 1 to 4, but was in well 5 and, as with total coliforms, in decreasing numbers from the beginning (7.6×10^2 *E. coli*/100 mL in sample 4) towards the end of the rainy season (7.4 *E. coli*/100 mL in sample 6) (Table 3). It is worth noticing that the microbial counts found in well 5 (and essentially only there) is consistent with the groundwater flow direction and with the relatively shallow water table in this well compared to others (Fig. 3 and Table 2).

The presence of coliform bacteria in groundwater has long been considered an indicator of contamination by organic material, in particular, faecal material or decomposing flesh (Young *et al.*, 2002). In Australia, Dent & Knight (1998) recorded variable but low numbers of faecal coliforms, faecal streptococci and *Pseudomonas aeruginosa* in piezometers placed within a burial ground. Pacheco *et al.* (1991), examining three cemeteries with shallow water tables in Brazil, found significant total and faecal coliforms and faecal streptococci. In addition, lipolytic and proteolytic bacteria were found in large numbers, indicating that the products of organic decomposition were being actively transported to the groundwater. Sulfide-reducing *Clostridia* were also frequently detected. Measurements at a control site away from the cemeteries showed an absence of lipolytic and proteolytic bacteria in groundwater. Furthermore, the presence and counts of all these indicator organisms were statistically correlated. Similar results were

Table 3 - Total coliforms and *E. coli* numbers (NMP/100 mL) in groundwater samples during the raining season, Tabuleiro, MG, Brazil, 2007-2008.

Sample	Well	Total coliforms	<i>Escherichia coli</i>
2 (Sep 2007)	1	7.4	ND
	2	ND	ND
	3	6.5×10^2	ND
	4	2.4×10^3	ND
	5	1.0	ND
4 (Dec 2007)	1	ND	ND
	2	ND	ND
	3	ND	ND
	4	2.0	ND
	5	1.0×10^3	7.6×10^2
5 (Jan 2008)	1	ND	ND
	2	ND	ND
	3	ND	ND
	4	2.3×10^1	ND
	5	2.5×10^2	4.8×10^1
6 (Feb 2008)	1	1.0	ND
	2	ND	ND
	3	1.0	ND
	4	1.0	ND
	5	2.8×10^1	7.4

ND: not detected.

found by Rodrigues & Pacheco (2003) in three cemeteries in Portugal. In South Africa, Engelbrecht (1998) showed increased numbers of indicators organisms in well points in a cemetery, as compared to the reference groundwater quality at a municipal borehole. The 95 percentile values for each indicator was found to be: 7.8×10^4 faecal coliforms per 100 mL, 5.7×10^4 *E. coli* per 100 mL, 2.1×10^5 faecal streptococci per 100 mL, and 5.4×10^3 *Staphylococcus aureus* per 100 mL. All these results, including those of the present study, suggest that in some hydrogeological settings microbial organisms can be carried into de groundwater.

3.4. Physical and chemical groundwater quality

Overall, the pH registered throughout the monitoring period ranged from 6.0 to 7.0, which did not substantially differ from the pH of water samples collected from the control well (Fig. 5). Such results suggest that the pH readings do not convey further inferences on eventual impacts of the cemetery upon the local aquifer. Electrical conductivity (EC) tests clearly indicated impacts upon groundwater quality, especially at monitoring well 5 (Fig. 6) located down-

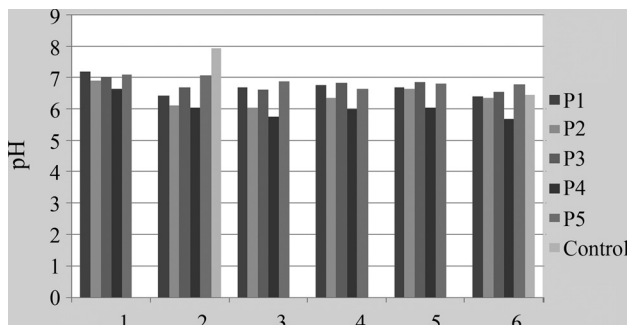


Figure 5 - pH readings in ground water samples, Tabuleiro, MG, Brazil, 2007-2008.

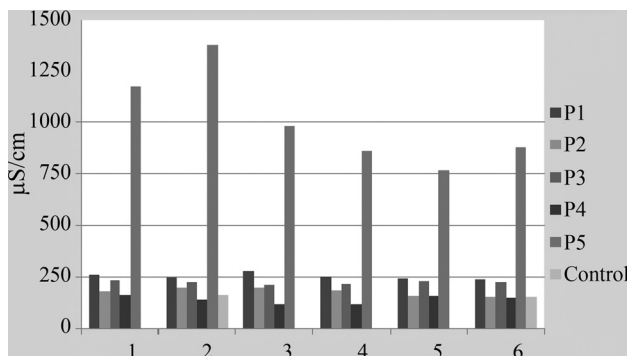


Figure 6 - Electrical conductivity readings in ground water samples, Tabuleiro, MG, Brazil, 2007-2008.

stream from the cemetery both for superficial and underground flow. Monitoring wells 1 to 4, as well as the control one, recorded EC levels ranging from 120 to 280 $\mu\text{S}/\text{cm}$ suggesting low salinity. EC in well 5 was much higher, ranging from 770 to 1380 $\mu\text{S}/\text{cm}$, typical readings for saline or wastewaters (Rhoades *et al.*, 1992; Metcalf & Eddy, 2004). The higher EC readings at well 5 maybe associated to its higher levels of ammonia, calcium, magnesium and sodium (Table 4). On Table 5 statistical values for all measured parameters are presented. These results, however, do not convey further inferences on eventual and aggregated impacts of rainfall.

In all groundwater samples, but those from well 5, ammonia remained below detection limit (5 mg/L) (Table 4). In well 5 the ammonia content was even higher than that usually found in municipal sewage (von Sperling & Chernicharo, 2005). These results indicate contamination from on the local aquifer; but as with EC, it does not convey further inferences on eventual and aggregated impacts of rainfall.

Nitrate concentration in groundwater samples varied from 2.5 to 6.4 mg/L in wells 1, 2, 3 and 5, although lesser values were sometimes found in well 5; the exception to its behavior was the result for well 1 at the end of dry season (32.8 mg/L). Taking into account the nitrate content recorded in the control well, overall the results indicate im-

pacts on the aquifer, mostly on well 4 in which higher concentrations were found: around 6 to 8 mg/L during the dry season and from 6 to close to the usual guideline value for drinking-water (10 mg/L) during the rainy season (WHO, 2004). Given that the presence of ammonia and nitrates can be taken as an evidence of pollution and based upon the results found during the study period, it is most likely that the cemetery is a continuous source of ammoniacal nitrogen, especially downstream in sampling well 5, which showed high levels of ammonia, lacking therefore the required time to allow the nitrification cycle to take place both in the soil and in the groundwater.

The content of phosphorus in the sampling wells was low, which is consistent with its low mobility in the soil (Table 4). In general, the results do not indicate that the cemetery is sourcing phosphorus to the aquifer. Nevertheless, is worth noticing that higher concentrations were usually found in well 5 (located downstream) during the rainy season.

A comparison between calcium readings in the sampling wells and in the control well clearly suggests that the cemetery is impacting the aquifer; moreover this pattern is more evident in sampling well 5. The results also suggest some seepage of magnesium, although not as clear as for calcium (Table 4). Overall there was little evidence of sodium contribution from the cemetery into the groundwater. Notwithstanding, once again well 5 usually showed the highest concentrations of sodium (Table 4). In general potassium is found only in very low concentrations in groundwater. Thus, in spite of being found in low concentrations in the wells, there is some suggestion of the cemetery as a source of potassium feeding the aquifer. The concentrations found in sample 1, are clearly an exception and could be attributed to the presence of clay in the samples collected from the wells.

BOD concentration on groundwater samples was usually low; in contrast COD values were much higher. Thus the recorded high COD: BOD ratios suggest that the groundwater was polluted by organic matter least biodegradable or at its initial degradation stages. However, it should be noted that the control well revealed an unexpected high COD reading in sample 6.

The observed impact of burial ground effluent on groundwater is generally similar to that of landfill leachate. The common contaminants are labile organic compounds, ammoniacal nitrogen, mobile anions (*e.g.* Cl, NO_3 and SO_4) and alkali earth metals (*e.g.* Na, K) (Young *et al.*, 2002; Sawyer *et al.*, 2003). The physical and chemical parameters analyzed herein are among those usually recommended as monitoring guidelines and as a first approach for detecting the groundwater impacts from cemeteries (Environmental Agency, 2004; Tredoux *et al.*, 2004). Further, the findings of this study are in general agreement with those by others. For instance, high concentrations of ammonium and nitrate ions have been reported in a contamination plume which

Table 4 - Chemical groundwater quality, Tabuleiro, MG, Brazil, 2007-2008.

Sample	Well	N-NO ₃	N-NH ₃	BOD	COD	P	Ca	Mg	Na	K
1	1	32.8	NM	NM	60.0	0.01	21.2	5.9	13.2	110.0
	2	3.7	NM	NM	85.0	0.14	14.4	4.3	11.4	83.6
	3	6.4	NM	NM	111.0	0.03	39.7	6.2	NM	NM
	4	6.4	NM	NM	126.0	0.02	20.4	3.6	6.8	83.6
	5	6.4	NM	NM	82.4	NM	31.7	2.8	81.4	70.4
	Control	NM	NM	NM	NM	NM	NM	NM	NM	NM
2	1	4.0	< 5.0	0.3	75.2	0.04	20.4	14.8	2.8	9.8
	2	3.8	< 5.0	1.5	27.3	0.07	18.8	11.2	2.2	5.0
	3	5.2	< 5.0	1.6	268.4	0.19	38.5	11.7	3.4	9.4
	4	8.0	< 5.0	0.4	110.5	0.05	20.4	NM	2.2	4.2
	5	1.5	73.5	6.1	126.6	0.09	35.3	NCO	1.6	1.4
	Control	1.0	< 5.0	0.4	57.1	0.11	16.0	16.0	12.0	3.2
3	1	4.4	< 5.0	3	27.3	0.06	32.9	0.9	10.4	5.2
	2	3.1	< 5.0	NM	57.1	0.09	23.2	NM	5.2	2.8
	3	2.4	< 5.0	3	27.3	0.10	38.1	NM	1.8	0.8
	4	7.6	< 5.0	2	27.3	0.06	15.2	NM	2	0.8
	5	7.4	NM	10	110.5	0.09	60.9	5.2	15.6	5.8
	Control	NM	NM	NM	NM	NM	NM	NM	NM	NM
4	1	3.3	< 5.0	3	NM	0.02	24.8	5.3	10.3	4.0
	2	4.8	< 5.0	3	NM	0.03	15.6	1.2	8.8	3.8
	3	4.6	< 5.0	6	NM	0.03	34.9	1.0	3.3	0.8
	4	6.1	< 5.0	5	NM	0.01	13.6	0.5	4.5	0.5
	5	0.5	45.7	2	NM	0.11	44.5	17.0	21.5	7.0
	Control	NM	NM	NM	NM	NM	NM	NM	NM	NM
5	1	4.8	< 5.0	NM	110.7	0.01	16.4	4.1	10.4	3.2
	2	4.3	< 5.0	NM	111.3	0.03	12.4	0.5	5.2	2.2
	3	6.2	< 5.0	NM	111.3	0.03	36.1	1.5	3.4	0.4
	4	9.2	< 5.0	NM	110.4	0.0	16.8	1.5	4.8	0.6
	5	0.6	68.9	NM	109.4	0.17	38.5	4.4	14.6	4.2
	Control	NM	NM	NM	NM	NM	NM	NM	NM	NM
6	1	5.2	< 5.0	NM	110.4	0.01	12.0	1.0	11.0	3.2
	2	4.1	< 5.0	NM	107.8	0.02	8.4	1.9	5.4	2.0
	3	4.9	< 5.0	NM	110.7	0.11	29.7	1.0	4.6	0.4
	4	9.8	< 5.0	NM	110.0	0.01	9.2	0.2	5.4	0.2
	5	0.3	33.3	NM	98.0	0.09	44.9	5.7	16.2	3.8
	Control	0.4	< 5.0	NM	109.8	0.01	11.2	1.7	6.0	2.2
7	1	4.9	< 5.0	2	108.5	0.07	17.6	3.4	NM	NM
	2	3.8	< 5.0	1	108.7	0.02	11.6	0.7	NM	NM
	3	5.0	< 5.0	3	109.4	0.13	33.7	0.5	NM	NM
	4	9.8	< 5.0	2	109.6	0.03	14.8	0.2	NM	NM
	5	0.5	< 5.0	8	106.3	0.27	40.1	3.2	NM	NM
	Control	0.6	< 5.0	3	109.8	0	16.0	1.0	NM	NM

NM: not measured; NCO: Not collected. All units are (mg.L⁻¹).

Table 5 - Average values and variation coefficients of chemical parameters

Well	Value	N-NO ₃	N-NH ₃	BOD	COD	P	Ca	Mg	Na	K
1	Average	4.43	< 5.0	2.08	82.02	0.03	20.76	5.06	9.68	5.08
	Std. Dev.	0.63	N.D.	1.10	31.24	0.02	6.21	4.36	3.24	2.47
2	Average	3.94	< 5.0	1.83	82.87	0.06	14.91	3.30	6.37	3.16
	Std. Dev.	0.49	N.D.	0.85	31.23	0.04	4.54	3.75	2.95	1.11
3	Average	4.96	< 5.0	3.40	123.02	0.09	35.81	3.65	3.30	2.36
	Std. Dev.	1.22	N.D.	1.61	71.78	0.06	3.17	4.08	0.89	3.52
4	Average	8.13	< 5.0	2.35	98.97	0.03	15.77	1.20	4.28	1.26
	Std. Dev.	1.52	N.D.	1.66	32.57	0.02	3.65	1.29	1.71	1.48
5	Average	2.46	55.35	6.53	105.53	0.14	41.80	4.26	13.90	4.44
	Std. Dev.	2.84	16.53	2.95	13.39	0.07	4.71	1.12	6.60	1.90
Control	Average	0.67	< 5.0	1.70	92.23	0.04	14.40	6.23	9.00	2.70
	Std. Dev.	0.25	N.D.	1.30	24.84	0.05	2.26	6.91	3.00	0.50

NM: not measured; All units are in (mg.L⁻¹).

rapidly diminished with distance from graves in Germany, whereas in Holland a very saline (2300 µS/cm) plume of chloride, sulfate and bicarbonate ions was found beneath graves. Studies in Australia showed an increase in electrical conductivity close to graves; also, elevated chloride, nitrate, nitrite, ammonium, orthophosphate, iron, sodium, potassium and magnesium ions were found beneath the cemetery. Index measures of organic contamination, including total organic carbon (TOC), BOD and COD have also been reported in groundwater analyses from burial grounds (Üçisik & Rushbrook, 1998). In the above mentioned work of Engelbrecht (1998) an increase in concentration above the regional groundwater quality was found for several chemical parameters in well points inside the cemetery; the maximum recorded values were: 37 mg K/L, 88.9 mg NH₃/L, 55.4 mg NO₃+NO₂/L, 0.99 mg PO₄/L, and 218 dissolved organic carbon per liter. In two of the three cemeteries studied by In Brazil, Pacheco *et al.* (1991) found nitrate concentrations as high as 2.1 and 75.7 mg/L. Similar results have been reported by Migliorini (1994), who observed high concentrations of nitrogenous products in the groundwater of Vila Formosa Cemetery (São Paulo, Brazil), and this was found to be a direct result of human remains' decomposition. Migliorini (1994) also came across high concentrations of calcium in the groundwater of Vila Formosa Cemetery, but suggested that the use of lime in the cemetery was the most probable source of calcium. On the other hand, it is well known that saponification reactions in corpses could be a source of calcium and magnesium (Fiedler & Graw, 2003).

In general, water samples have shown underground water contamination, but further studies are necessary to define whether this contamination is caused by corpse de-

composition and/or by other sources such as septic tanks or malfunctioning of sewage systems.

4. Conclusions

The results arising from this study adds further evidence that groundwater is subjected to contamination from burials leakage from cemeteries. The studied cemetery, as several other existing burial grounds in Brazil, was sited without any prior geological and hydrogeological assessment, thus not surprisingly the most evident impacts have been observed in the sampling well located downstream of the cemetery site. Such impacts were confirmed mainly by the following water quality parameters: electrical conductivity, ammoniacal nitrogen, nitrates, calcium, COD, total coliforms and *Escherichia coli*. It must be pointed out that these last two parameters (total coliforms and *Escherichia coli*) cannot be related to corpse decomposition, but its presence must be related to sources existing in the cemetery surroundings, as there are no administration or visitors services within the cemetery area.

The evidences resulting from this study shows that there is a need of addressing a more detailed characterization of cemeteries leakages, including pathogenic organisms and toxic amines, and the fate of chemical and microbial contaminants from cemeteries through the soil. Proper hydrogeological assessments of new or extension of existing burial sites must be sought to mitigate environmental impacts and health risks.

The results have shown contamination of underground water but this cannot be definitely pointed as only been derived from Tabuleiro Cemetery leakage.

Acknowledgments

The authors are most thankful for the financial support provided for by the Brazilian agencies FAPEMIG and CAPES.

References

- ABNT (1992) Construção de Poço Para Captação de Água Subterrânea - NBR 12244. ABNT, São Paulo, Brazil, 10 p.
- APHA (1998) Standard Methods for the Examination of Water and Wastewater. American Public Health Association. 20th ed. Washington - DC.
- Brasil (2003) Brazilian Environment National Council. Directive N. 335 - 03 apr. 2003. Cemetery Environmental Licensing. Diário Oficial da União, Brasília, n. 1, Section 1, p. 98-99 (In Portuguese).
- Dent, B.B. & Knight, M.J. (1998) Cemeteries: A special kind of landfill. The context of their sustainable management. Proceedings of IAH Sustainable Solutions Conference, IAH, Kenilworth, Melbourne, p. 451-456.
- Engelbrecht, J.F.P. (1998) Groundwater pollution from cemeteries. In: Proceedings of the Water Institute of Southern Africa, Biennial Conference and Exhibition, Cape Town (CD-ROM).
- Environmental Agency (2004) Assessing the Groundwater Pollution Potential of Cemetery Developments. UK Environmental Agency, Bristol, 24 p.
- Fiedler, S. & Graw, M. (2003) Decomposition of buried corpses, with special reference to the formation of adipocere. *Naturwissenschaften*, v. 90:7, p. 291-300.
- Metcalf and Eddy, Inc. (2004) Wastewater Engineering - Treatment and Reuse. International edition. McGraw-Hill, Boston, 1820 p.
- Migliorini, R.B. (1994) Cemeteries as Source of Pollution in Aquifers. Study of the Vila Formosa Cemetery in the Sedimentary Basin of São Paulo. MSc Dissertation, Instituto de Geociências, Universidade de São Paulo, São Paulo, 74 p. (In Portuguese).
- Morgan, O. (2004) Infectious disease risks from dead bodies following natural disasters. *Pan American Journal of Public Health*, v. 15:5, p. 307-312.
- Pacheco, A.; Mendes, J.M.B.; Martins, T.; Hassuda, S. & Kimmelman, A.A. (1991) Cemeteries - A potential risk to groundwater. *Water Science and Technology*, v. 24:11, p. 97-104.
- Rhoades, J.D.; Kandiah, A. & Mashali, A.M. (1992) The Use of Saline Waters for Crop Production. FAO, Rome, 117 p. (FAO Irrigation and Drainage paper 48).
- Rodrigues, L. & Pacheco, A. (2003) Groundwater contamination from cemeteries. Cases of study. Proceedings of Environmental 2010: Situation and Perspectives for the European Union, Porto, Portugal (CD-ROM).
- Rodriguez III, W.C. & Bass, W.M. (1985) Decomposition of buried bodies and methods that aid in their location. *Journal of Forensic Science*, v. 30:3, p. 836-852.
- Sawyer, C.N.; McCarthy, P.L. & Parkin, G.F. (2003) Chemistry for Environmental Engineering and Science. 5th ed. McGraw-Hill, New York, 752 p.
- Tredoux, G.; Cavé, L. & Engelbrecht, P. (2004) Groundwater pollution: Are we monitoring appropriate parameters? *Water SA*, v. 30:5 (Special edition), p. 114-119.
- Üçisik A.S. & Rushbrook, P. (1998) The Impact of Cemeteries on the Environment and Public Health. An Introductory Briefing. WHO Regional Office for Europe, Copenhagen, 15 p.
- Vass, A.A. (2001) Beyond the grave - Understanding human decomposition. *Microbiology Today*, v. 28, p. 190-192.
- Vass, A.A.; Bass, W.M.; Wolt, J.D.; Foss, J. & Ammons, J.T. (1992) Time since death determinations of human cadavers using soil solution. *Journal of Forensic Science*, v. 37:5, p. 1236-1253.
- Von Sperling, M. & Chernicharo, C.A.L. (2005) Biological Wastewater Treatment in Warm Climate Regions. V. 1. IWA Publishing, London, 835 p.
- WHO (2004) Guidelines for Drinking-Water Quality. 3rd ed. World Health Organization, Geneva, 515 p.
- Young, C.P.; Blackmore, K.M.; Reynolds, P.J. & Leavens, A. (2002) Pollution Potential of Cemeteries. UK Environmental Agency, Bristol, 71 p (R & D Technical Report P223).

The Influence of Cement Content and Water to Cement Ratio on Capillary Absorption of Root-Pile Mortars

E. Laister, P.J.R. Albuquerque, G. Camarini, D. Carvalho

Abstract. For the design of mortar mixes for filling root piles, the Brazilian standard NBR 6122, establishes a minimum compressive strength of 20 MPa (28 days), minimum cement content of 600 kg/m³ and a water to cement ratio between 0.5 and 0.6 and allows the use of water-reducing admixtures; however, the definition of a minimum cement content is a controversial topic about the guarantee of durability. Besides, cement content at these levels, will lead to axial compressive strength higher than 20 MPa, which is the minimum required by the standard, without much technological effort. The present study shows the influence of cement content and water to cement ratio on capillary absorption of mortars. It was found that, cement content, water to cement ratio and grain size distribution have an influence on capillary absorption. The study also demonstrates that it is possible to obtain mortars with low absorption for cement content lower than 600 kg/m³ by controlling the overall grain size distribution and by adding chemical admixtures to control the amount of mixing water. However, for mortars where grain size control is not possible, such as mortars mixed on site, the minimum cement content of 600 kg/m³ should be used to ensure low permeability.

Keywords: root piles, mortar, cement, durability.

1. Introduction

Root piles are widely used as a foundation in medium-to-large sized construction projects, mostly being the only alternative for the reinforcement of foundations of buildings and special structures. The pile is filled with a paste of cement or mortar, the latter being the most commonly used in Brazil. To obtain sufficient strength and durability, the Brazilian standard NBR 6122 (ABNT, 2010) specifies a minimum cement content of 600 kg/m³ and water to cement ratio ranging between 0.5 and 0.6 for the production of mortar for filling the piles; superplasticizer admixtures, among others, may be employed to improve the performance of the mortar. The minimum cement content required by the NBR 6122 is high and has become a controversial topic in technical circles being heavily discussed as a result of trends in global sustainability and in terms of the cost of carrying out this type of foundation. Besides, such high cement contents will result in axial compressive strengths above the 20 MPa required by the standard.

From the durability point of view, cementitious materials can be deteriorated by action of external agents. For structures in contact with soil or buried, the most important deterioration agents are sulfates. Mortar is made of materials held together by a porous binder forming a complex of solids and pores (hydrated cement paste). The binder is the continuous phase in the composite and pores are critical with respect to movement of water and chemicals substances into or out of the mortar. This is a feature relevant to the durability of the mortar in service (Diamond, 2007).

According to Dhir *et al.* (1994), durability tests are restricted to specialist laboratories; they take a long time to perform and are expensive. As durability is directly linked to the paste permeability for a defined cement, the lower the permeability the greater the durability.

Wassermann *et al.* (2009) highlight some of the reasons why the technical standards define minimum cement content for concrete. Firstly, this value goes back to a time when the water to cement ratio was controlled by means of cement content; secondly, there were few options in terms of water-reducing admixtures. Another important reason to have minimum cement content in the concrete or mortar is to guarantee a minimum amount of fines, ensuring workability and increased cohesion. Today, this is achieved by the addition of inert fines in order to increase the efficiency of the mortar without increasing cement content. These authors also evaluated the influence of cement content on the durability of concrete with cement content in the order of 230 to 450 kg/m³ and w/c ratios varying between 0.45 and 0.70. They concluded that cement content is not a parameter that can be used to guarantee durability. With smaller values of cement content, there was a reduction in capillary absorption, which was caused by the refinement of the pores in the matrix due to the use of superplasticizer admixtures.

Neville (1997) emphasizes that in soils and groundwater, it is common to find sulfates of sodium, potassium, magnesium and calcium. These sulfates may originate naturally or they may come from industrial effluents or fertil-

Eliézer Laister, Civil Engineer, MSc, Universidade de Campinas, Campinas, SP, Brazil. e-mail: eliezer.laister@vcimentos.com.br.

Paulo José Rocha de Albuquerque, Associate Professor, DSc, Universidade de Campinas, Campinas, SP, Brazil. e-mail: pjra@fec.unicamp.br.

Gladis Camarini, Associate Professor, DSc, Universidade de Campinas, Campinas, SP, Brazil. e-mail: camarini@fec.unicamp.br.

David de Carvalho, Associate Professor, DSc, Universidade de Campinas, Campinas, SP, Brazil. e-mail: david@feagri.unicamp.br.

Submitted on December 9, 2013; Final Acceptance on July 18, 2014; Discussion open until December 31, 2014.

izers. The sources of sulfates, such as calcium sulfate, react with alumina compounds present in the cement paste, forming ettringite (hydrated calcium sulfoaluminate). As this reaction is expansive and occurs in the mature stages, when the material has already hardened, it can cause cracks in the paste with a consequent increase in permeability and loss of strength.

According to Mehta & Monteiro (2008), the best protection against attack from sulfate sources includes: low permeability, adequate cement content and low w/c ratio, good consolidation of the concrete, proper curing and, if possible, the use of a sulfate-resisting cement.

Schulze (1999) shows that the capillary absorption of mortar is a function of its w/c ratio and its cement content (Fig. 1).

In porous solids, water has an enormous impact on their degradation; the more impermeable they are, the more durable (Diamond, 2007). As this is the case with mortar, the capillary absorption test was chosen to provide indirect information in terms of mortar durability, mainly because this is a simple, low-cost and easy to perform test.

In the present work, a study of mortars prepared at construction sites and in laboratory, and industrial ones is presented. These mortars were evaluated by capillary absorption and axial compressive strength tests

2. Material and Methods

2.1. Mortars

Nine types of mortar were studied. Two were collected from construction sites that used root piles (Sites 1 and 2), four were industrialized mortars (named Grout 15, Grout 20, Grout 25 and Grout 30) and three were produced in the laboratory (Lab 336, Lab 475 and Lab 616). The mortars produced in the laboratory were prepared by adding filler to substitute part of the cement. Table 1 shows the composition of the studied mortars. These mortars were studied in fresh (consistency) and hardened state (compressive strength and capillary absorption).

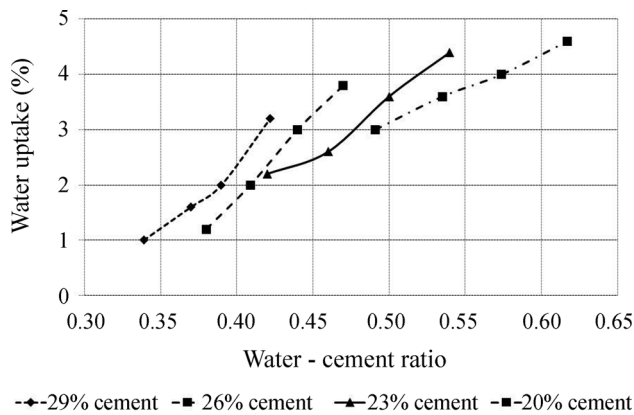


Figure 1 - Capillary absorption study conducted by Schulze (1999).

Table 1 - Characteristics of the mortars used in the study.

Mortar	Cement content (kg/m ³)	Filler (kg/m ³)	Aggregate - material passing through 0.15 mm sieve (%)	w/c	Water content (L/m ³)
Site 1	605	0	n/d	0.72	436
Site 2	636	0	n/d	0.82	522
Grout 15	242	n/d	23	1.09	264
Grout 20	286	n/d	19	0.92	263
Grout 25	330	n/d	21	0.80	264
Grout 30	374	n/d	25	0.71	266
Lab 336	336	336	19	0.80	269
Lab 475	475	204	20	0.57	271
Lab 616	616	68	20	0.44	271

Note: Mortars with minimum consistency of 90 mm by mini-slump test measured 30 min after mixing. The mortars site 1 and site 2 were made according to current regulations at the time of execution (1996). The setting of a range for the w/c was established in 2010 (NBR 6122/2010).

For all the mortars studied, 5 cm x 10 cm cylindrical specimens (diameter x height) were shaped manually according to the Brazilian standard NBR 7215 (ABNT, 1991).

Mortar curing was made as follows: the specimens from sites 1 and 2 remained at the site for the first 24 h; the specimens cast in laboratory were kept in moulds in a wet chamber for the first 24 h. After that, they were demolded and remained immersed in water until the time of the tests.

2.2. Consistency

The consistency of the mortar was measured using Kantro mini-slump (Kantro, 1980) (Figs. 2 and 3), which is a test used for fluid mortars. The test consists of measuring the diameter formed by the spreading of the fluid mortar over a glass dish after removing the mini-slump apparatus. The minimum value set as a reference for the mortars mixed in the laboratory and the grouts was a diameter of 90 mm measured 30 min after mixing, which is similar to the value obtained in mortars collected in the field (sites 1 and 2).

2.3. Compressive strength

Mortars compressive strength tests were made in four specimens for each age and for each mortar. The tests followed NBR 7215 (ABNT, 1991).

2.4. Capillary absorption test

The capillary absorption test was carried out at the age of 28 days in three specimens for each mortar. The tests followed NBR 9779 (ABNT, 1995). The specimens remained in the oven (105 ± 5 °C) until constant mass and were stored in a desiccator until they reached 23 ± 2 °C. The specimens were weighted and were subsequently placed over a grill in a container with water. The water level remained constant during the test at 5 ± 1 mm above the surface in contact with water.

The specimens were weighted after 3, 6, 24, 48 and 72 h. Before weighting, they were dried with a damp cloth to remove the excess water.

To ensure a unidirectional capillary absorption flow, a technique employed by the Laboratório de Aglomerantes e Resíduos (Laboratory of Binders and Wastes) at FEC/UNICAMP (Camarini *et al.*, 2011), was used. In this procedure, the lateral surface of the specimens are sealed with a latex-based waterproofing agent, thereby restricting the flow of water in just one direction, i.e. perpendicular to its axis.

The coefficient of capillary absorption was calculated using the Eq. 1.

$$C = \frac{A - B}{Area} \tag{1}$$

where *C* = absorption of water through capillarity (g/cm²), *A* = mass of the specimen after immersion in the test receptacle in the respective period of time (g), *B* = mass of the specimen when dry in oven (105 ± 5 °C) until constant mass, as soon as it attains a temperature of 23 ± 2 °C (g), in the desiccator and *Area* = cross-sectional area of specimen (cm²).

3. Results and Discussions

3.1. Consistency

Table 1 shows the quantity of water needed to obtain the consistency required for the mortar pumping. A diameter of 90 mm measured by the mini-slump test was required 30 min after mixing. If the water to cement ratios (between 0.5 and 0.6) proposed by NBR6122 (ABNT, 2010) were used for these water contents, it would be obtained:

- For mortars collected from the construction sites, a water to cement ratio of 0.5 and water content between 436 and 522 L/m³, leading to cement contents of 872 kg/m³ and 1044 kg/m³, respectively; for mortars with a water to ce-

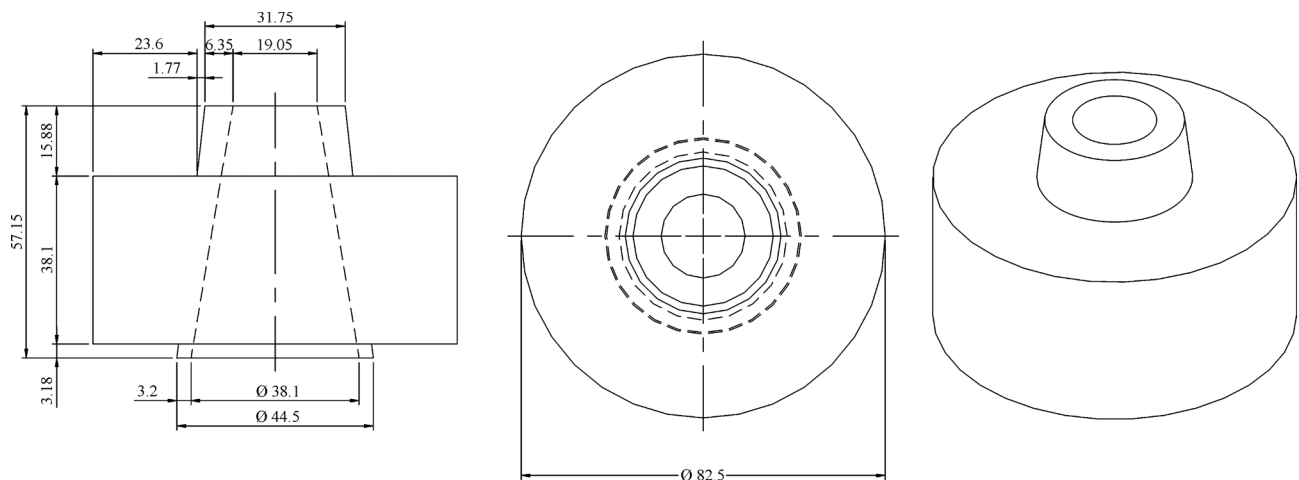


Figure 2 - Project design of mini-slump apparatus (units in mm) (Based on Kantro, 1980).

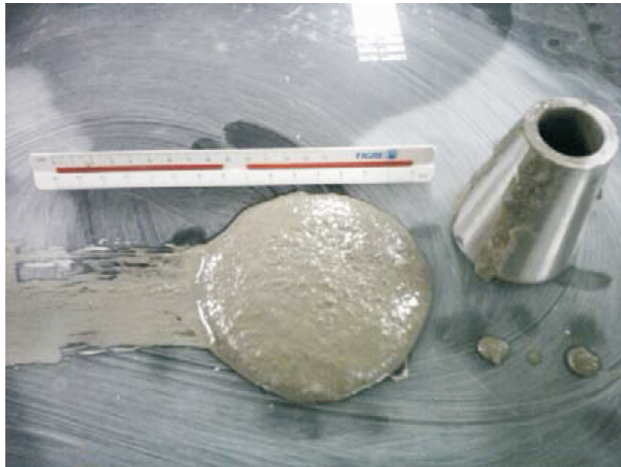


Figure 3 - Mini-slump test (Laister, 2012).

ment ratio 0.6 and water content between 436 and 522 L/m³, the cement content would be 726 kg/m³ and 870 kg/m³;

- For laboratory (Lab) and industrial mortars (Grout), a water to cement ratio of 0.5 and water content ranging from 263 to 271 L/m³, result in a cement content of 526 kg/m³ to 542 kg/m³. These same mortars with a w/c of 0.6 result in a cement content of 438 kg/m³ to 451 kg/m³.

These results indicate that to maintain the w/c ratio and the fluidity with cement content of 600 kg/m³ it is necessary to use a water-reducing admixture.

In laboratory conditions it was not possible to mix mortars with a cement content lower than 600 kg/m³ using superplasticizer admixture without segregation. However, it was possible to mix mortar with a cement content lower than 600 kg/m³ by replacing a part of the cement with limestone filler.

3.2. Compressive strength

Figure 4 displays the axial compressive strength obtained for the different types of mortar. Dotted line is the minimum value established by the Brazilian standard.

The mortars designated as Grout 15 (242 kg cement/m³) and Lab 336 (336 kg cement/m³) had strength under 20 MPa. On the other hand, the mortars Grout 20 (286 kg cement/m³), Grout 30 (374 kg cement/m³) and Lab

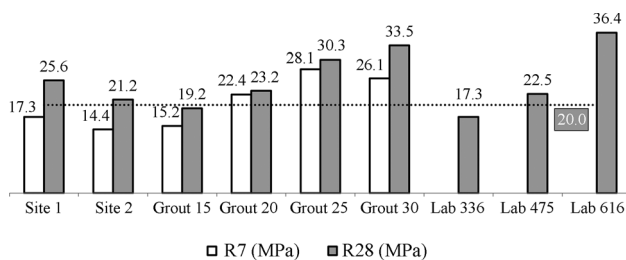


Figure 4 - Axial compressive strengths of the mortars studied (Laister, 2012).

475 (475 kg cement/m³), had strength above 20 MPa, with a cement content lower than 600 kg/m³. The results also showed that the mortar Lab 475, which was the one with the lowest cement content, attained a compressive strength 20 MPa.

2.3. Capillary absorption

Figure 5 shows the capillary absorption of the studied mortars.

The Site 2 mortar was adopted as reference of capillary absorption test (absorption limit), because it was collected in the field, was prepared according to the prevailing standards and by an experienced company.

From the capillary absorption results (Fig. 5), it can be seen that Grout 15 and the mortars Lab 336 and 474 showed capillary absorption above that of the mortar used in Site 2 (reference). They are not therefore efficient in terms of capillary absorption. The Lab 616 mortar was the only one mixed in the laboratory which met the reference, both in terms of strength and capillary absorption (absorption below the reference value). It was not possible to obtain mortars mixed in the laboratory with capillary absorption less than or equal to the reference mortar using a cement content of less than 600 kg/m³ (Site 2).

Grout 20 had a capillary absorption similar to that of Site 2 (reference), while Grouts 25 and 30 displayed capillary absorption lower than that of the mortar on Site 2 (reference). Grouts 25 and 30 were generally more effective because, with their smaller cement content, they had lower capillary absorption (Fig. 5).

Grout 30 had the second lowest capillary absorption (Fig. 5). This sample contains the highest quantity of total fines (Table 1), which may have contributed to a better particle packing density, producing a smaller quantity of capillary pores or even interrupting the interconnecting capillary pores.

Table 2 summarizes the compressive strength and capillary absorption of the studied mortars.

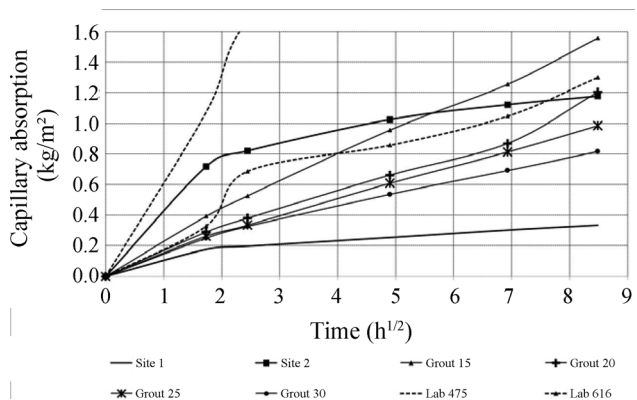


Figure 5 - Capillary absorption of the mortars studied (Laister, 2012).

Table 2 - Compressive strength and capillary absorption of mortars. Site 2 mortar was taken as reference.

Mortar	Compressive strength $f_c \geq 20$ MPa*	Capillary absorption**
Site 1	Yes	-
Grout 15	No	No
Grout 20	Yes	Yes
Grout 25	Yes	Yes
Grout 30	Yes	Yes
Lab 336	Yes	No
Lab 475	Yes	No
Lab 616	Yes	Yes

f_c = axial compressive strength.

*"Yes" - mortars with compressive strength ≥ 20 MPa (reference). "No" - mortars with compressive strength < 20 MPa.

**"Yes" - mortars with capillary absorption \leq site 2. "No" - mortars with capillary absorption $>$ site 2.

These results show that industrial mortars can have an excellent performance in terms of compressive strength and capillary absorption, demonstrating that is possible to use them for root piles. With industrial mortar it is possible to have a more appropriate technological control. Mortars produced on site must have a high cement content to guarantee the desired absorption.

4. Conclusions

The present study found that the quantity of fines in the cement matrix helps to ensure that segregation does not occur. Therefore, for mortars where grain-size control is not possible, such as those mixed on construction sites, a minimum cement content of 600 kg/m^3 should be used, in order to guarantee low mortar permeability. To obtain fluid mortar and to maintain the w/c between 0.5 and 0.6, a water-reducing admixture should be used.

The study also showed that the grouts were the products with lowest capillary absorption, even though they had the lowest cement content. These formulations contain a higher quantity of fines than conventional mortar, contributing to a better overall grain-size distribution, making possible to work with cement content lower than 600 kg/m^3 without negative impacts on permeability. In other words, it is possible to work with smaller cement content if adequate technological procedures are adopted.

In the case of construction sites where it is not possible to perform a grain size control of the mixture, neither the use chemical admixtures, the addition of filler and a cement content of a least 600 kg/m^3 are good measures to ensure low permeability and to increase robustness in the whole manufacture process. A cement content of 600 kg/m^3 leads to a lower w/c ratio and provides a quantity of fines so that segregation does not occur.

The setting of a range for the w/c ratio could promote a significant increase in the content of cement. Depending on the high fluidity and the characteristics of the inputs

available at the construction site it could possibly demand more water. Therefore, it is also necessary to define the range of consistency for pumping and also the capillary absorption performance, which could promote more economical, more durable mortars, making the content of cement more flexible maintaining the performance, both in its fresh state (avoiding segregation) and also in the hardened state (minimum compressive strength and limiting capillary absorption).

References

- ABNT NBR 6122 (2010) Projeto e Execução de Fundações. Associação Brasileira de Normas Técnicas, Rio de Janeiro, Brasil, 91 p.
- ABNT NBR 7215 (1996) Cimento Portland - Determinação da Resistência à Compressão. Associação Brasileira de Normas Técnicas, Rio de Janeiro, Brasil, 8 p.
- ABNT NBR 9779 (2012) Argamassa e Concreto Endurecidos - Determinação da Absorção de Água por Capilaridade. Associação Brasileira de Normas Técnicas, Rio de Janeiro, Brasil, 3 p.
- Camarini, G.; Pereira, V.M.; Freitas, P.M.G. & Tirello, R.A. (2011) Methods to measure the transfer properties of mortars. *Applied Mechanics and Materials*, v. 148:149, p. 184-187.
- Dhir, R.K.; Jones, M.R.; Byars, E.A. & Shaaban, I.G. (1994) Predicting concrete durability from its absorption. *Durability of concrete. Third International Conference*, Malhotra, Nice, ACI - SP - 145:62, p. 1177-1194.
- Diamond, S. (2007) Physical and chemical characteristics of cement composites, In: Page, C.L. & Page, M.M. (eds) *Durability of Concrete and Cement Composites*. Woodhead Publishing and Maney Publishing, CRC Press, p. 10-44.
- Kantro, D.L. (1980) Influence of water-reducing admixtures on properties of cement paste - A mini slump test.

- Cement and concrete aggregates. Winter, v. 2:2, p. 95-102.
- Laister, E. (2012) Influência do Consumo de Cimento e da Relação Água/Cimento em Argamassas para Execução de Estaca Raiz. Dissertação de Mestrado, FEC, Unicamp, 160 p.
- Mehta, P.K. & Monteiro, P.J.M. (2008) Concreto, Microestrutura, Propriedades e Materiais. Ibracon, São Paulo, 674 p.
- Neville, A.M. (1997) Propriedades do Concreto. PINI, São Paulo, 828 p.
- Schulze, J. (1999). Influence of water-cement ratio and cement content on the properties of polymer-modified mortars. Cement and Concrete Research, v. 29:6, p. 909-915.
- Wassermann, A.; Katz, A. & Bentur, A. (2009) Minimum cement content requirements: A must or a myth? Materials and Structures, v. 42:7, p. 973-982.

SOILS and ROCKS

An International Journal of Geotechnical and Geoenvironmental Engineering

Publication of

ABMS - Brazilian Association for Soil Mechanics and Geotechnical Engineering

SPG - Portuguese Geotechnical Society

Volume 37, N. 2, May-August 2014

Author index

Albuquerque, P.J.R.	171	Guedes, J.	133
Alonso, Eduardo E.	3	He, M.C.	73
Aoki, N.	61	Janin, J.P.	39
Arêde, A.	133	Karam, K.	133
Bacellar, L.A.P.	51	Laister, E.	171
Barreto, G.W.	61	Mahler, C.F.	133
Bastos, R.K.X.	161	Maiñas, L.M.S.	85
Betim, L.S.	161	Marques, E.A.G.	161
Borgatto, A.V.A.	133	Massad, Faiçal	113
Boskov, M.E.G.	85	Menezes, J.E.Q.	133
Camarini, G.	171	Mitchell, J.K.	99
Carvalho, D.	171	Münnich, K.	133
Cintra, J.C.A.	61	Paupério, E.	133
Costa, A.	133	Ribeiro e Sousa, L.	133
Dias, D.	39	Sousa, L.R.	73
Feng, J.L.	73	van Elk, A.G.P.	85
Ferreira, Q.C.G.	51	Viana da Fonseca, A.	133
Fineza, A.G.	161	Wang, C.G.	73
		Webler, A.D.	133

SOLOS MOLES?



CPR[®]

CONSOLIDAÇÃO PROFUNDA RADIAL

**O MAIS RÁPIDO E EFETIVO
TRATAMENTO PARA SOLOS MOLES**

Processo de adensamento de solo mole, eficientemente controlado, monitorando-se o grau de consolidação desejado.



Vantagens do CPR

- 100% específico para solos moles;
- Mobilização rápida;
- Ausência de transtornos à obra;
- Ampla gama de aplicações;
- Ausência de aterros, refugos e lama;
- Técnica não destrutiva;
- Alternativa super econômica, além de prazos extremamente curtos em relação à substituição de solos, aterros temporários, colunas granulares e estaqueamentos;
- Alcança profundidades de tratamento onde técnicas clássicas são limitadas;
- Acesso a locais restritos, limitados e difíceis, sem interferência com a rotina do cliente;
- Melhor custo benefício;
- Perfeito para reforço de fundação.

www.engegraut.com.br



Reforced Retaining Walls Terramesh®



Gabions Retaining Walls

RETAINING WALLS PROBLEMS? WE HAVE THE SOLUTION



Gabions Retaining Walls



Reforced Retaining Walls Terramesh®

BRASIL
Phone: 55 (11) 4525-5000
Fax: 55 (11) 4599-4275
maccaferri@maccaferri.com.br
www.maccaferri.com.br

PORTUGAL
Phone: (351) 218 968 282
Fax: (351) 218 968 078
portugal@abianchini.pt
www.abianchini.es

MACCAFERRI
Engineering a better solution

Geotechnics and Foundation Engineering



HEAD OFFICE
Edifício Edifer
Estrada do Seminário , 4 - Alfragide
2610 - 171 Amadora - PORTUGAL
Tel. 00 351 21 475 90 00 / Fax 00 351 21 475 95 00

Madrid
 Calle Rodríguez Marín, Nº 88 1º Dcha
 28016 Madrid - ESPANHA
 Tel. 00 34 91 745 03 64 / Fax 00 34 91 411 31 87

Angola
 Rua Alameda Van-Dúnem, n.º 265 R/c
 Luanda - ANGOLA
 Tel. 00 244 222 443 559 / Fax 00 244 222 448 843

Porto
 Rua Eng. Ferreira Dias, nº 161 2º Andar
 4100-247 Porto - PORTUGAL
 Tel. 00 351 22 616 74 60 / Fax 00 351 22 616 74 69

Barcelona
 Calle Comte d' Urgell, 204-208 6.º A
 08036 Barcelona - ESPANHA
 Tel. 00 34 93 419 04 52 / Fax 00 34 93 419 04 16

Madeira
 Rampa dos Piornais, n.º 5 - Sala 1
 9000-248 Funchal - PORTUGAL
 Tel. 00 351 291 22 10 33 / Fax 00351 291 22 10 34

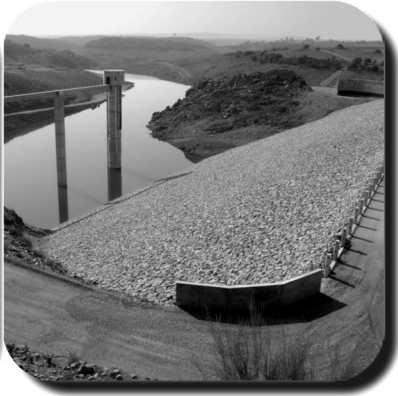
Sevilla
 Polígono Industrial de Guadalquivir, C/ Artesania, 3
 41120 Gelves (Sevilla) - ESPANHA
 Tel. 00 34 955 762 833 / Fax 00 34 955 76 11 75



Geotechnic and Rehabilitation

TEIXEIRA DUARTE
ENGENHARIA E CONSTRUÇÕES, S.A.

- **Head Office**
Lagoas Park – Edifício 2
2740-265 Porto Salvo - Portugal
Tel.: (+351) 217 912 300
Fax: (+351) 217 941 120/21/26
- **Algeria**
Parc Miremont – Rua A, Nº136 - Bouzareah
16000 Alger
Tel.: (+213) 219 362 83
Fax: (+213) 219 365 66
- **Spain**
Avenida Alberto Alcocer, nº24 – 7º C
28036 Madrid
Tel.: (+34) 915 550 903
Fax: (+34) 915 972 834
- **Angola**
Alameda Manuel Van Dunen 316/320 - A
Caixa Postal 2857 - Luanda
Tel.: (+34) 915 550 903
Fax: (+34) 915 972 834
- **Brazil**
Rua Iguatemi, nº488 – 14º - Conj. 1401
CEP 01451 - 010 - Itaim Bibi - São Paulo
Tel.: (+55) 112 144 5700
Fax: (+55) 112 144 5704
- **Mozambique**
Avenida Julyus Nyerere, 130 – R/C
Maputo
Tel.: (+258) 214 914 01
Fax: (+258) 214 914 00



GEOLOGY - GEOTECHNICS - SUPERVISION OF GEOTECHNICAL WORKS



EMBANKMENT DAMS - UNDERGROUND WORKS - RETAINING STRUCTURES



SPECIAL FOUNDATIONS - SOIL IMPROVEMENT - GEOMATERIALS

CENOR Consultores, S. A.

PORTUGAL | ANGOLA | ALGERIA | BRAZIL | CAPE VERDE | COLOMBIA
MALAWI | MOROCCO | MOZAMBIQUE | EAST TIMOR | VENEZUELA

Rua das Vigias, 2. Piso 1 | Parque das Nações | 1990-506 LISBOA . PORTUGAL
T. +351.218 437 300 | F. +351.218 437 301 | E. cenor@cenor.pt





- > **Prospecção Geotécnica**
Site Investigation
- > **Consultoria Geotécnica**
Geotechnical Consultancy
- > **Obras Geotécnicas**
Ground Treatment-Construction Services
- > **Controlo e Observação**
Field Instrumentation Services and Monitoring Services
- > **Laboratório de Mecânica de Solos**
Soil and Rock Mechanics Laboratory

Certificada ISO 9001 por

BVQI



Geocontrole



Parque Oriente, Bloco 4, EN10
2699-501 Bobadela LRS
Tel. 21 995 80 00
Fax. 21 995 80 01
e.mail: mail@geocontrole.pt
www.geocontrole.pt


Geocontrole
Geotecnia e Estruturas de Fundação SA



Where engineering begins.

Behind a great work there's always a great company.

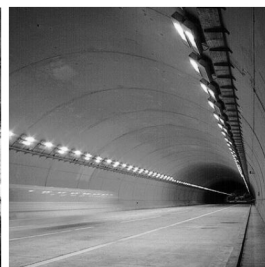
tgeotecnia enters in national and Spanish market with a wide range of solutions, with state of the art technology and qualified means necessities to engage geotechnical studies, projects and works.

Currently, tgeotecnia is specialised in all kinds of work, from geologic-geotechnical studies and project development to slope stabilisation, reinforcement, soil treatment and special foundations.

The works carried out and client satisfaction, as well as the growing number of projects, are the proof that it is worth making innovation the lever of development.

tgeotecnia
In the origin of construction

a dst group company



COBA

GEOLOGY AND GEOTECHNICS

Hydrogeology • Engineering Geology • Rock Mechanics • Soil Mechanics • Foundations and Retaining Structures • Underground Works • Embankments and Slope Stability
Environmental Geotechnics • Geotechnical Mapping



- Water Resources Planning and Management
- Hydraulic Undertakings
- Electrical Power Generation and Transmission
- Water Supply Systems and Pluvial and Wastewater Systems
- Agriculture and Rural Development
- Road, Railway and Airway Infrastructures
- Environment
- Geotechnical Structures
- Cartography and Cadastre
- Safety Control and Work Rehabilitation
- Project Management and Construction Supervision



PORTUGAL

CENTER AND SOUTH REGION
Av. 5 de Outubro, 323
1649-011 LISBOA
Tel.: (351) 210125000, (351) 217925000
Fax: (351) 217970348
E-mail: coba@coba.pt
www.coba.pt

Av. Marquês de Tomar, 9, 6º.
1050-152 LISBOA
Tel.: (351) 217925000
Fax: (351) 213537492

NORTH REGION

Rua Mouzinho de Albuquerque, 744, 1º.
4450-203 MATOSINHOS
Tel.: (351) 229380421
Fax: (351) 229373648
E-mail: engico@engico.pt

ANGOLA

Praceta Farinha Leitão, edifício nº 27, 27-A - 2º Dto
Bairro do Maculusso, LUANDA
Tel./Fax: (244) 222338 513
Cell: (244) 923317541
E-mail: coba-angola@netcabo.co.ao

MOZAMBIQUE

Pestana Rovuma Hotel. Centro de Escritórios.
Rua da Sé nº114. Piso 3, MAPUTO
Tel./Fax: (258) 21 328 813
Cell: (258) 82 409 9605
E-mail: coba.mz@tdm.co.mz

ALGERIA

09, Rue des Frères Hocine
El Biar - 16606, ARGEL
Tel.: (213) 21 922802
Fax: (213) 21 922802
E-mail: coba.alger@gmail.com

BRAZIL

Rio de Janeiro
COBA Ltd. - Rua Bela 1128
São Cristóvão
20930-380 Rio de Janeiro RJ
Tel.: (55 21) 351 50 101
Fax: (55 21) 258 01 026

Fortaleza

Av. Senador Virgílio Távora 1701, Sala 403
Aldeota - Fortaleza CEP 60170 - 251
Tel.: (55 85) 3261 17 38
Fax: (55 85) 3261 50 83
E-mail: coba@esc-te.com.br

UNITED ARAB EMIRATES

Corniche Road - Corniche Tower - 5th Floor - 5B
P. O. Box 38360 ABU DHABI
Tel.: (971) 2 627 0088
Fax: (971) 2 627 0087

STATIC LOAD TESTING

HYDRODYNAMIC EXPANSION CELLS[®]

ELIMINATES REACTION SYSTEM

- Ideal for any load capacity.
- Cost savings, safety and speed in execution.
- Recommended for all types of foundations.
- Worldwide pioneer in bidirectional static load testing.

“44 years developing advanced technologies, intelligent and creative solutions in the field of soil engineering.”

REINFORCEMENT OF FOUNDATIONS

ARCOS MICROPILES[®]:

- Ideal for strengthening of foundations and pile driving in hard to reach places.
- Cost savings, safety and speed in execution.



Desde 1969

+55 31 3274.0155 | www.arcos.eng.br
Belo Horizonte - MG - Brasil



ARCOS 44
engenharia de solos anos

1. TECCO® SYSTEM® teste em escala real, Suíça, outubro 2012
2. TECCO® SYSTEM® Instalação, B462, Alemanha
3. Ângulo máximo de inclinação de 85° durante o teste de campo



TECCO® SYSTEM³ – Seu talude estabilizado

... validado por teste em escala real com inclinação do talude de até 85°.

A malha de aço de alta resistência TECCO®, as placas de ancoragem e garras de conexão TECCO®, juntas, estabilizaram com sucesso 230 toneladas de cascalho com 85° de inclinação em um ensaio em escala real.

- moldura de teste com dimensões 10 x 12 x 1,2m
- espaçamento dos grampos 2,5m x 2,5m, utilizando Gewi 28mm

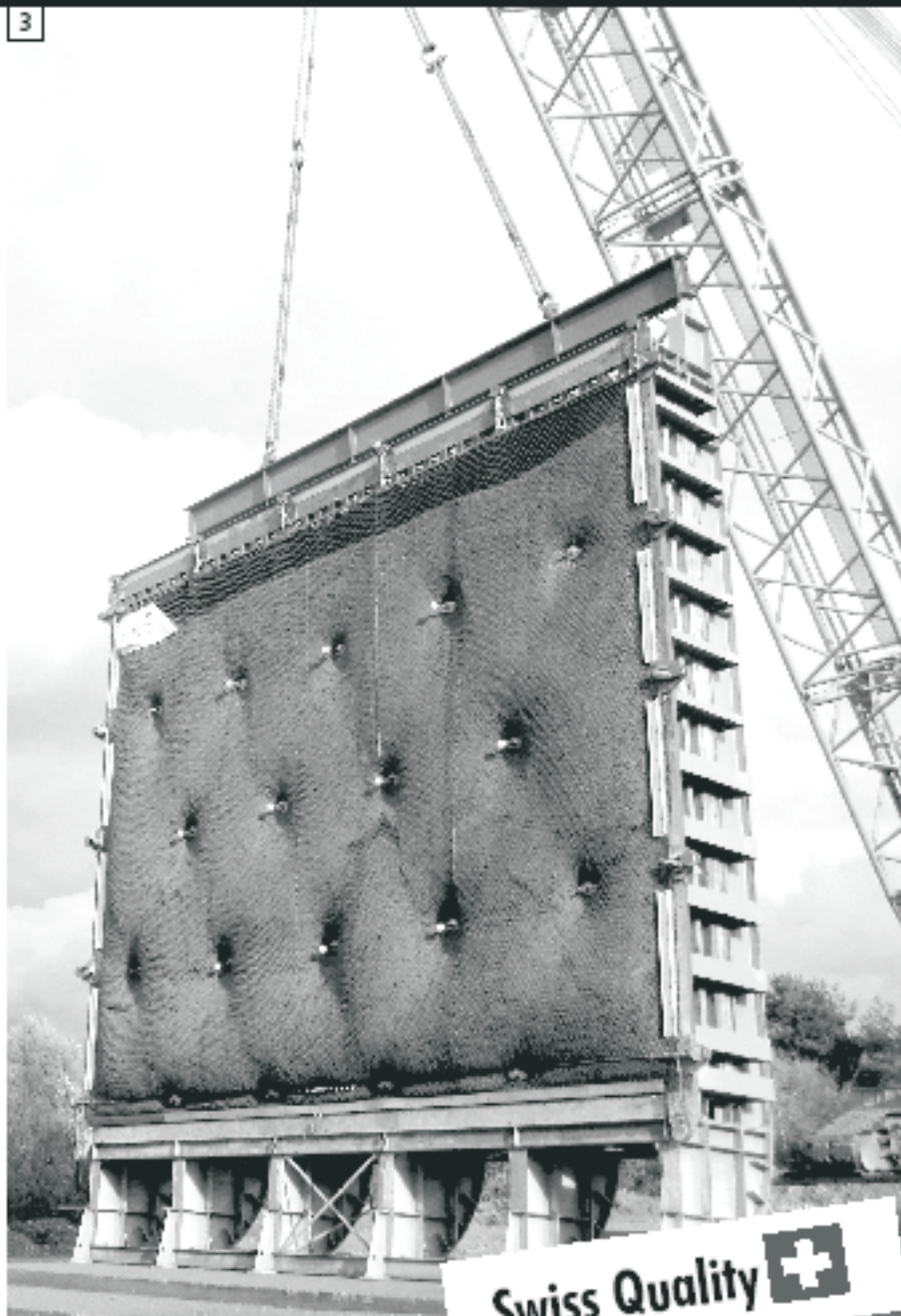
Para um estudo preliminar de solução de estabilização ou de riscos de desastres naturais nas obras em que você atua, entre em contato conosco através do e-mail info@geobrugg.com



Assista ou escaneie nosso filme com instalação TECCO® em www.geobrugg.com/slopes



Geobrugg AG, Geohazard Solutions
Rua Visconde de Pirajá, 82 sl.606
Ipanema - Rio de Janeiro • 22410-003
Fone: +55 21 3624.1449
Cel: +55 21 99979.1288
www.geobrugg.com

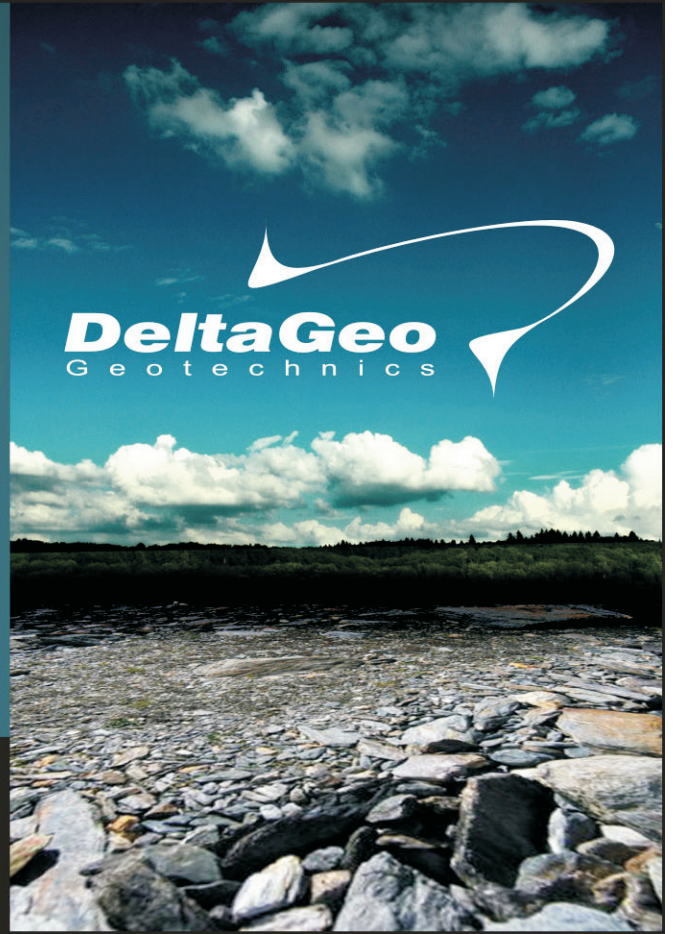


Swiss Quality 

SPECIALISTS IN GEOTECHNICAL IN-SITU TESTS AND INSTRUMENTATION

GEOTECHNICAL SERVICES (onshore and offshore)

- **IN-SITU TESTS**
 - Seismic CPT
 - Cone Penetration Testing Undrained-CPTu (cordless system)
 - Vane Shear Testing (electrical apparatus)
 - Pressuremeter Testing (Menard)
 - Flat Dilatometer Test-DMT (Machetti)
 - Standard Penetration Test-SPT-T
- **INSTRUMENTATION**
 - Instrumentation, installation and direct import
 - Routine Monitoring
 - Operation and Maintenance
 - Engineering analyses
 - Consultancy, design & geotechnical engineering services
- **SAMPLING**
 - Soil sampling and monitoring
 - Groundwater sampling and monitoring
 - Field and laboratory testing
- **ENVIRONMENTAL**
 - Environmental Services
 - Soil and groundwater sampling and monitoring
 - Field and laboratory testing



0800 979 3436

São Paulo: +55 11 8133 6030

Minas Gerais: +55 31 8563 2520 / 8619 6469

www.deltageo.com.br deltageo@deltageo.com.br



The largest portfolio of private clients in Brazil, and the highest rate of absolute repetition.

geofix

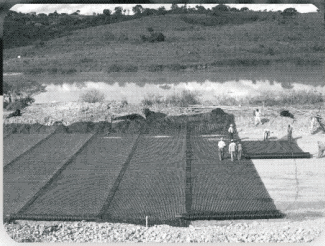
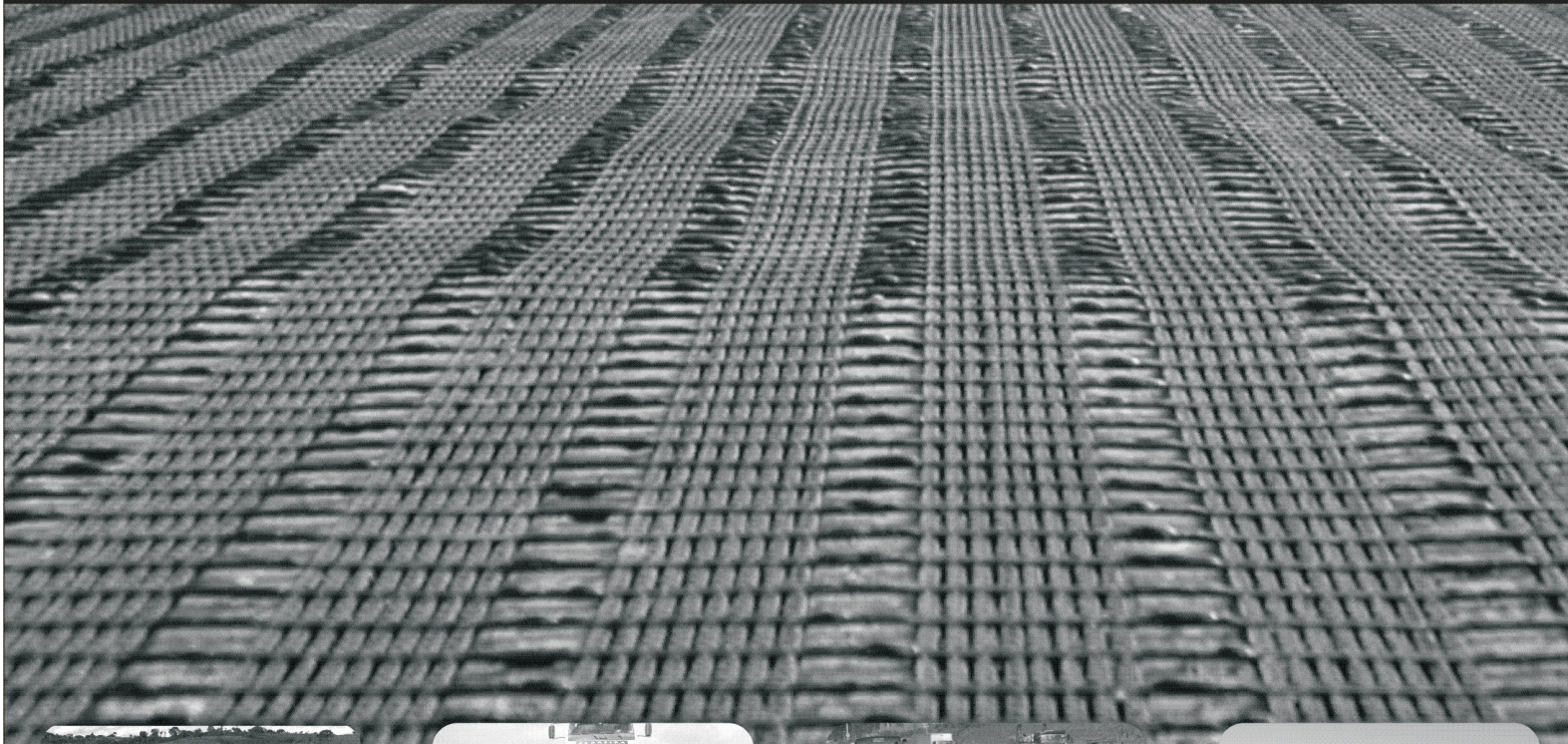
Among the types of services, we highlight environmental control projects, such as: recovery of degraded soils; containment of contaminated groundwater; construction of filters and capture of material; containment of pollutants.

Pioneering which translates into confidence and quality to your site.



www.geofix.com.br

» We're known for our strength «



Fortrac®

High tensile stiffness geogrid
for soil reinforcement



HaTelit® C

Flexible grid for
asphalt reinforcement



Fornit®

Flexible geogrid for
base reinforcement



HaTe®

Fabric for separation,
stabilization and filtration



Ringtrac®

Ring reinforcement for granular
columns on soil improvement



Stabilenka®

High strength woven
geosynthetic for soil reinforcement



NaBento®

Geosynthetic clay liner
for sealing



Incomat®

Construction system for
slope and bed protection

HUESKER
Engineering with Geosynthetics

Instructions to Authors

Category of the Papers

Soils and Rocks is the scientific journal edited by the Brazilian Association for Soil Mechanics and Geotechnical Engineering (ABMS) and the Portuguese Geotechnical Society (SPG). The journal is intended to the divulgation of original research works from all geotechnical branches.

The accepted papers are classified either as an Article paper, a Technical Note, a Case Study, or a Discussion according to its content. An article paper is an extensive and conclusive dissertation about a geotechnical topic. A paper is considered as a technical note if it gives a short description of ongoing studies, comprising partial results and/or particular aspects of the investigation. A case study is a report of unusual problems found during the design, construction or the performance of geotechnical projects. A case study is also considered as the report of an unusual solution given to an ordinary problem. The discussions about published papers, case studies and technical notes are made in the Discussions Section.

When submitting a manuscript for review, the authors should indicate the category of the manuscript, and is also understood that they:

- a) assume full responsibility for the contents and accuracy of the information in the paper;
- b) assure that the paper has not been previously published, and is not being submitted to any other periodical for publication.

Manuscript Instructions

Manuscripts must be written in English. The text is to be typed in a word processor (MS Word or equivalent), using ISO A4 page size, left, right, top, and bottom margins of 25 mm, Times New Roman 12 font, and line spacing of 1.5. All lines and pages should be numbered. The text should be written in the third person.

The first page of the manuscript is to include the title of the paper in English, followed by the names of the authors with the abbreviation of the most relevant academic title. The affiliation, address and e-mail is to be indicated below each author's name. An abstract of 200 words is to be written in English after the author's names. A list with up to six keywords at the end of the abstract is required.

Although alteration of the sequence and the title of each section may be required, it is suggested that the text contains the following sections: Introduction, Material and Methods, Results, Discussions, Conclusion, Acknowledgements, References and List of Symbols. A brief description of each section is given next.

Introduction: This section should indicate the state of the art of the problem under evaluation, a description of the problem and the methods undertaken. The objective of the work is to be clearly presented at the end of the section.

Materials and Methods: This section should include all information needed to the reproduction of the presented work by other researchers.

Results: In this section the data of the investigation should be presented in a clear and concise way. Figures and tables should not repeat the same information.

Discussion: The analyses of the results should be described in this section. **Conclusions:** The text of this section should be based on the presented data and in the discussions.

Acknowledgements: If necessary, concise acknowledgements should be written in this section.

References: References to other published sources are to be made in the text by the last name(s) of the author(s), followed by the year of publication, similarly to one of the two possibilities below:

“while Silva & Pereira (1987) observed that resistance depended on soil density” or “It was observed that resistance depended on soil density (Silva & Pereira, 1987).”

In the case of three or more authors, the reduced format must be used, e.g.: Silva *et al.* (1982) or (Silva *et al.*, 1982). Two or more citations belonging to the same author(s) and published in the same year are to be distinguished with small letters, e.g.: (Silva, 1975a, b, c.). Standards must be cited in the text by the initials of the entity and the year of publication, e.g.: ABNT (1996), ASTM (2003).

Full references shall be listed alphabetically at the end of the text by the first author's last name. Several references belonging to the same author shall be cited chronologically. Some examples are listed next:

Papers: Bishop, A.W. & Blight, G.E. (1963) Some aspects of effective stress in saturated and unsaturated soils. *Géotechnique*, v. 13:2, p. 177-197.

Books: Lambe, T.W & Whitman, R.V. (1979) *Soil Mechanics*, SI Version, 2nd ed. John Wiley & Sons, New York, p. 553.

Book with editors: Sharma, H.D.; Dukes, M.T. & Olsen, D.M. (1990) *Field measurements of dynamic moduli and Poisson's ratios of refuse and underlying soils at a landfill site*. Landva A. & Knowles, G.D. (eds) *Geotechnics of Waste Fills - Theory and Practice*, American Society for Testing and Materials - STP 1070, Philadelphia, p. 57-70.

Proceedings (printed matter or CD-ROM): Jamiolkowski, M.; Ladd, C.C.; Germaine, J.T & Lancellotta, R. (1985) *New developments in field and laboratory testing of soils*. Proc. 11th Int. Conf. on Soil Mech. and Found. Engr., ISSMFE, San Francisco, v. 1, pp. 57-153. (specify if CD – ROM)

Thesis and dissertations: Lee, K.L. (1965) *Triaxial Compressive Strength of Saturated Sands Under Seismic Loading Conditions*. PhD Dissertation, Department of Civil Engineering, University of California, Berkeley, 521 p.

Standards: ASTM (2003) *Standard Test Method for Particle Size Analysis of Soils - D 422-63*. ASTM International, West Conshohocken, Pennsylvania, USA, 8 p.

Internet references: *Soils and Rocks* available at <http://www.abms.com.br>.

On line first publications must also bring the digital object identifier (DOI) at the end.

Figures shall be either computer generated or drawn with India ink on tracing paper. Computer generated figures must be accompanied by the corresponding digital file (.tif, .jpg, .pcx, etc.). All figures (graphs, line drawings, photographs, etc.) shall be numbered consecutively and have a caption consisting of the figure number and a brief title or description of the figure. This number should be used when referring to the figure in text. Photographs should be black and white, sharp, high contrasted and printed on glossy paper.

Tables shall be numbered consecutively in Arabic and have a caption consisting of the table number and a brief title. This number should be used when referring to the table in text. Units should be indicated in the first line of the table, below the title of each column. Abbreviations should be avoided. Column headings should not be abbreviated. When applicable, the units should come right below the corresponding column heading. Any necessary explanation can be placed as footnotes.

Equations shall appear isolated in a single line of the text. Numbers identifying equations must be flush with the right margin. International System (SI) units are to be used. The symbols used in the equations shall be listed in the List of Symbols. It is recommended that the used symbols

be in accordance with Lexicon in 8 Languages, ISSMFE (1981) and the ISRM List of Symbols.

The text of the submitted manuscript (including figures, tables and references) intended to be published as an article paper or a case history should not contain more than 30 pages formatted according to the instructions mentioned above. Technical notes and discussions should have no more than 15 and 8 pages, respectively. Longer manuscripts may be exceptionally accepted if the authors provide proper explanation for the need of the required extra space in the cover letter.

Discussion

Discussions must be written in English. The first page of a discussion paper should contain:

- The title of the paper under discussion in the language chosen for publication;
- Name of the author(s) of the discussion, followed by the position, affiliation, address and e-mail. The discussor(s) should refer himself (herself, themselves) as “the discussor(s)” and to the author(s) of the paper as “the author(s)”.

Figures, tables and equations should be numbered following the same sequence of the original paper. All instructions previously mentioned for the preparation of article papers, case studies and technical notes also apply to the preparation of discussions.

Editorial Review

Each paper will be evaluated by reviewers selected by the editors according to the subject of the paper. The au-

thors will be informed about the results of the review process. If the paper is accepted, the authors will be required to submit a version of the revised manuscript with the suggested modifications. If the manuscript is refused for publication, the authors will be informed about the reasons for rejection. In any situation comprising modification of the original text, classification of the manuscript in a category different from that proposed by the authors, or refusal for publication, the authors can reply presenting their reasons for disagreeing with the reviewers' comments

Submission

The author(s) must submit for review:

1. A hard copy of the manuscript to Editors - Soils and Rocks, Av. Prof. Almeida Prado, 532 – IPT, Prédio 54 – DEC/ABMS, 05508-901 - São Paulo, SP, Brazil. The first page of the manuscript should contain the identification of the author(s), or

2. The digital file of the manuscript, omitting the authors' name and any information that eventually could identify them, should be sent to **abms@ipt.br**. The following must be written in the subject of the e-mail message: “*Paper submitted to Soils and Rocks*”. The authors' names, academic degrees and affiliations should be mentioned in the e-mail message. The e-mail address from which the digital file of the paper was sent will be the only one used by the editors for communication with the corresponding author.

Follow Up

Authors of manuscripts can assess the status of the review process at the journal website (www.soilsandrocks.com.br) or by contacting the ABMS secretariat.